# Thiolate containing N-heterocyclic amine based ligands; Investigations of intermediates in $O_2^-$ and $O_2$ reactivity and application towards new ligand design for modelling the active site of Superoxide Reductase.

Morgan Gleaves

A dissertation submitted in partial fulfilment of the requirements for the degree

of

Doctor of Philosophy

University of Washington

2012

Reeding Committee:

Julia A. Kovacs, Chair

Daniel R. Gamelin

D. Michael Heinekey

Program Authorized to Offer Degree:

Chemistry

University of Washington

Abstract

Thiolate containing N-heterocyclic amine based ligands; Investigations of intermediates in $O_2^-$ and $O_2$ reactivity and application towards new ligand design for modelling the active site of Superoxide Reductase.

Morgan Gleaves

Chair of the Supervisory Committee:

Professor Julia A. Kovacs

Chemistry

Detoxification of superoxide ($O_2^-$) in anaerobic organisms is performed by the iron (Fe) containing metalloenzyme Superoxide Reductase (SOR) via reduction to hydrogenperoxide. To understand the mechanism involved and how small molecular changes affect the properties and reactivity of SOR model complexes $[Fe^{(II)}(S^{Me2}N_4(6\text{-H-DPPN}))](PF_6)$, $[Fe^{(II)}(S^{Me2}N_4(2\text{-QuinoEN}))](PF_6)$ and $[Co^{(II)}(S^{Me2}N_4(6\text{-Me-DPEN}))](PF_6)$ were used in an attempt to reproduce the functionality of SOR and to characterize intermediates of reactivity. Intermediates of reaction with ($O_2^-$) were investigated through spectroscopic analysis as well as reactivity with a variety of substrates. Geometric alterations resulted in the reversible binding of neutral solvent ligands to $[Fe^{(II)}(S^{Me2}N_4(6\text{-H-DPPN}))](PF_6)$. The thermodynamics of binding were studied.

Based on these observations, new ligand designs incorporating steric bulk or electron donating substituents were proposed with the goal of stabilizing and isolating intermediate compounds.

Table of Contents

Page

# Contents

# List of Figures

# List of Abbreviations

$cm^{-1}$: reciprocal centimeters

DCM: dichloromethane

DMA: dimethylamide

EAS: electronic absorption spectroscopy

ESI-MS: electrospray ionization mass spectroscopy

EPR: electron paramagnetic resonance

$Et_2O$: diethyl ether

$[FeCP_2](PF_6)$: ferricenium hexafluorophosphate

IR: infrared

$^1H$: proton nucleus

J: coupling constant in Hz

MeCN: acetonitrile

MeOH: methanol

mL: milliliter

mmol: millimole

mol: mole

mV: millivolts

MW: molecular weight

m/z: mass to charge ratio

NMR: nuclear magnetic resonance

rR: resonance Raman

SOR: superoxide reductase

THF: tetrahydrofuran

# Compound Numbering Scheme

**1**: $[Fe^{II}(S^{Me2}N_4)(tren)]^+$

**2**: $[Fe^{II}(cyclam\text{-}PrS)]^+$

**3**: $[Fe^{(II)}(S^{Me2}N_4(6\text{-}Me\text{-}DPEN))]^+$

**4**: $[Co^{(II)}(S^{Me2}N_4(6\text{-}Me\text{-}DPEN))](PF_6)$

**5**: $[Co^{(III)}(S^{Me2}N_4(6\text{-}Me\text{-}DPEN))](PF_6)_2$

**7**: $[Fe^{(II)}(S^{Me2}N_4(6\text{-}H\text{-}DPPN))](PF_6)$

**8**: $[(Fe^{(III)}(S^{Me2}N_4(6\text{-}H\text{-}DPPN)))_2O](PF_6)_2$

**9**: $[Fe^{(II)}(S^{Me2}N_4(2\text{-}QuinoEN))]^+$

**10**: $[(Fe^{(III)}(S^{Me2}N_4(2\text{-}QuinoEN)))_2\text{-}\mu\text{-}O]^{2+}$

**12**: $[Mn^{(II)}(S^{Me2}N_4)(6\text{-}Me\text{-}DPEN)]^+$

**14**: $[Fe^{(II)}(S^{Me2}N_4)(6\text{-}Me\text{-}DPPN)]^+$

**15**: $[Fe^{(II)}(S^{Me2}N_4)(6\text{-}H\text{-}DPPN)]^+$

# Acknowledgements

This thesis represents the culmination of a great deal of work over the past years. Despite my name solely being presented on the cover of this dissertation I could not have accomplished this alone. I would like to thank my advisor Julia Kovacs for assisstance, guidance and the opportunity to contribute my own ideas and skills to research in her lab. All my group members present and past, Dr. Rodney Swartz, Dr. Jessica Pikul, Dr. Santiago Toledo, Dr. Elaine Nam, Dr. Pauline Alokolaro, Dr. Gloria Villar, Michael Coggins, Ben Leipzig, Audra Johansen, Julian Rees, Helen Ferreria, Erika Shaffer and Ganapathi Venkatesh. I appreciate the assisstance of Dr. Mohammed Ibrahim of the Spiro lab and Jim Mayer for allowing me to use some important equipment. Finally I would like to thank everyone that helped support me through this whole process, my friends, family and co-workers.

# 1 General Introduction

## 1.1 Metaloenzymes

Metalloenzymes are a vital and common element in biology. Comprising approximately one-third of all enzymes, metalloenzymes represent the pinnacle of metal based catalysts. Commonly utilizing readily available first-row transition metals they promote a wide range of chemical transformations under mild conditions and ambient temperatures. Examples of these functions include stereo- and region-selective chemical transformations,[1,2] molecular transport,[3] electron and proton transfer reactions,[4] oxidant scavenging[5] and dioxygen conversions.[6] The importance of metals in biology cannot be understated as they include systems such as the oxygen evolving complex,[7,8] responsible for the production of $O_2$ for all oxygen breathing lifeforms, and Hemeoglobin,[3] which transports oxygen from the lungs to the cells. In the former case oxo-bridged manganese atoms cluster in a protein framework and produce $O_2$ in a not yet fully elucidated pathway, while in the latter an iron atom in a porphyrin ring is fine tuned to have an affinity to bind $O_2$ without activating it.

The protein environment of metalloenzymes significantly direct the reactivity as is highlighted in comparing the unreactive hemoglobin to other iron enzymes such as methane monooxygenase (MMO),[9] cytochrome P450 (P450)[10] or Superoxide Reductase (SOR).[11] MMO involves a diiron core bound by histidine and glutamate residues, which catalyzes the insertion of one oxygen atom into methane, forming methanol. P450 enzymes contain a porphyrin ligated iron with a cysteine coordinated *trans* to a binding site for $O_2$, which is activated to hydroxylate a wide variety of organic compounds. SOR has a similar coordination sphere to P450s but contains 4 histidine residues in an equatorial plane rather than a porphyrin. SOR reduces superoxide ($O_2^-$) and re-

leases $H_2O_2$, and is a vital means of combating the radical oxygen species in anaerobic lifeforms where production of $O_2$ would be detrimental if the more classically known aerobic enzymes, superoxide dismutase (SOD), were utilized.[12] The variety of chemical transformations, diversity of reactivity and importance towards the complexity of life provides a compelling reason for the investigations of metalloenzymes. Through more thorough understanding we may be able to harness the incredible chemical and reactive properties of metalloenzymes to further medical and industrial progress.

One important function of a set of metalloenzymes is the degradation of reactive oxygen species such as $O_2^-$. Oxygen is a reactive element and the use of oxygen as the ultimate electron acceptor in aerobic biology results in the adventitious production of $O_2^-$, a toxic radical species, via the one $e^-$ reduction of $O_2$. A common component of cellular oxidative stress $O_2^-$ is also linked to disease states, such as heart attacks, where it is produced in high concentration[13] and can result in tissue damage or cell death. Biological countermeasures to $O_2^-$ that are prevalent in aerobic organisms are the SOD metalloenzymes[14] which catalyse the disproportionation $O_2^-$ to $O_2$ and $H_2O_2$. However, in anaerobic organisms transient exposure to $O_2$ is a key component of $O_2^-$ formation. Reforming $O_2$ would not be beneficial to the anaerobic organism and an alternative enzyme, SOR, is used to degrade $O_2^-$ by reduction to $H_2O_2$.

## 1.2 Superoxide Reductase

SOR[15–24] is a blue, non-heme iron enzyme and has been crystallographically characterized in several forms. The structures of SOR obtained from *Treponema pallidum*[23] and *Pyrococcus furiosus*[15] have SOR as a dimer of homodimers and a homotetramer respectively, each containing a single non-heme iron per subunit. The structure obtained from sulphate-reducing bacteria *D. desulfuricans*[22] is a homodimer with two iron atoms per

unit (Figure 1). The second iron atom is part of a $[Fe(Cys)_4]$ center originally thought to be necessary for the reduction of the ferric state of the reactive iron center but its role is now uncertain as full reactivity is observed in its absence. The active site for SOR consists of a square-pyramidal high-spin ferrous iron ligated by four histidine nitrogens in an equatorial plane and one axial cysteine sulphur *trans* to an exposed coordination site (Figure 2). In the oxidized $Fe^{III}$ resting state a glutamate carboxylate acts as a sixth ligand to form an overall octahedral structure.[15]

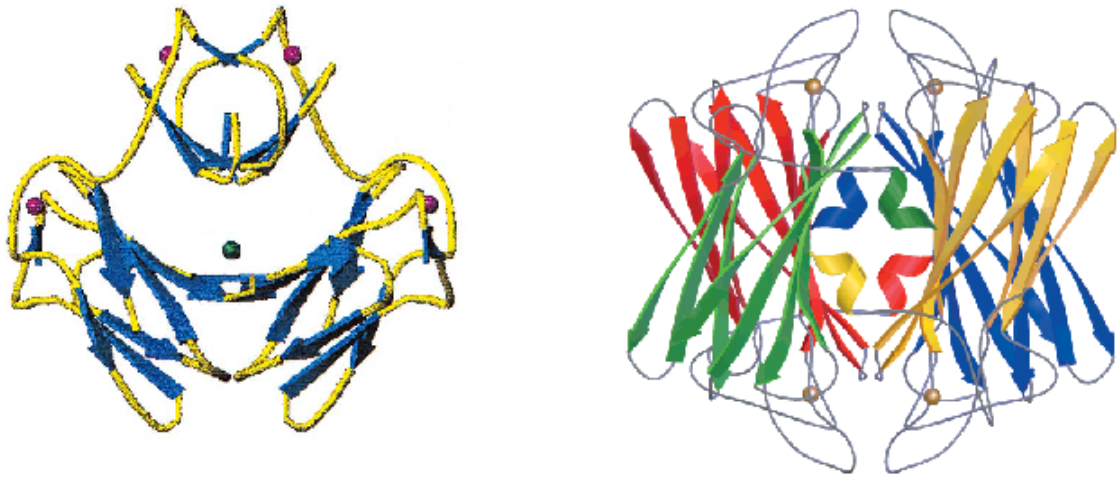

Figure 1: X-ray crystal structures (ribbon diagram) of *Pyrococcus furiosus* monomer at 1.7Å resolution (right);[15] crystal structure of *D. desulfuricans* homotetramer at 1.9Å resolution. Gold dots (right) and purple dots (left) represent iron atoms. Green dot (left) represents a calcium atom.

Neighboring amino acids are believed to play a role in orientating $O_2^-$, in acting as proton donors to facilitate the formation of $H_2O_2$, in regulating the electron density of the sulphur through hydrogen bonding and in affecting the binding strength of substrates and the redox properties of the iron center.[25] The catalytic cycle that occurs at the SOR active site has been thoroughly studied for over a decade[20] and some aspects are well

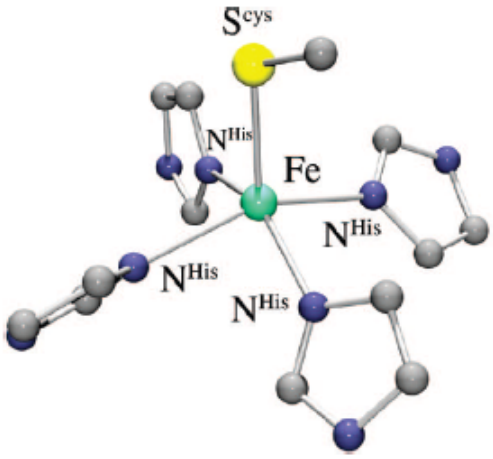


Figure 2: Representation of the active site of superoxide reductase.

established. The mechanism involves the formation of two transient intermediates ($T_1$ and $T_2$) upon reaction with $O_2^-$ [24] (Figure 3).

The first step is proposed to involve the oxidative addition of $O_2^-$ to the iron center, which occurs at diffusion controlled rates to form $T_1$, which is proposed to be an Fe-peroxo species.[26] Several SOR enzyme mutants have been studied that yielded spectroscopic data relevent to $T_1$. An E47A mutant first obtained resonance Raman parameters of an Fe-peroxo species from reaction with $H_2O_2$, that appeared to support an side on peroxo species.[27] However, more recently, when an E114A mutant was reacted with $H_2O_2$ and characterized by both resonance Raman and X-ray crystallographic techniques it revealed an end-on bound hydroperoxo species.[28] At this time no vibrational data to support either conclusion has been reported for the native enzyme.

The second intermediate, $T_2$, forms less quickly and has been shown to be an $Fe^{(III)}-OH$ species[29] with a pH dependent $\nu$Fe-O stretch, which shifts with $^{18}OH_2$ and $D_2O$. $T_2$ is believed to be formed when $T_1$ is protonated at the proximal oxygen, releasing $H_2O_2$, followed by the subsequent binding of $OH^-$. Reduction of $T_2$ in the presence

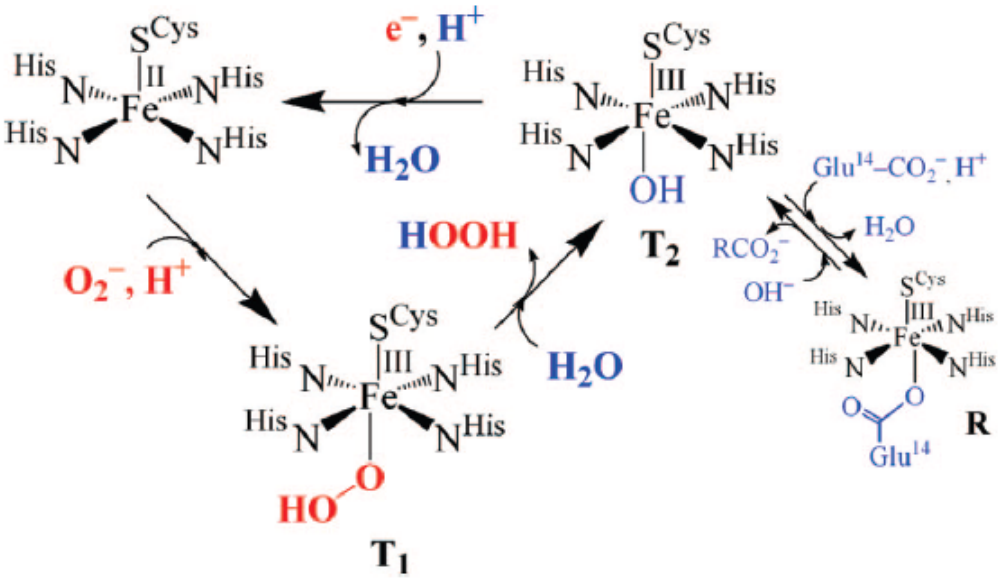


Figure 3: Proposed catalytic cycle for SOR.[24]

of protons releases $H_2O$ and regenerates the catalytically active $Fe^{(II)}$ form. In the absence of substrate or reductant the $Fe^{(III)}$-glutamate bound resting state of the enzyme is observed.

## 1.3 Biomimetic Modelling

Benchmark spectroscopic parameters for the proposed $T_1$ intermediate are needed to more fully investigate the enzymes and work in biomimetic chemistry towards synthesizing such species is ongoing. The key means of obtaining these benchmark parameters is via biomimetic chemistry, which is based on the preparation of small molecules that mimic the active site of enzymes. Understanding how the local ligand environment of the active site directs and controls the reactivity of SOR, and of all metalloenzymes, is vital towards understanding how nature created such effective catalysts. Carefully designed

model systems allow for the reproduction of active site geometry, coordination sphere and ligand environments but in a smaller molecule than the natural enzyme, simplifying efforts at characterization. The ability to modify custom ligands is far greater than the modifications that can be performed upon enzymes and through these modifications the properties governing the desired reactivity can be investigated.

Such investigations led to the first functional model of SOR reported in the literature,[30,31] the $[Fe^{II}(S^{Me2}N_4)(tren)]^+$ (**1**) (Figure 4) synthesized in the Kovacs lab. While not a structural model, as the sulphur is coordinated *cis* to the binding site as opposed to *trans*, **1** was observed to reduce $O_2^-$ to $H_2O_2$. In methanol, at -90℃, an intermediate species was formed upon $O_2^-$ addition, characterized by EXAFS, IR, EAS and EPR spectroscopies as an end-on hydroperoxo.[30] The second functional model synthesized by the Kovacs lab was the $[Fe^{II}(\text{cyclam-PrS})]^+$ (**2**), which used a 14 member cyclam ring with a tethered thiolate to place the sulphur *trans* to the proposed binding site.[32] $[Fe^{II}(\text{cyclam-PrS})]^+$ reacted with $O_2^-$ and a proton donor at -78℃ to form the first example of a thiolate-containing, high-spin iron-hydroperoxo complex. The high-spin state was in accordance with that proposed for the SOR intermediate and the vibrational data showed the weakest $\nu$Fe-O stretch reported for a ferric-peroxo.

Results from comparison of these complexes reveal the significant influence of the thiolate upon the spectroscopic, magnetic and electronic properties of the complex and help to understand how alterations to various parameters affect reactivity and stability of intermediates in regard to alkyl $N_4S$ ligated iron complexes. The changes between these two functional models were large though and a greater understanding of how the properties of the ligand influence the complex towards reactivity, and affect the hydroperoxo intermediates, requires ligand models that are more amenable to slight alterations.

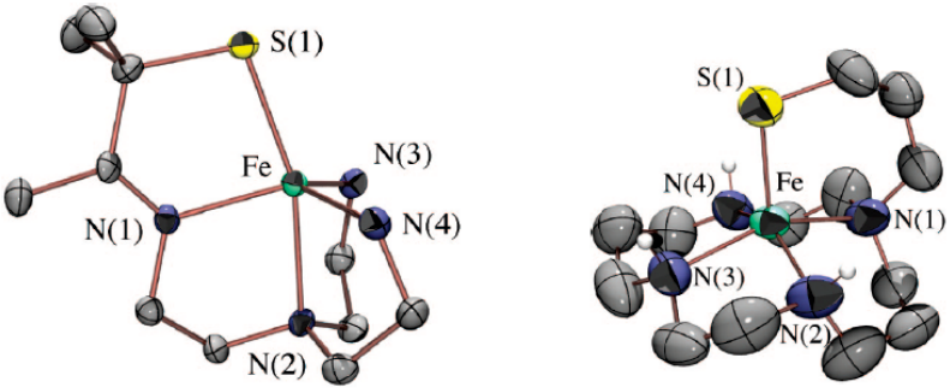


Figure 4: ORTEP diagrams of SOR functional models $[Fe^{II}(S^{Me2}N_4)(tren)]^+$ **1** (left) and $[Fe^{II}(cyclam\text{-}PrS)]^+$ **2** (Right). Hydrogen atoms, solvent and counterions omitted for clarity.

Previous work by Goldberg *et al.*[33,34] with a cyclic $N_4$ ligand and an untethered aryl-thiolate (Figure 5) has shown the ability to form stable alkylperoxo intermediates and probe the effects of the trans thiolate upon the $\nu$Fe-O and $\nu$O-O stretches. Work by Halfen *et al.*[35,36] created structural models for the SOR active site and highlight how ligand modifications can alter magnetic, spectroscopic and redox properties. However in all these cases reduction of $O_2^-$ to form an iron hydroperoxo was not reported. The similar nature yet divergent reactivity of SOR models highlights how much is still unknown about the influences and governing factors in reactivity.

## 1.4 DPEN ligand system

In the pursuit of creating a series of model complexes that were amendable to fine-tuning of the ligand, as to affect desired properties from the metal complex, Santiago Toledo,[37] in the Kovacs lab, designed an $N_4S$ ligand system utilizing an N,N-di(2-methylpyridyl)ethylenediamine (DPEN) framework (Figure 6). When complexed to a

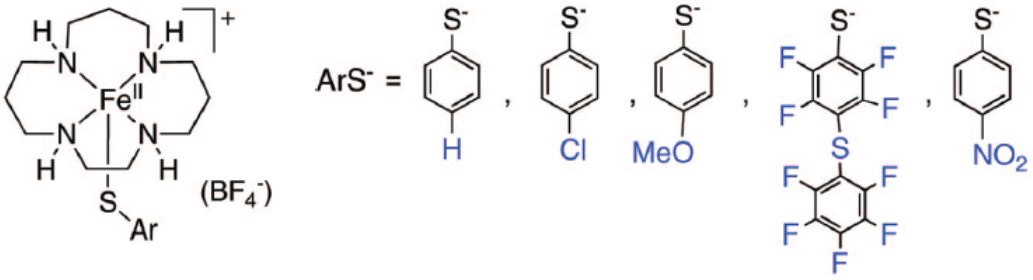


Figure 5: SOR model complex with modified, untethered aryl-thiolates studied by Goldberg *et al.*.[33]

metal ion, via the Schiff-base condensation with 3-mercapto-3-methylbutanone, the resultant compound was similar in structure to that of the $[Fe^{II}(S^{Me2}N_4)(tren)]^+$ system but with the primary amines replaced with pyridine rings. Modification of the pyridine rings, through electron dontating, electron withdrawing and sterically congestive substituents provide a means for the fine-tuning desired to fully investigate how the ligand properties and environment govern reactivity in SOR model complexes. In comparison to the $[Fe^{II}(S^{Me2}N_4)(tren)]^+$ system the DPEN ligands also had handles in the UV-Vis spectra, simplifying characterization and investigation.

The potential for the DPEN ligand system is well highlighted when compared to investigations of other pyridine containing non-heme iron complexes, lacking thiolates, which formed stabilized Fe-peroxo species.[38–41] Modifications of the pyridine rings, in terms of electron donating and withdrawing substituents, had already been reported and used to investigate the contributions to other model systems.[42–45] Several versions of the DPEN ligand have been synthesized by S. Toledo, including the 6-H and 6-Me modifications and the replacement of pyridine for quinoline. Preliminary studies of these compounds provided characterization of the basic electronic, magnetic and structural properties as well as reactivity in regard to $O_2$ and $O_2^-$. Several compelling leads were

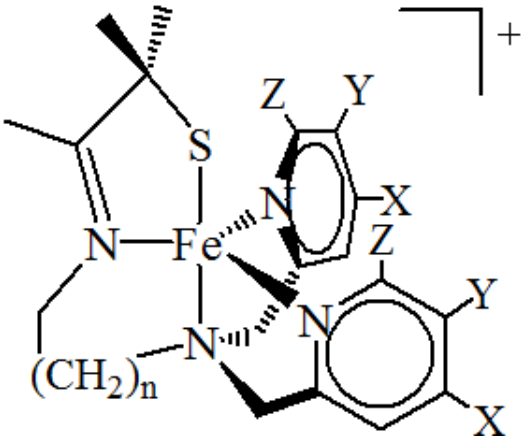


Figure 6: $[Fe^{II}(S^{Me2}N_4(DPEN))]^+$ ligand system and target modification sites. (n = 0-1)

identified for future study and investigations into these compounds are reported hereafter. Lessons learned from the first series of DPEN ligands are applied towards synthesis of new DPEN ligand modifications and towards future targets.

# Bibliography

[1] Peter L. Roach, Ian J. Clifton, Charles M. H. Hensgens, Norio Shibata, Christopher J. Schofield, and Janos Hajdu Jack E. Baldwin. *Nature*, 387:827–830, 1997.

[2] Bernard Meunier, Samuel P. de Visser, and Sason Shaik. *Chem. Rev.*, 104:3947–3980, 2004.

[3] M.D. Connie C.W. Hsia. *N. Engl. J. Med.*, 338:239–248, 1998.

[4] Hartmut Michel. *Biochemistry*, 38:15129–15140, 1999.

[5] Jochen Wuerges, Jin-Won Lee, Yang-In Yim, Hyung-Soon Yim, Sa-Ouk Kang, and Kristina Djinovic Carugo. *PNAS*, 101:8569–8574, 2004.

[6] David T Gibson and Rebecca E Parales. *Curr. Op. Biotech.*, 11:236–243, 2000.

[7] Bessel Kok, Bliss Forbush, and Marion McGloin. *Photobiol.*, 11:457–475, 1970.

[8] Yasufumi Umena, Keisuke Kawakami, Jian-Ren Shen, and Nobuo Kamiya. *Nature*, 473:55–60, 2011.

[9] Amanda S. Hakemian and Amy C. Rosenzweig. *Annual Review of Biochemistry*, 76:223–241, 2007.

[10] Gilda H. Loew and Danni L. Harris. *Chem. Rev.*, 100:407–420, 2000.

[11] Donald M. Kurtz Jr. *Acc. Chem. Res.*, 37:902–908, 2004.

[12] Stefan I. Liochev and Irwin Fridovich. *Free Radical Biology and Medicine*, 42:1465–1469, 2007.

[13] Giuliana Fortunato, Antonella Pastinese, Mariano Intrieri, Maria M Lofrano, Giovanni Gaeta, Marcello Bolletti Censi, Aldo Boccalatte, Francesco Salvatore, and Lucia Sacchetti. *Clin. Biochem.*, 30:569–571, 1997.

[14] Joe M. McCord and Irwin Fridovich. *J. Biol. Chem.*, 244:6049–6055, 1969.

[15] Andrew P. Yeh, Yonglin Hu, Francis E. Jenney Jr., Michael W. W. Adams, and Douglas C. Rees. *Biochemistry*, 39:2499–2508, 2000.

[16] Murielle Lombard, Chantal Houee-Levin, Daniele Touati, Marc Fontecave, and Vincent Niviere. *Biochemistry*, 40:5032–5040, 2001.

[17] Francis E. Jenney Jr., Marc F. J. M. Verhagen, Xiaoyuan Cui, and Michael W. W. Adams. *SCIENCE*, 286:306–309, 1999.

[18] Michael D. Clay, Francis E. Jenney Jr., Peter L. Hagedoorn, Graham N. George, Michael W. W. Adams, and Michael K. Johnson. *J. Am. Chem. Soc.*, 124:788–805, 2002.

[19] Eric D. Coulter, Joseph P. Emerson, Donald M. Kurtz Jr., and Diane E. Cabelli. *J. Am. Chem. Soc.*, 122:11555–11556, 2000.

[20] Isabel A. Abreu, Ligia M. Saraiva, Claudio M. Soares, Miguel Teixeira, and Diane E. Cabelli. *J. Biol. Chem.*, 276(42):38995–39001, 2001.

[21] Michael D. Clay, Christopher A. Cosper, Jr. Francis E. Jenney, Michael W. W. Adams, and Michael K. Johnson. *PNAS*, 100:3796–3801, 2003.

[22] Ana V. Coelho, Pedro Matias, Vilmos Fulop, Andrew Thompson, Ana Gonzalez, and Maria A. Carrondo. *J. Biol. Inorg. Chem.*, 2:680–689, 1997.

[23] Teresa Santos-Silva, Jose Trincao, Ana Luisa Carvalho, Cecilia Bonifa cio, Francoise Auchere, Patricia Raleiras, Isabel Moura, Jose J. G. Moura, and Maria Joao Romao. *J. Biol. Inorg. Chem.*, 11:548–558, 2006.

[24] Joao V. Rodrigues, Isabel A. Abreu, Diane Cabelli, and Miguel Teixeira. *Biochemistry*, 45:9266–9278, 2006.

[25] Christelle Mathe, Claire O. Weill, Tony A. Mattioli, Catherine Berthomieu, Chantal Houee-Levin, Emilie Tremey, and Vincent Niviere. *J. Biol. Chem.*, 282(30):22207–22216, 2007.

[26] Donald M. Kurtz Jr. *J. Biol. Chem.*, 100:679–693, 2006.

[27] Christelle Mathe, Tony A. Mattioli, Olivier Horner, Murielle Lombard, Jean-Marc Latour, Marc Fontecave, and Vincent Niviere. *J. Am. Chem. Soc.*, 124:4966–4967, 2002.

[28] Gergely Katona, Philippe Carpentier, Vincent Niviere, Patricia Amara, Virgile Adam, Jeremy Ohana, Nikolay Tsanov, and Dominique Bourgeois. *Science*, 316:449–453, 2007.

[29] Christelle Mathe, Vincent Niviere, and Tony A. Mattioli. *J. Am. Chem. Soc.*, 127:16436–16441, 2005.

[30] Jason Shearer, Robert C. Scarrow, and Julie A. Kovacs. *J. Am. Chem. Soc.*, 124:11709–11717, 2002.

[31] Elaine Nam, Pauline E. Alokolaro, Rodney D. Swartz, Morgan C. Gleaves, Jessica Pikul, and Julie A. Kovacs. *Inorg. Chem.*, 50:1592–1602, 2011.

[32] Terutaka Kitagawa, Abhishek Dey, Priscilla Lugo-Mas, Jason B. Benedict, Werner Kaminsky, Edward Solomon, and Julie A. Kovacs. *J. Am. Chem. Soc.*, 128:14448–14449, 2006.

[33] Frances Namuswe, Gary D. Kasper, Amy A. Narducci Sarjeant, Takahiro Hayashi, Courtney M. Krest, Michael T. Green, Pierre Moenne-Loccoz, and David P. Goldberg. *J. Am. Chem. Soc.*, 130:14189–14200, 2008.

[34] Divya Krishnamurthy, Gary D. Kasper, Frances Namuswe, William D. Kerber, Amy A. Narducci Sarjeant, Pierre Moenne-Loccoz, and David P. Goldberg. *J. Am. Chem. Soc.*, 128:14222–14223, 2006.

[35] Adam T. Fiedler, Heather L. Halfen, Jason A. Halfen, and Thomas C. Brunold. *J. Am. Chem. Soc.*, 127:1675–1689, 2005.

[36] Jason A. Halfen, Heather L. Moore, and Derek C. Fox. *Inorg. Chem.*, 41:3935–3943, 2002.

[37] S.A. Toledo. Synthesis and Reactivity of an Expanded Family of Superoxide Reductase (SOR) Model Complexes Using N-Heterocyclic, Thiolate-Containing Ligands: Towards a Better Understanding of Structural-Functional Relationships., Ph.D. Thesis, University of Washington, Seattle, Wa, 2009.

[38] A. Jalila Simaan, Susanne Dopner, Frederic Banse, Sophie Bourcier, Guy Bouchoux, Alain Boussac, Peter Hildebrandt, and Jean-Jacques Girerd. *Eur. J. Inorg. Chem.*, pages 1627–1633, 2000.

[39] Veronique Balland, Frederic Banse, Elodie Anxolabehere-Mallart, Martine Nierlich, and Jean-Jacques Girerd. *Eur. J. Inorg. Chem.*, pages 2529–2535, 2003.

[40] Yan Zang, Jinheung Kim, Yanhong Dong, Elizabeth C. Wilkinson, Evan H. Appelman, and Lawrence Que, Jr. *J. Am. Chem. Soc.*, 119:4197–4205, 1997.

[41] A. Jalila Simaan, Frederic Banse, Jean-Jacques Girerd, Karl Wieghardt, and Eckhard Bill. *Inorg. Chem.*, 40:6538–6540, 2001.

[42] Gerard Roelfes, Vladislav Vrajmasu, Kui Chen, Raymond Y. N. Ho, Jan-Uwe Rohde, Charon Zondervan, Rene M. la Crois, Ebe P. Schudde, Martin Lutz, Anthony L. Spek, Ronald Hage, Ben L. Feringa, Eckard Munck, , and Lawrence Que Jr. *Inorg. Chem.*, 42:2639–2653, 2003.

[43] Christiana Xin Zhang, Susan Kaderli, Miguel Costas, Eun il Kim, Yorck-Michael Neuhold, Kenneth D. Karlin, and Andreas D. Zuberbuhler. *Inorg. Chem.*, 42:1807–1824, 2003.

[44] Masakazu Tamura, Yasuteru Urano, Kazuya Kikuchi, Tsunehiko Higuchi, Masaaki Hirobe, and Tetsuo Nagano. *Chem. Pharm. Bull.*, 48:1514–1518, 2000.

[45] Bernhard Kohl, Ernst Sturm, Jorg Senn-Bilfinger, W. Alexander Simon, Uwe Kruger, Hartmann Schaefer, Georg Rainer, Volker Figala, and Kurt Klemm. *J. Med. Chem.*, 35:1049–1057, 1992.

# 2 $[Co^{(II)}(S^{Me2}N_4(6\text{-Me-DPEN}))]^+$

Use of a Cobalt Analogue to Stabilize Potential Intermediates of $[Fe^{(II)}(S^{Me2}N_4(6\text{-Me-DPEN}))]^+ + O_2^-$ Reactivity

## 2.1 Introduction

Previous work in the Kovacs lab[1] showed that a low temperature stabilized intermediate forms in the reaction between $O_2^-$ and $[Fe^{(II)}(S^{Me2}N_4(6\text{-Me-DPEN}))]^+$ **3**. This intermediate, proposed to be a peroxo or hydroperoxo, was proton sensitive and would convert to a second species with addition of triethylamine and revert with addition of MeOH. Iron-peroxo complexes that convert between the end-on hydroperoxo and the side-on peroxo with addition of base have been reported previously in the literature.[2,3] It was proposed that a similar reactivity was being observed for **3**. However, vibrational and/or structural characterizations of these **3** derived species have yet to be obtained.

Cobalt peroxo species are known to be more stable than those of related iron complexes. Octahedral $Co^{(III)}$ is generally low spin $d^6$ and considered to be substitution inert. This helps stabilize $Co^{(III)}$ compounds to the extent that crystal structures of $Co^{(III)}$ side-on peroxo,[4] bridging $\mu$-peroxo,[5] alkylperoxo[6] and even a hydroperoxo[5,7] are known. Cobalt has the additional stabilizing property of avoiding the formation of Co=O species as it is to the right of the 'oxo-wall'.[8] This is relevant as the Fe intermediate decomposes into $[(Fe^{(III)}(S^{Me2}N_4(6\text{-Me-DPEN})))_2O]^{2+}$ which likely involves a transient Fe=O species. A low-spin $d_6$ octahedral electronic configuration is also diamagnetic, enabling the use of NMR as a tool to probe the identity of the proposed intermediate.

In order to utilize the potentially enhanced stability and spectroscopic properties an attempt was made to synthesize and isolate a cobalt analogue of the observed intermediate species **3** using $[Co^{(II)}(S^{Me2}N_4(6\text{-Me-DPEN}))](PF_6)$ **4**.

## 2.2 Experimental

*General Methods*

All reactions were performed using standard Schlenk techniques under an atmosphere of dinitrogen in a glove box. Reagents were obtained from commercial sources at the highest purity available and were used without further purifications. Acetonitrile (MeCN) and diethyl ether ($Et_2O$) were dispensed under argon from a solvent delivery system. Methanol (MeOH) was refluxed over magnesium and iodine, and dichloromethane ($CH_2Cl_2$) was dried over $CaH_2$. 3-Methyl-3-mercapto-2-butanone was prepared according to a published procedure. NMR spectra were recorded on either a Bruker AV 301 or Bruker AV 300 FTNMR spectrometer and referenced to the residual protio solvent. Electron paramagnetic resonance (EPR) spectra were obtained using a Varian CW-EPR spectrometer at 4 K equipped with an Oxford helium cryostat. Electronic absorption spectra (EAS) were recorded using either a Hewlett-Packard 8453 diode array or a Cary 50 spectrometer.

*Synthesis of* $[Co^{(II)}(S^{Me2}N_4(6\text{-Me-DPEN}))](PF_6)$ **4**:

3-mercapto-3-methyl-2-butanone (79 mg, 0.67 mmol) was dissolved in a solution of NaOMe (37 mg, 0.68 mmol) in MeOH (2 mL) and cooled to -30℃ forming a peach colored solution. Separately N,N-Bis(6-methyl-2-pyridylmethyl)-1,2-ethylenediamine (179 mg, 0.66 mmol) ligand precursor was dissolved in MeOH (2 mL) and cooled to -30℃ as an orange solution. Separately anhydrous $CoCl_2$ (86 mg, 0.66 mmol) was dissolved into MeOH (2 mL) and cooled to -30℃ as a pink solution. The peach thiol solution was added dropwise to the pink cobalt solution while stirring causing the color to change to red/brown. After 5 minutes orange ligand solution was added dropwise to the cobalt mixture and the color changed to brown/green. After 2 hours $NaPF_6$ (111 mg, 0.66

mmol) was added to solution and stirring continued for 48 hours. The solvent was removed in *vacuo* and solids were dissolved in MeCN, filtered to remove insolubles and layered with ten times the volume of $Et_2O$. After 24 hours the solution was filtered to obtain green needles. Electronic Absorption Spectrum (MeCN): $\lambda$max ($\epsilon$ ($M^{-1}cm^{-1}$)): 263 (8900), 379 (2200) nm. ESI-MS: 428 m/z. Redox Potential: $E_{1/2}(Co^{(II/III)})$ = +473 mV (reversible) MeCN vs. SCE, $E_{1/2}(Co^{(II/III)})$ = 628 mV (reversible) in $CH_2Cl_2$ vs. SCE.

*Synthesis of* $[Co^{(III)}(S^{Me2}N_4(6\text{-}Me\text{-}DPEN))](PF_6)_2$ **5**:

**4** (0.043 g, 0.075 mmol) was dissolved in $CH_2Cl_2$ (5 mL). Separately tri(p-tolyl)aminium hexafluorphosphate ($[(p{-}CH_3C_6H_4)_3N](PF_6)$) was dissolved in $CH_2Cl_2$ (5 mL). Both solutions were cooled to -30℃. In a precooled Schlenk flask was added the solution of 4 followed by dropwise addition of $[(p{-}CH_3C_6H_4)_3N](PF_6)$. The color of the reaction solution changed from green/brown to orange/red as addition progressed. Reaction mixture was stirred one hour at room temperature then solvent was removed in *vacuo*. The solid material was dissolved in minimum $CH_2Cl_2$ and layered with ether. After 24 hours the solution was filtered to obtain **5** as a brick-red solid. Yield 37%, EAS: (MeCN): $\lambda$max ($\epsilon$ ($M^{-1}cm^{-1}$)): 267, 405, 495nm.

Table 1: *X-ray crystallography data*

| Bonds/Angles | **4** | | **4** |
|---|---|---|---|
| Co(1)-S(1) | 2.2744(7) | MW | 573.45 |
| Co(1)-N(1) | 2.068(2) | T (K) | 130(2) K |
| Co(1)-N(2) | 2.179(2) | unit cell | Monoclinic |
| Co(1)-N(3) | 2.134(4) | a (Å) | 10.9469(2) |
| Co(1)-N(4) | 2.118(3) | b (Å) | 18.7705(4) |
| S(1)-Co(1)-N(1) | 84.73(8) | c (Å) | 16.1331(3) |
| S(1)-Co(1)-N(2) | 157.86(8) | $\alpha$ (∘) | 90 |
| S(1)-Co(1)-N(3) | 102.96(8) | $\beta$ (∘) | 132.911(2) |
| S(1)-Co(1)-N(4) | 122.67(8) | $\gamma$ (∘) | 90 |
| N(1)-Co(1)-N(2) | 78.6(1) | V (Å$^3$) | 2428.02(10) |
| N(1)-Co(1)-N(3) | 124.2(1) | Z | 4 |
| N(1)-Co(1)-N(4) | 113.5(1) | $d_{calcd}$ | 1.569 Mg/m$\hat{3}$ |
| N(2)-Co(1)-N(3) | 75.4(1) | space group | P21/c |
| N(2)-Co(1)-N(4) | 77.8(1) | $R_1$ | 0.0530 |
| N(3)-Co(1)-N(4) | 107.9(1) | $wR_2$ | 0.1243 |
| | | GOF | 1.078 |
| Select bond lengths and angles | | Crystal data, intensity collections and structure refinement parameters | |

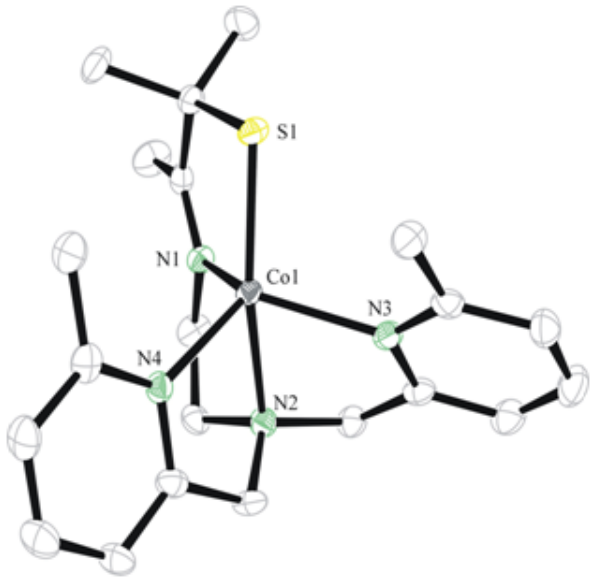


Figure 7: ORTEP diagram of [$Co^{(II)}$($S^{Me2}N_4$(6-Me-DPEN))]($PF_6$) **4** with hydrogen atoms, counterion and solvents of crystallization omitted (50% prob. ellipsoids)

## 2.3 Synthesis and Characterization

$[Co^{(II)}(S^{Me2}N_4(6\text{-Me-DPEN}))](PF_6)$ **4** forms forest green needles in the solid state and is green/brown in solution with $\lambda$max at 263 (8900), 378 (2200) (Figure 8). **4** was not observed to react with or decay upon exposure to $O_2$ in solution or in the solid state. **4** did not show affinity for binding anions in solution, shown by the lack of EAS spectral changes upon the addition of $OAc^-$ or $N_3^-$ in excess.

The EPR spectrum has g-values at $g_1 = 6.84$ and $g_2 = 2.16$, consistent with a high-spin (S = 3/2) $Co^{(II)}$ system.[9] The cyclic voltamagram of **4** in MeCN and $CH_2Cl_2$ show a single reversible wave with $E_{(1/2)}$ $(Co^{(II/III)}) = +473$ mV and +628 mV vs. SCE respectively (Figures 9 and 10). The shift of nearly 150 mV is presumed to be a result of the polarity of the solvent as addition of MeCN to a $CH_2Cl_2$ solution shows no new waves in the CV to indicate a separate coordinated species.

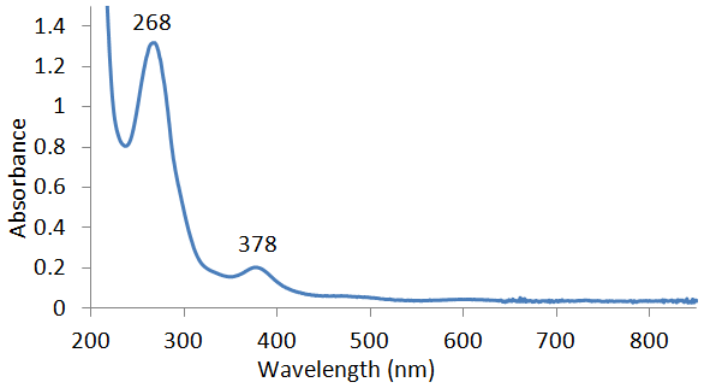


Figure 8: Electronic absorption spectra of $[Co^{(II)}(S^{Me2}N_4(6\text{-Me-DPEN}))](PF_6)$ in MeCN **4**

*Structural Characterization*

A crystal suitable for X-ray diffractometry was obtained from an MeCN solution layered with $Et_2O$. Selected bond lengths and angles for **4** are listed in Table (2.2). The bond lengths for **4** are similar to those observed for the **3**.[1] Each bond to the $Co^{(II)}$ metal is shorter by 0.03-0.07 angstroms, as would be expected for the smaller metal ion.

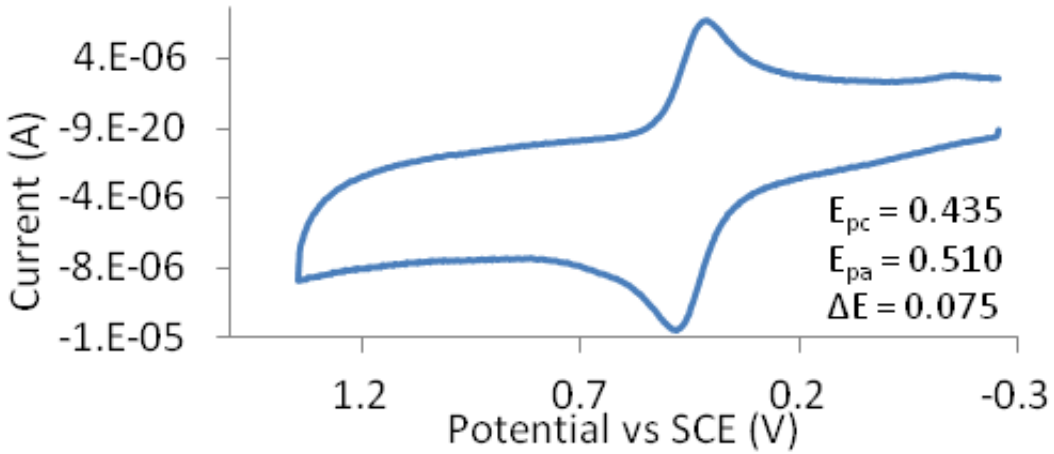


Figure 9: Cyclic Voltamagram of $[Co^{(II)}(S^{Me2}N_4(6\text{-Me-DPEN}))](PF_6)$ **4** in MeCN. 0.1M $Ag/AgNO_3$

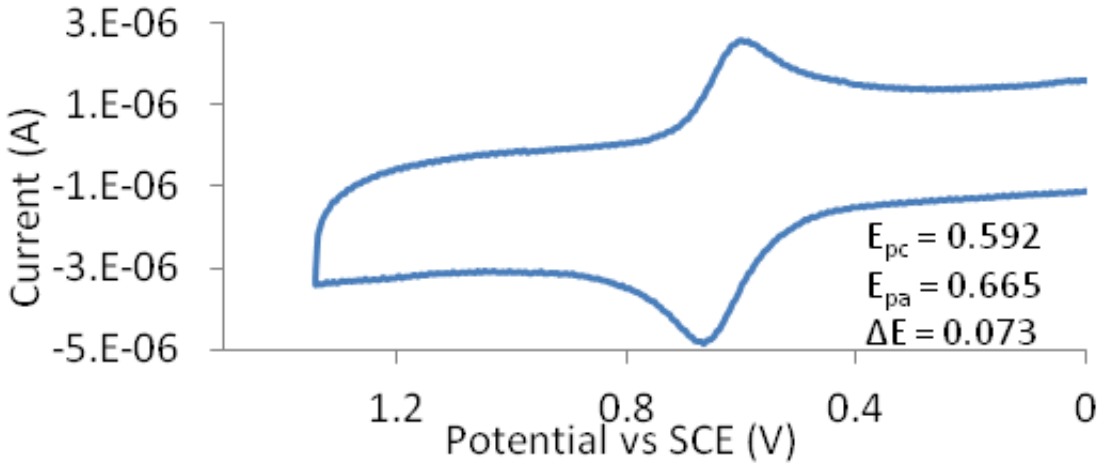


Figure 10: Cyclic Voltamagram of $[Co^{(II)}(S^{Me2}N_4(6\text{-Me-DPEN}))](PF_6)$ **4** in $CH_2Cl_2$. 0.1M $Ag/AgNO_3$

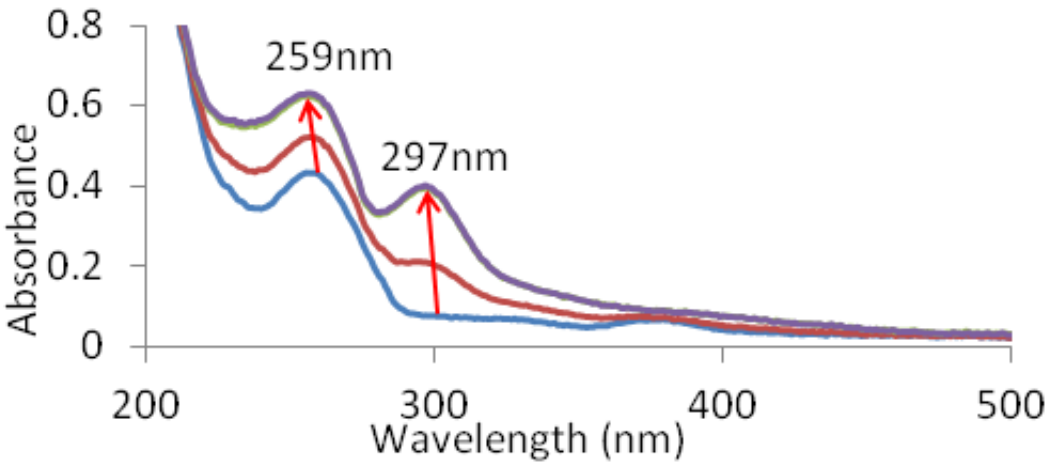


Figure 11: $[Co^{(II)}(S^{Me2}N_4(6\text{-Me-DPEN}))](PF_6)$ **4** + $O_2^-$ in MeCN at -40℃

*Formation of **6**: Reactivity of **4** with $O_2^-$ and peroxides*

Addition of 1 eq of $O_2^-$, from $KO_2$ solubilized in THF by 18-crown-6, to an MeCN solution of **4** at -40℃ showed varied reactivity dependent on solvent conditions. When **4** was reacted with $O_2^-$ at -40℃ in MeCN no reaction was observed unless a proton donor (350eq MeOH) was present *in situ*. When MeOH was present addition of $O_2^-$ resulted in the formation of a species with a new absorption in the EAS spectrum at $\lambda$max = 297 nm over the course of 15 minutes, species **6** (Figure 11). The product was stable at low temperatures but the EAS spectra bleach upon warming to room temperature. ESI-MS analysis of the reaction solution showed a peak at M + 16, indicating the incorporation of an oxygen atom, but no evidence of the half-mass of $[(Co^{(III)}(S^{Me2}N_4(6\text{-Me-DPEN})))_2O]^{2+}$ was observed.

Addition of $H_2O_{2(aq)}$ 30% dissolved in MeCN 1:2, tert-butylhydroperoxide (t-BuOOH) or cumene hydroperoxide to a solution of **4** in MeCN at -40℃ resulted in an EAS spectrum similar to **6** with an absorption at $\lambda$ = 297 nm.

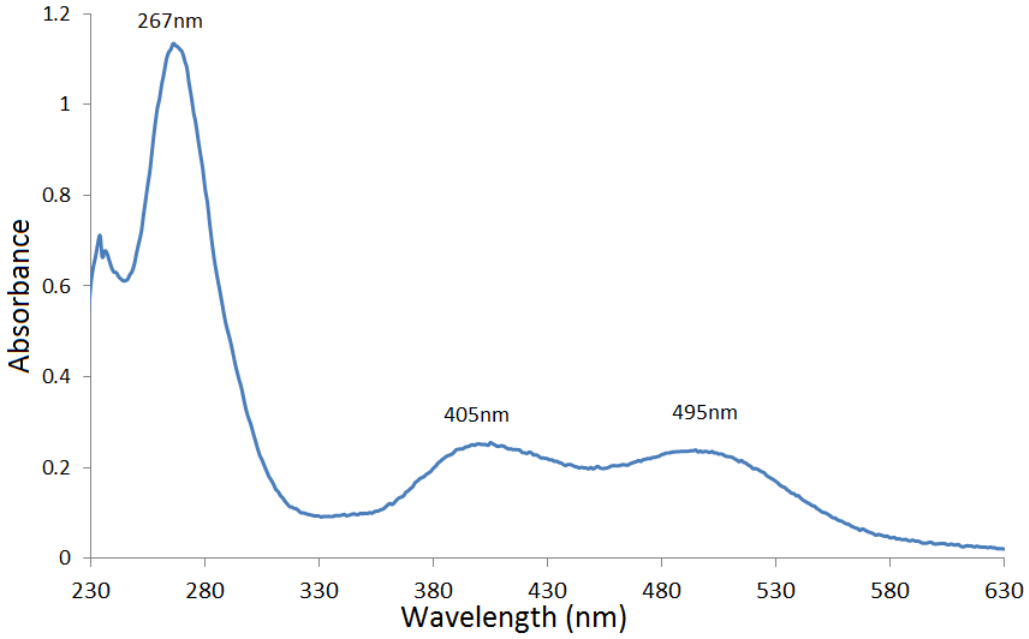


Figure 12: $[Co^{(III)}(S^{Me2}N_4(6\text{-Me-DPEN}))](PF_6)_2$ **5** in $CH_2Cl_2$

*$[Co^{(III)}(S^{Me2}N_4(6\text{-Me-DPEN}))](PF_6)_2$*

The oxidized compound $[Co^{(III)}(S^{Me2}N_4(6\text{-Me-DPEN}))](PF_6)_2$ **5** was synthesized by the one electron oxidation of **4** in $CH_2Cl_2$. Use of the strong oxidant tri(p-tolyl)aminium hexafluorphosphate $[(p{-}CH_3C_6H_4)_3N](PF_6)$ was necessary due to the fairly positive potential of **4** at 628 mV in $CH_2Cl_2$. Stepwise addition of oxidant to a solution of **4** in the dipprobe showed the growth of new peaks by EAS at 405 and 495 nm (Figure 12). This same spectrum was observed for the brick-red solid obtained from bulk synthesis of **5**.

In contrast to **4** the anions $OAc^-$ and $N_3^-$ were observed to react with **5** in solution. Upon addition of either anion the absorbances at 405 and 495 nm disappear and a new band at 325 nm is observed (Figure 13). To a solution of **5** in MeCN at -40°C was added $O_2^-$ but no reaction was observed to occur regardless of whether a proton donor was present. However when peroxides were added to a solution of **5** the growth of a band in the EAS spectrum as 297nm was observed. This product appeared by EAS and ESI-MS methods to be the same as **6**.

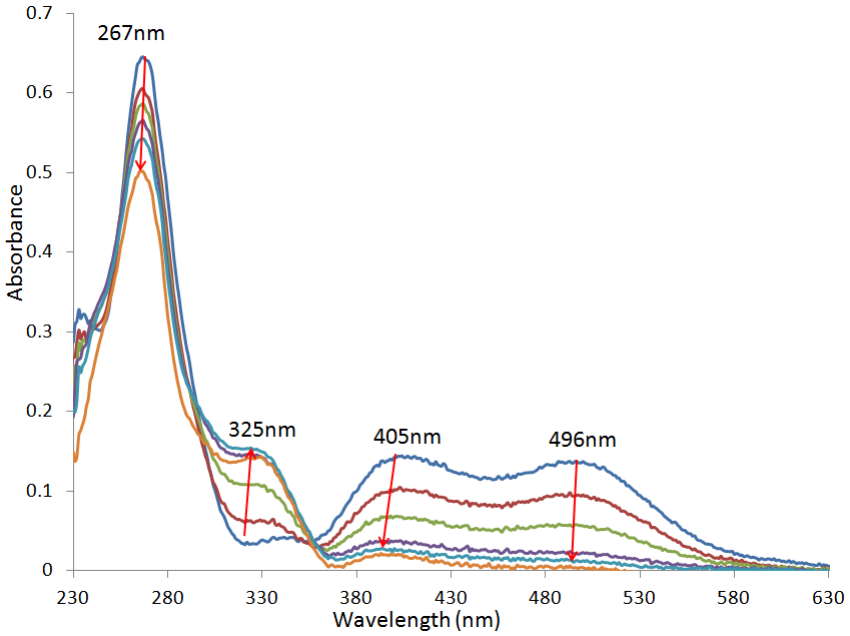


Figure 13: $[Co^{(III)}(S^{Me2}N_4(6\text{-Me-DPEN}))](PF_6)_2$ **5** + $NBu_4OAc$ in $CH_2Cl_2$

To a solution of **4** in deuterated MeCN in a J-Young tube was added aliquots of cumene hydroperoxide. Products of reaction were monitored by NMR. After addition of 1 eq cumene hydroperoxide both acetophenone and cumenol were observed in a nearly equal proportion (Figure 14). With continued additions of cumene hydroperoxide it was observed that 3 eq were required before unreacted cumene hydroperoxide was observed by NMR. After 3 eq were added the integration ratio of acetophenone to cumenol was observed to be 1:2.

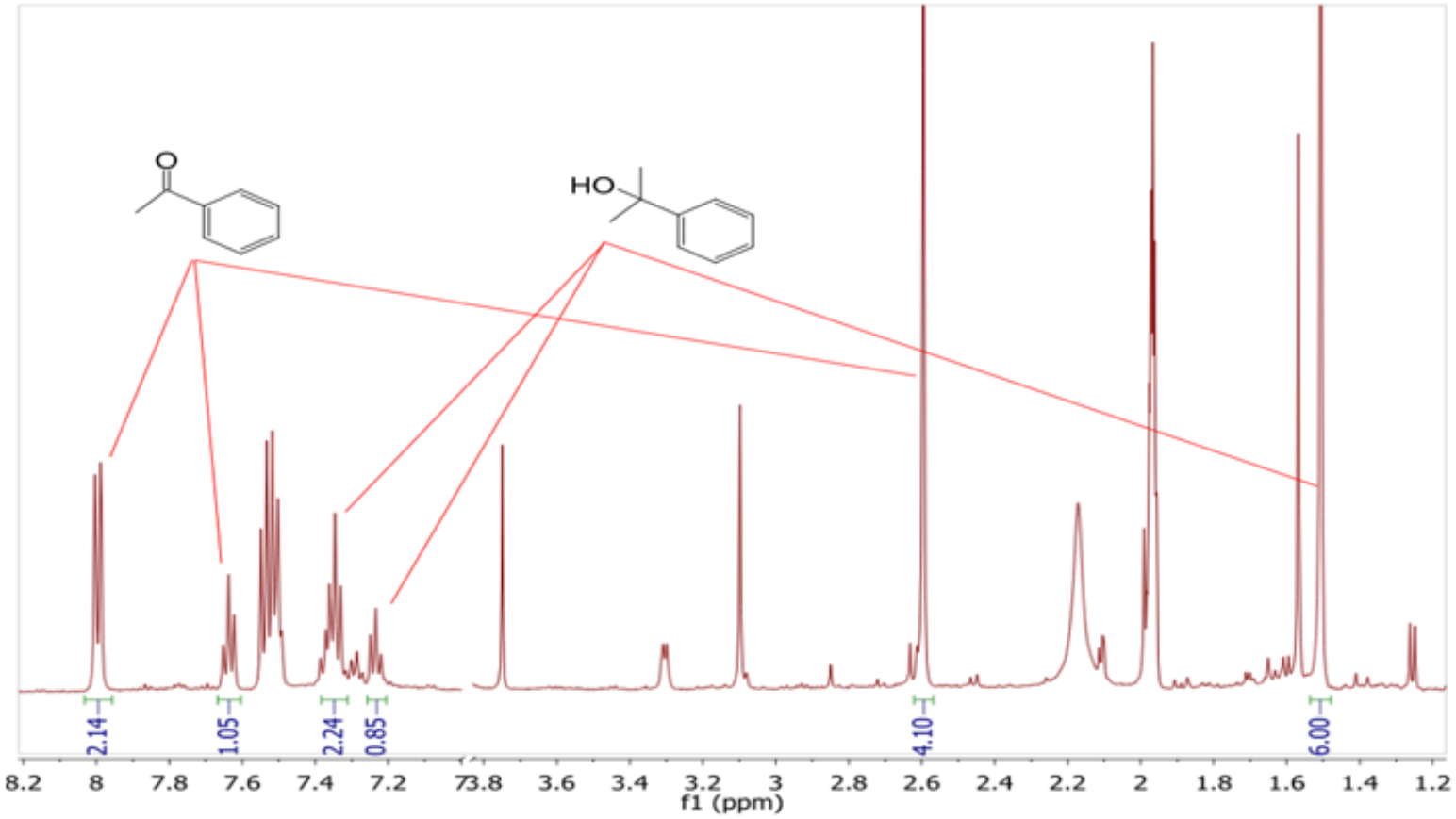


Figure 14: $^{1}$H NMR spectrum of **4** plus 1 eq cumene hydroperoxide

## 2.4 Discussion

$[Co^{(II)}(S^{Me2}N_4(6\text{-Me-DPEN}))](PF_6)$ **4** was synthesized with the intent of creating a cobalt analogue of $[Fe^{(II)}(S^{Me2}N_4(6\text{-Me-DPEN}))]^+$ **3** in the hopes of exploiting the potentially enhanced stability of cobalt towards peroxo intermediates. A comparison of the cobalt and iron analogues' spectroscopic and electronic properties shows significant similarities. Both complexes had simple EAS spectra, primarily containing higher energy absorptions around 300 nm. The CV in MeCN for the iron complex showed that the redox potential was more negative than for the cobalt by only 66 mV. This difference is smaller than the effect solvent was observed to cause upon the redox potential of **4**. Comparison of the crystal structures of both materials reveal that the structures are geometrically similar. The $\tau$ value gives a measure of the complex's structure relative to the trigonal bipyramidal ($\tau = 1.0$) or the square pyramidal ($\tau = 0.0$) coordination geometries. In the case of **4** $\tau = 0.56$ while the iron analogue, **3**, has $\tau = 0.59$. Both complexes are distorted roughly halfway between the two optimum geometries, slightly favoring trigonal bipyramidal. The bond lengths of each complex are similar with the cobalt complex having 0.03-0.07Å shorter bonds between the metal and ligand atoms, which would be expected for the smaller metal ion.

Despite these similarities the two complexes showed markedly different reactivity (*vide infra*). Notably **4** was not reactive to $O_2$ either in solution or in the solid state whereas the iron analogue reacted readily with $O_2$ to form the oxo-bridged dimer species $[(Fe^{(III)}(S^{Me2}N_4(6\text{-Me-DPEN})))_2O]^{2+}$. One possible reason for this change in reactivity may be the shorter bond lengths between the ligand and metal. It has been observed for the DPEN series that the 6-Me substituent causes significant steric hinderance with the geminal methyls protecting the sulphur atom, as evidenced by increased bond lengths for the M-$N_{py}$ bonds observed in the crystal structures of the $Fe^{(III)}$ oxo-bridged dimers.[1] If $O_2$ were to coordinate and oxidize the $Co^{(II)}$ to $Co^{(III)}$ the metal ion radius would

decrease even further causing additional steric strain upon the ligand. $O_2$ may not be a sufficiently powerful oxidant to overcome the ligand steric effects.

To investigate the ability of **4** to form stabilized peroxo species, akin to those proposed to be the intermediates of the iron analogue, **4** was reacted in solution with $O_2^-$ both in the presence and the absence of the proton donor MeOH. In MeCN, when a proton donor was present in solution, **4** was observed to react with $O_2^-$ over the course of 15 minutes to form **6**. Complex **6** was characterized by the formation of an EAS absorption at 297nm (Figure 11). ESI-MS of **6** solutions showed no indication of a $[(Co^{(III)}(S^{Me2}N_4(6\text{-Me-DPEN})))_2O]^{2+}$ oxo-bridged dimer but did indicate the addition of an oxygen atom to the complex with a signal at m/z = 444.

Often, in the literature, peroxo containing complexes are formed by addition of excess hydrogen peroxide or alkylperoxide compounds[10–12] rather than $O_2^-$. When **4** was reacted with various peroxides, $H_2O_2$, t-BuOOH and cumene hydroperoxide, the spectra obtained were very similar to that of **6**, with the 297nm band appearing as a shoulder rather than a distinct peak. It appeared that the same species was being formed. ESI-MS data supported this conclusion, containing the same primary peaks observed upon reaction of **4** with $O_2^-$.

To better characterize complex **6**, cold aliquots of the reaction mixtures were subjected to ESI-MS analysis. Both the **4** + $O_2^-$ and **4** + peroxide reactions show similar sets of m/z peaks. 428, 444 m/z are prominent and consistent in both reactions. 428 m/z corresponds to the starting material, while 444 m/z indicates the addition of an oxygen atom. The similar ESI-MS strongly indicates that the product of $O_2^-$ and peroxide reaction with **4** are the same. No peak suggesting $[(Co^{(III)}(S^{Me2}N_4(6\text{-Me-DPEN})))_2O]^{2+}$ is observed and no evidence of peroxide bound material is observed.

To test that **6** was not simply the product of metal centered oxidation of **4** a direct synthesis of $[Co^{(III)}S^{Me2}N_4$6-Me-DPen$](PF_6)_2$ **5** was undertaken. $[(p{-}CH_3C_6H_4)_3N](PF_6)$ had a sufficiently positive potential to achieve this transformation[13,14] and was used to perform the one electron oxidation of **4** to form **5**, which was collected as a brick-red powder. The EAS spectrum was distinctly different from that of **6**, indicating that **6** was not simply oxidized **4**. **5** had $\lambda_{max}$ at 405 and 495 nm in $CH_2Cl_2$ and MeCN, was stable towards $O_2$ and $O_2^-$ but decomposed in solution over a few days. The EPR spectrum was featureless, as would be expected for a $d^6$ metal ion. Attempts to observe an NMR spectrum were unsuccessful, no diamagnetic signals were observed for the compound. **5** reacted upon addition of anions ($OAc^-$ and $N_3^-$) to solution and had been formed in non-coordinating $CH_2Cl_2$ from the 5-coordinate **4**. This suggests that **5** was not octahedral and remained 5-coordinate until anionic ligands were present. This could explain the lack of diamagnetic NMR signals as a trigonal bipyramidal or square pyramidal compound may more easily achieve higher spin states than the S = 0 expected for octahedral $Co^{(III)}$. Attempts to obtain an X-ray quality crystal were thus far unsuccessful but due to the rarity of 5-coordinate $Co^{(III)}$[15,16] may warrant further investigation.

In one possible reaction scenario when $O_2^-$ is reacted with **4** the expected products would be a peroxide and an oxidized cobalt complex. The newly formed peroxide could continue to react with **4** or the oxidized cobalt species. Reactions of **5** with peroxides resulted in similar spectra to those observed in the reaction of **4** with $O_2^-$, though it was clearly shown that **5** did not react with $O_2^-$. This evidence suggested that the 297 nm species, **6**, was formed in a secondary reaction from the byproducts of **4** oxidation by $O_2^-$. **4** would be oxidized to **5** by $O_2^-$ which is reduced to a peroxide and then reacts with **5** to

form **6**. As was observed, proton donor availability would greatly enhance reactivity by providing the hydrogen atoms necessary to stabilize the negative charge on the peroxide.

The likely reaction of **5** with hydrogen peroxide would be the oxidation of the ligand sulphur atom. Ligand sulphur oxidation has been observed in the Kovacs lab previously in various cases of thiolate ligated cobalt complexes.[16,17] If the sulphur of **6** were oxidized it would explain the observed peak at 444 m/z in the ESI-MS which indicated addition of an oxygen to the complex.

S=O stretches would appear in the IR spectra in the range of 1225-980 $cm^{-1}$. However IR spectra for the solutions of **6** or of solids precipitated from solution with $Et_2O$ were not sufficiently resolved to characterize. An alternate method to probe for the occurrence of sulphur oxidation was undertaken utilizing cumene hydroperoxide.[18,19] Reaction of cumene hydroperoxide in one or two electron oxidation processes result in different organic by-products. In one electron reactions, such as oxidizing the $Co^{(II)}$, the O-O bond breaks homolytically producing a radical organic compound that converts into the easily identifiable acetophenone. In a two electron process, such as oxygenating a sulphur atom, the O-O bond breaks heterolytically forming cumenol. Both products can be monitored easily by NMR.

Stepwise additions of cumene hydroperoxide to a solution of **4** in deuterated MeCN showed that both acetophenone and cumenol were observed to grow in in roughly equal proportions for the first full equivalent of cumene hydroperoxide added (Figure 14). As addition was continued it was observed that 3 eq were required before the complex had fully reacted. Beyond 3 eq unreacted cumene hydroperoxide was observed by NMR with no further acetophenone nor cumenol formation. This suggested that both oxidation of **4** to **5** and oxidation of the sulphur atom were occurring at the same time in solution.

As additional cumene hydroperoxide is added a second oxidation of sulphur may become favorable leading to the final 3 eq requirement for complete reaction and the 1:2 ending ratio of acetophenone to cumenol observed by NMR. ESI-MS analysis of the reaction solution has not been able to clearly identify the final product from 3 eq of cumene hydroperoxide addition.

At this time it does not appear that use of cobalt in the DPEN ligands leads to good analogues for the reactivity of the equivalent iron complexes. It may be that steric problems arising from the substituents on the pyridine rings interfere with reactivity and use of cobalt in non-sterically crowded complexes may still be of use in future investigations. Comparison of structural data for 6-coordinate $Fe^{III}$DPEN compounds[1] shows a trend where modifications to the 6-position of the pyridine ring results in elongation of the M-$N_{py}$ bond by 0.2Å-0.3Å. The X-ray structures suggest that intramolecular steric interactions with the geminal methyls protecting the thiolate contribute to the observed elongation, destabilizing the complex in comparison to DPEN ligands with unmodified 6-positions.

In the case of **4** the $Co^{II}$ is a smaller metal ion than $Fe^{II}$ to begin with, having 0.03-0.07Å shorter bonds between the metal and ligand atoms than observed for **3**. In a 6-coordinate $Co^{III}$ the smaller metal ion radius would result in comparatively greater steric interactions than the $Fe^{III}$ complex. The result may be that the desired oxidative addition of $O_2^-$ is unfavorable due to the destabilized 6-coordinate structure and instead the observed reactivity occurs, which leads to a less sterically congested 5-coordinate compound.

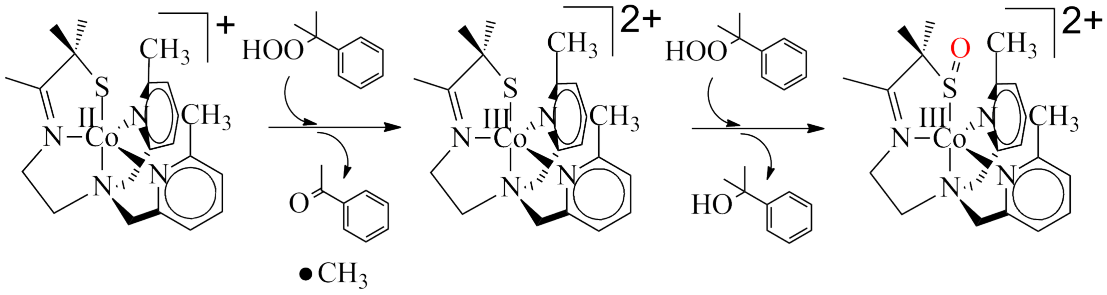


Figure 15: Proposed stepwise reaction of Compound **4** plus first equivalent of cumene hydroperoxide

## 2.5 Conclusions

In conclusion we have synthesized and characterized $[Co^{(II)}(S^{Me2}N_4(6\text{-Me-DPEN}))](PF_6)$ 4, a cobalt analogue to the $[Fe^{(II)}(S^{Me2}N_4(6\text{-Me-DPEN}))](PF_6)$ previously synthesized in the Kovacs lab. **4** was electronically, spectroscopically and structurally similar to the original iron compound however it displayed markedly different reactive properties. No potential peroxo intermediates were observed and reactions with $O_2^-$ and peroxides appear to result in metal and ligand oxidation.

At this time it does not appear that use of cobalt in the DPEN ligands leads to good analogues for the reactivity of the equivalent iron complexes. It may be that steric problems arising from the substituents on the pyridine rings interfere with reactivity and use of cobalt in non-sterically crowded complexes may still be of use in future investigations.

# Bibliography

[1] S.A. Toledo. Synthesis and Reactivity of an Expanded Family of Superoxide Reductase (SOR) Model Complexes Using N-Heterocyclic, Thiolate-Containing Ligands: Towards a Better Understanding of Structural-Functional Relationships., Ph.D. Thesis, University of Washington, Seattle, Wa, 2009.

[2] Ariane Jalila Simaan, Frederic Banse, Pierre Mialane, Alain Boussac, Sun Un, Taraneh Kargar-Grisel, Guy Bouchoux, and Jean-Jacques Girerd. *Eur. J. Inorg. Chem.*, pages 993–996, 1999.

[3] A. Jalila Simaan, Frederic Banse, Jean-Jacques Girerd, Karl Wieghardt, and Eckhard Bill. *Inorg. Chem.*, 40:6538–6540, 2001.

[4] A. F. M. Mokhlesur Rahman, W. Gregory Jackson, and Anthony C. Willis. *Inorg. Chem.*, 43:7558–7560, 2004.

[5] R.D. Swartz II. Synthesis, Structure, and Reactivity of Biomimetic Catalysts Modeling Non-Heme and Non-Corrinoid Thiolate Ligated Iron and Cobalt Enzymes, Ph.D. Thesis, University of Washington, Seattle, Wa, 2010.

[6] Ferman A. Chavez, Jorge A. Briones, Marilyn M. Olmstead, and Pradip K. Mascharak. *Inorg. Chem.*, 38:1603–1608, 1999.

[7] Ilia A. Guzei and Andreja Bakac. *Inorg. Chem.*, 40:2390–2393, 2001.

[8] Subhasish Mukerjeea, Kirsten Skogersona, Susan DeGalaa, and John P. Caradonna. *Inorg. Chim. Acta.*, 297:313–329, 2000.

[9] C. Benelli and D. Gatteschi. *Inorg. Chem.*, 21:1788–1790, 1982.

[10] Frances Namuswe, Gary D. Kasper, Amy A. Narducci Sarjeant, Takahiro Hayashi, Courtney M. Krest, Michael T. Green, Pierre Moenne-Loccoz, and David P. Goldberg. *J. Am. Chem. Soc.*, 130:14189–14200, 2008.

[11] Divya Krishnamurthy, Gary D. Kasper, Frances Namuswe, William D. Kerber, Amy A. Narducci Sarjeant, Pierre Moenne-Loccoz, and David P. Goldberg. *J. Am. Chem. Soc.*, 128:14222–14223, 2006.

[12] A. Jalila Simaan, Susanne Dopner, Frederic Banse, Sophie Bourcier, Guy Bouchoux, Alain Boussac, Peter Hildebrandt, and Jean-Jacques Girerd. *Eur. J. Inorg. Chem.*, pages 1627–1633, 2000.

[13] Neil G. Connelly and Willian E. Geiger. *Chem. Rev.*, 96:877–910, 1996.

[14] Vitaly V. Paclishchuk and Anthony W. Addison. *Inorg. Chim. Acta*, 298:97–102, 2000.

[15] William Levason and Mark D. Spicer. *J. Chem. Soc. Dalton Trans.*, pages 719–722, 1990.

[16] Irene Kung, Dirk Schweitzer, Jason Shearer, Wendy D. Taylor, Henry L. Jackson, Scott Lovell, and Julie A. Kovacs. *J. Am. Chem. Soc.*, 122:8299–8300, 2000.

[17] G. V. Acevedo. Mechanisms for probing metalloenzymes active sites and exploration of the post-translational modification of the enzyme nitrile hydratase (nhase), Ph.D. Thesis, University of Washington, Seattle, Wa, 2008.

[18] Shin ichi Adachi, Shingo Nagano, Koichiro Ishimori, Yoshihito Watanabe, Isao Morishima, Tsuyoshi Egawas, Teizo Kitagawa, and Ryu Makino. *Biochemistry*, 32:241–252, 1993.

[19] Shin ichi Adachi, Shingo Nagano, Koichiro Ishimori, Yoshihito Watanabe, and Isao Morishima. *Biochemistry*, 32:241–252, 1993.

# 3 $[Fe^{(II)}(S^{Me2}N_4(6\text{-H-DPPN}))](PF_6)$

Temperature Dependent $O_2$ Reaction Products and Thermodynamics of Neutral Ligand Binding

## 3.1 Introduction

Small structural modifications to ligands, as simple as the expansion of backbone alkyl linkers, has been shown previously to promote significant reactivity changes in known complexes.[1] Modified ligands with the expansion of the ethyl-backbone linker to a propyl-backbone linker were synthesized for the DPEN series. This change resulted in different geometric and reactive properties for several of the DPEN compounds as compared to the ethyl version.[2] The $[Fe^{(II)}(S^{Me2}N_4(6\text{-H-DPPN}))](PF_6)$ **7** was of particular interest. **7** was the first of the DPEN series to display reversible solvent coordination as well as solvent and temperature dependent $O_2$ reaction products. Understanding how the changes in the ligand environment led to such divergent behavior, as compared to the ethyl linker compound, is a crucial part of the synthetic strategy of biomimetic chemistry. Studies into the properties of **7** were undertaken to expand on the understanding of the DPEN ligand system.

While some molecules, $N_3^-$ and $CN^-$,[3] have been shown to inhibit SOR activity through competitive binding, the active site of SOR in the $Fe^{(II)}$ state appears to be 5-coordinate despite being exposed on the surface of the enzyme. Understanding how ligand lability is controlled in an SOR-like environment could enhance understanding of the specificity of reaction towards $O_2^-$. Investigations into the thermodynamics of ligand binding to **7** were undertaken for comparison in future DPEN compounds that may share this property.

Additionally, the reaction of **7** with $O_2$ at low temperatures in MeOH appeared to form an intermediate that was stable for several hours. The biological relevance of intermediates of $O_2$ reactivity with iron systems are of interest to modern chemistry.[4] While work in the field has been able to characterize examples of many species, such as the iron-oxo[5–7] -(hydro)peroxo[8–11] and -superoxo[12] compounds, more examples are needed to fill in our knowledge of such compounds and the possibility of **7** forming such an intermediate was further investigated.

## 3.2 Experimental

*General Methods*

All reactions were performed using standard Schlenk techniques under an atmosphere of dinitrogen in a glove box. Reagents were obtained from commercial sources at the highest purity available and were used without further purifications. Acetonitrile (MeCN), Tetrahydrofuran (THF) and Diethyl ether ($Et_2O$) were dispensed under argon from a solvent delivery system. Methanol (MeOH) was refluxed over magnesium and iodine, and dichloromethane ($CH_2Cl_2$) was dried over $CaH_2$. 3-Methyl-3-mercapto-2-butanone was prepared according to a published procedure. Electron paramagnetic resonance (EPR) spectra were obtained using a Bruker E580 CW/FT X-Band EPR Spectrometer at 4 K. Electronic absorption spectra (EAS) were recorded using either a Hewlett-Packard 8453 diode array, a Cary 50 spectrometer or a Unisoku Unispeks USP-203-A liquid nitrogen cooled spectrophotometer cell. Elemental analyses were performed by Atlantic Microlab, Inc. (Norcross, GA).

Solvent-dependent (EAS) were recorded in MeCN, THF, $CH_2Cl_2$ and MeOH at various temperatures. EAS and extinction coefficients for fully bound adducts (Figure 17) of THF and MeCN were obtained by cooling a solution of **7** in pure THF or MeCN to 203 K or 233 K respectively. Extinction coefficients for fully MeOH bound adduct were determined by preparation of a solution of **7** in $CH_2Cl_2$ containing 1.65 M MeOH cooled to 193 K. Cooling of this solution below 193 K resulted in a negligible change in extinction coefficient values.

*Synthesis of* $[Fe^{(II)}(S^{Me2}N_4(6\text{-H-DPPN}))](PF_6)$ **7**.

3-methyl-3-mercapto-2-butanone (0.158 g, 1.3 mmol) was dissolved in MeOH (3 mL). N,N-Bis(2-pyridylmethyl)-1,3-propanediamine (0.297 g, 1.2 mmol) ligand precursor was dissolved in MeOH (3 mL). Both solutions were combined in a 50 mL Schlenk flask.

$Fe(OAc)_2$ (0.202 g, 1.2 mmol) was suspended in MeOH (3 mL). NaOMe (0.055 g, 1 mmol) was dissolved in MeOH (3 mL). All solutions were cooled to -30℃. $Fe^{II}(OAc)_2$ suspension was added dropwise to a stirring ligand mixture over 5 min followed by NaOMe solution added dropwise to ligand mixture over 5 min. The yellow/orange solution was allowed to stir at room temperature for 24 hours. $NaPF_6$ (0.199 g, 1.2 mmol) was dissolved in MeOH (3 mL) and added to solution and the reaction mixture was stirred for 6 hours. Solvent was removed by vacuum and the residue was dissolved in MeCN (5 mL)and stirred for 1 hour. The Solution was filtered over a sintered glass frit to remove insolubles. Solvent was removed by vacuum and residue was redissolved in minimum MeCN (2 mL), layered with $Et_2O$ (10 mL) and cooled to -30℃. Orange/brown crystalline solids were collected by filtration after 2 days, rinsed with $Et_2O$ and dissolved in minimum THF (2 mL), layered with $Et_2O$ (10 mL) and cooled to -30℃. Orange solids were collected by filtration after 2 days. Solids were triturated with $Et_2O$ multiple times until a yellow color persisted, affording 0.260 g of powdered $[Fe^{(II)}(S^{Me2}N_4(6\text{-H-DPPN}))](PF_6)$. Yield: 40%. Yellow X-ray quality crystals were grown by vapor diffusion of $Et_2O$ to a saturated solution of **7** in THF. Electronic Absorption Spectrum ($CH_2Cl_2$, -70℃) $\lambda_{max}$ ($\epsilon$ ($M^{-1}cm^{-1}$)) 341 (1900), 390 (sh) nm; (MeOH, -70℃) $\lambda_{max}$ ($\epsilon$ ($M^{-1}cm^{-1}$)) 302 (2000), 446 (1900) nm; (MeCN, -40℃) $\lambda_{max}$ ($\epsilon$ ($M^{-1}cm^{-1}$)) 321 (1600), 444 (920) nm; (THF, -70℃) $\lambda_{max}$ ($\epsilon$ ($M^{-1}cm^{-1}$)) 320 (2600), 464 (2800) nm. Magnetic moment $\mu_{eff}$ = 5.2 (MeCN, 298 K, Evans method). Anal. Calcd for $C_{20}H_{27}F_6N_4P_1S_1Fe_1$: C, 43.18; H, 4.89; N, 10.07. Found: C, 39.32; H, 4.37; N, 8.97.

*X-ray crystallography*

| Bonds (Å) / Angles | **7** |
|---|---|
| Fe(1)-S(1) | 2.3186(10) |
| Fe(1)-N(1) | 2.077(3) |
| Fe(1)-N(2) | 2.299(3) |
| Fe(1)-N(3) | 2.092(3) |
| Fe(1)-N(4) | 2.094(3) |
| S(1)-Fe(1)-N(1) | 84.00(8) |
| S(1)-Fe(1)-N(2) | 174.86(8) |
| S(1)-Fe(1)-N(3) | 106.18(9) |
| S(1)-Fe(1)-N(4) | 105.73(8) |
| N(1)-Fe(1)-N(2) | 90.96(11) |
| N(1)-Fe(1)-N(3) | 114.29(12) |
| N(1)-Fe(1)-N(4) | 126.22(12) |
| N(2)-Fe(1)-N(3) | 76.79(11) |
| N(2)-Fe(1)-N(4) | 76.49(11) |
| N(3)-Fe(1)-N(4) | 113.12(12) |

Select bond lengths and angles

| | **7** |
|---|---|
| MW | 556.35 |
| T (K) | 130(2) K |
| unit cell | Orthorombic |
| a (Å) | 13.8216(14) |
| b (Å) | 12.5289(5) |
| c (Å) | 26.989(2) |
| $\alpha$ (∘) | 90 |
| $\beta$ (∘) | 90 |
| $\gamma$ (∘) | 90 |
| V (Å$^3$) | 4673.7)6) |
| Z | 8 |
| $d_{calcd}$ | 1.581 Mg/m$\hat{3}$ |
| space group | P b c a |
| $R_1$ | 0.0565 |
| $wR_2$ | 0.1055 |
| GOF | 0.923 |

Crystal data, intensity collections and structure refinement parameters

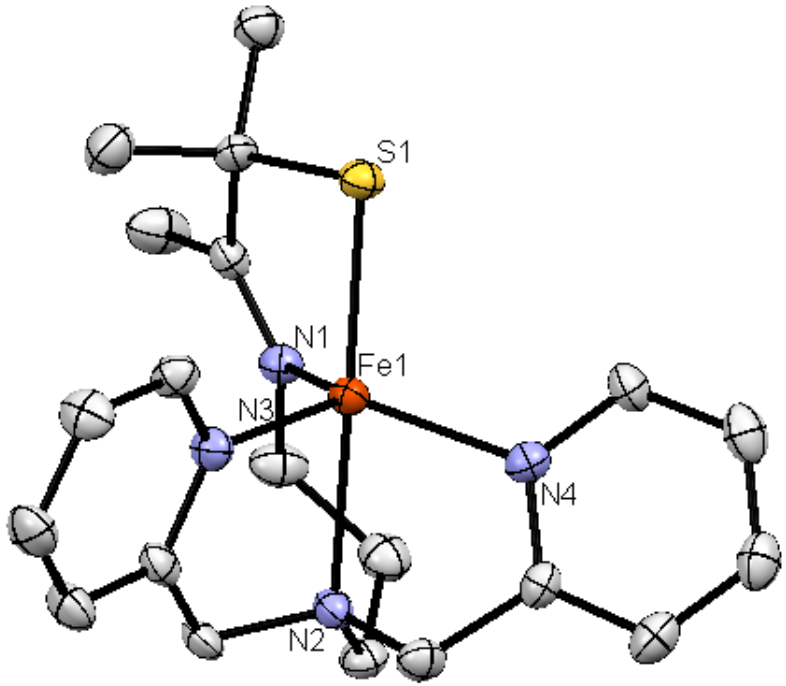


Figure 16: ORTEP diagram of $[Fe^{(II)}(S^{Me2}N_4(6\text{-H-DPPN}))](PF_6)$ **7** with hydrogen atoms, counterions and solvents of crystallization omitted (50% prob. ellipsoids)

## 3.3 Synthesis and Characterization

Solvent-dependent Electronic absorption spectra (EAS) were recorded in MeCN, THF, $CH_2Cl_2$ and MeOH at various temperatures.

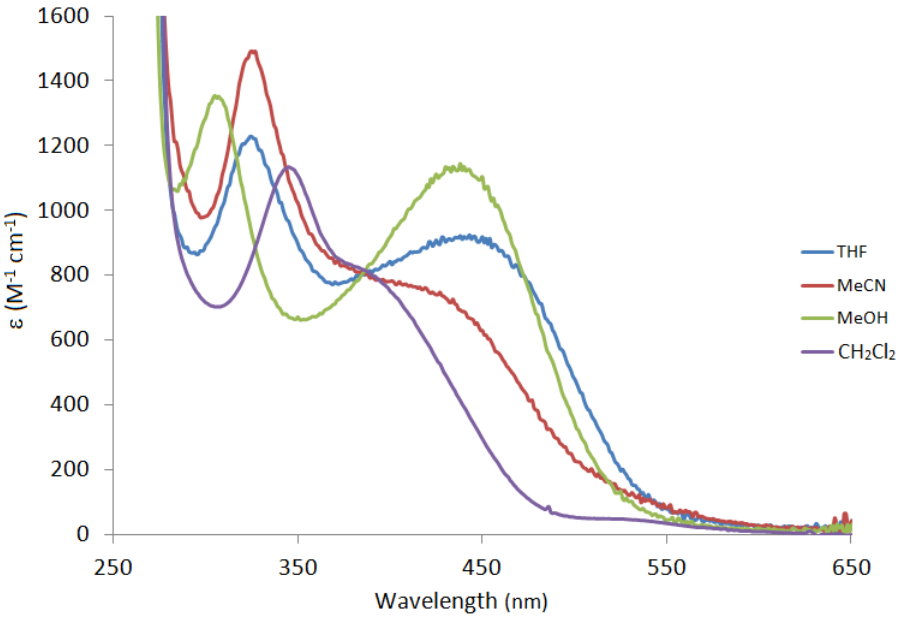


Figure 17: EAS of $[Fe^{(II)}(S^{Me2}N_4(6\text{-H-DPPN}))](PF_6)$ **7** in THF (Blue), MeCN (Red), MeOH (Green) and $CH_2Cl_2$ (Purple)

*Thermodynamics of neutral ligand binding*

Neutral ligands were found to bind reversibly to **7** and result in changes in the electronic absorption spectra (Figure 19, 20 and 21). Equilibrium constants ($K_{eq}$) for the binding of neutral ligands to **7** were determined by monitoring electronic absorption spectra of known concentrations of **7** and neutral solvent ligand in $CH_2Cl_2$. $K_{eq}$ values were calculated for each neutral ligand by standard methods[1] over the temperature range of 193 - 303 K. Concentrations for all low temperature measurements were corrected for changes in volume of $CH_2Cl_2$. To an aliquot of a standard solution of **7** in $CH_2Cl_2$ was placed an appropriate quantity of neutral ligand to result in final concentrations of **7**

$$Keq = \frac{[LX]}{([L]_0 - [LX])([X]_0 - [LX])} \quad (1)$$

$$ln(Keq) = \frac{\Delta H}{RT} + \frac{\Delta S}{R} \quad (2)$$

Figure 18: Van't Hoff Expression

(0.68 mM), MeCN (0.957 M), THF (0.616 M), or MeOH (0.165 M).

$K_{eq}$ is related to ΔH and ΔS through the Van't Hoff equation (Figure 18 equation 2). Use of a Van't Hoff plot (Figure 22, 23, 24), ln($K_{eq}$) vs 1/T, yields a linear graph with a slope of -ΔH/R and an intercept equal to ΔS/R where R is the gas constant. The parameters calculated for THF (ΔH = -3.14 ± 0.03 kcal/mol, ΔS = -14.5 ± 0.1 cal/mol • K) and MeCN (ΔH = -3.2 ± 0.15 kcal/mol, ΔS = -16.4 ± 2 cal/mol • K) are similar, however the parameters for MeOH are relatively larger (ΔH = -6.7 ± 0.5 kcal/mol, ΔS = -25 ± 2 cal/mol • K) indicating a more favorable binding.

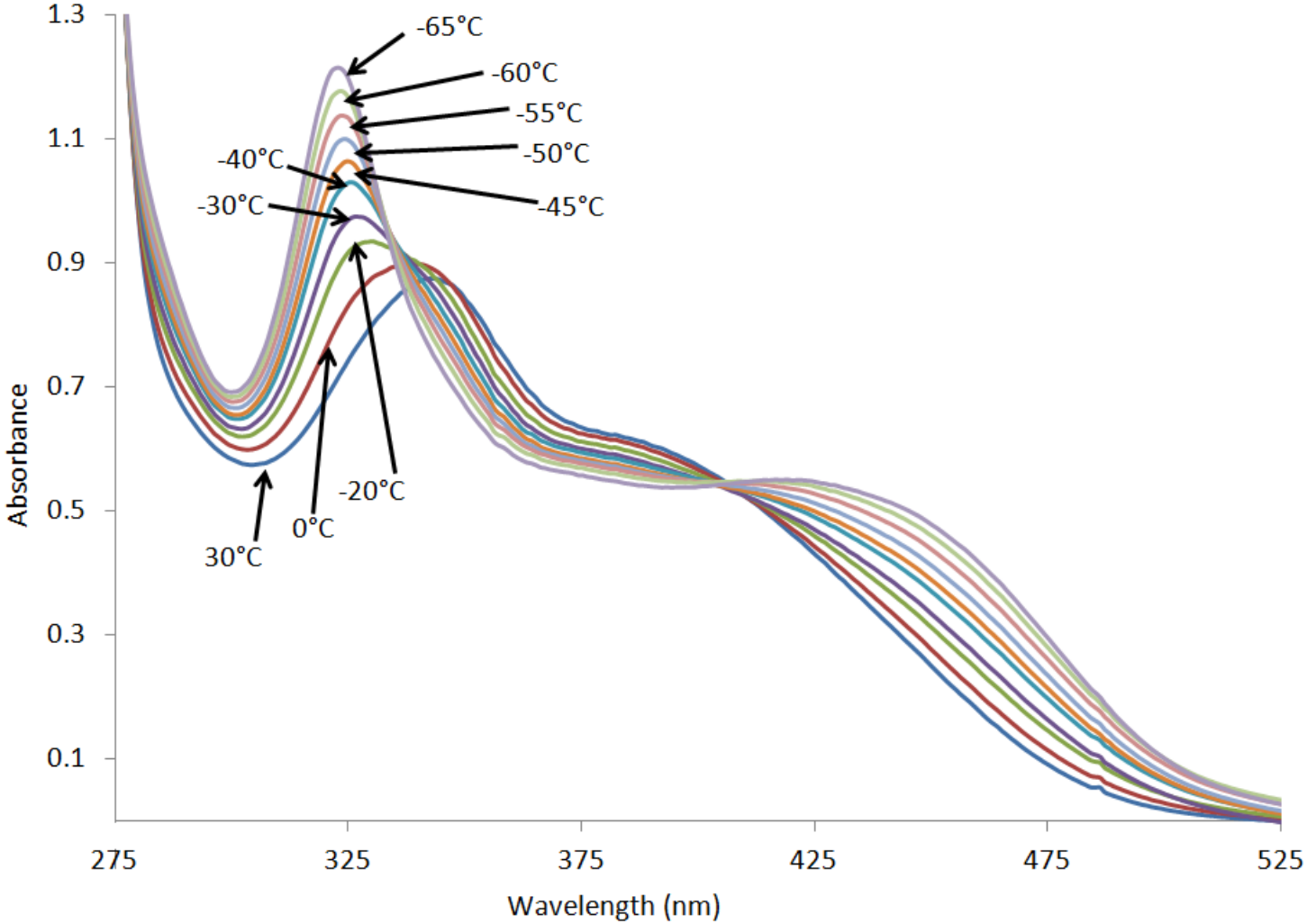


Figure 19: Temperature dependent EAS spectra of $[Fe^{(II)}(S^{Me2}N_4(6\text{-H-DPPN}))](PF_6)$ **7** + MeCN in $CH_2Cl_2$

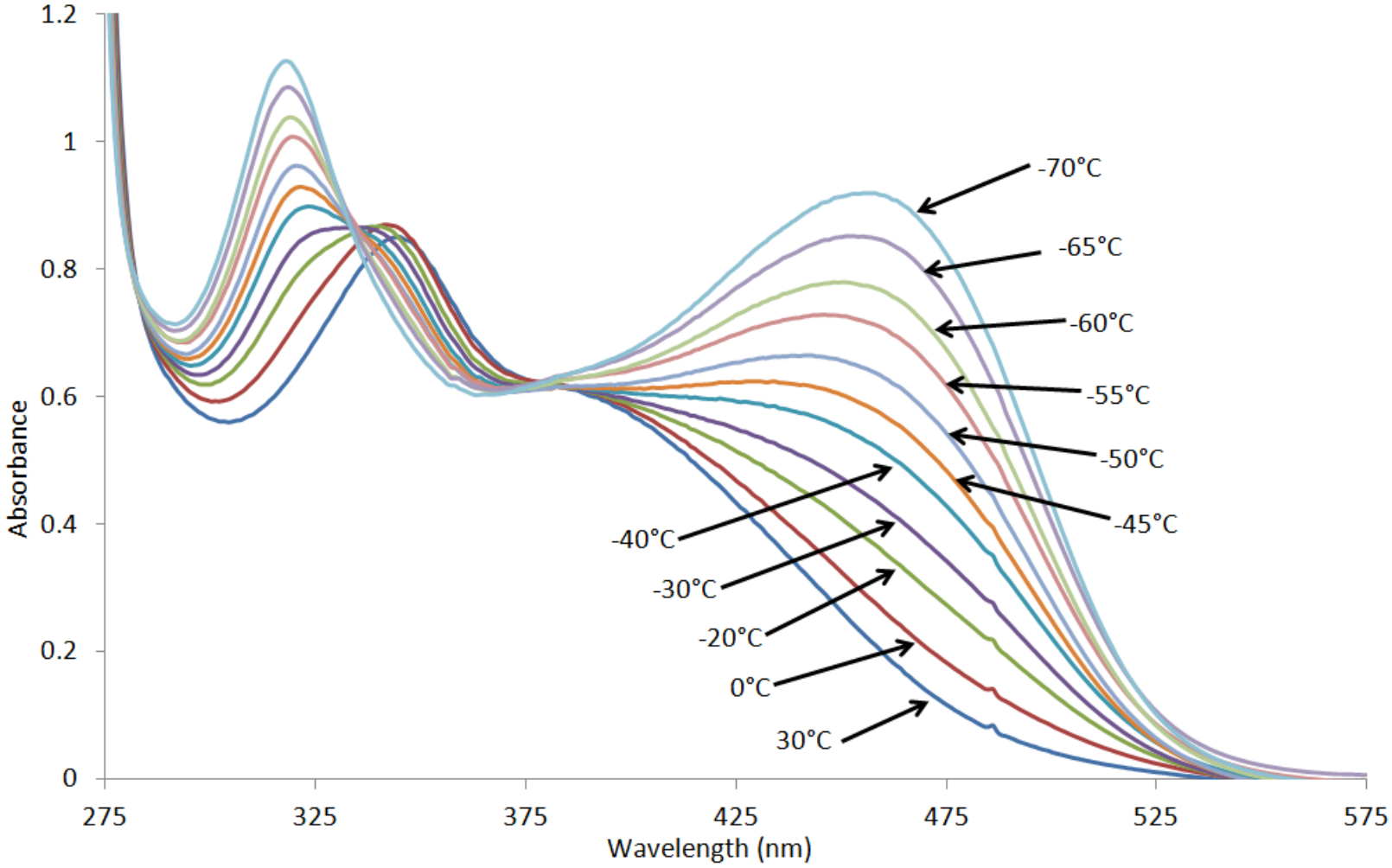


Figure 20: Temperature dependent EAS spectra of $[Fe^{(II)}(S^{Me2}N_4(6\text{-H-DPPN}))](PF_6)$ **7** + THF in $CH_2Cl_2$

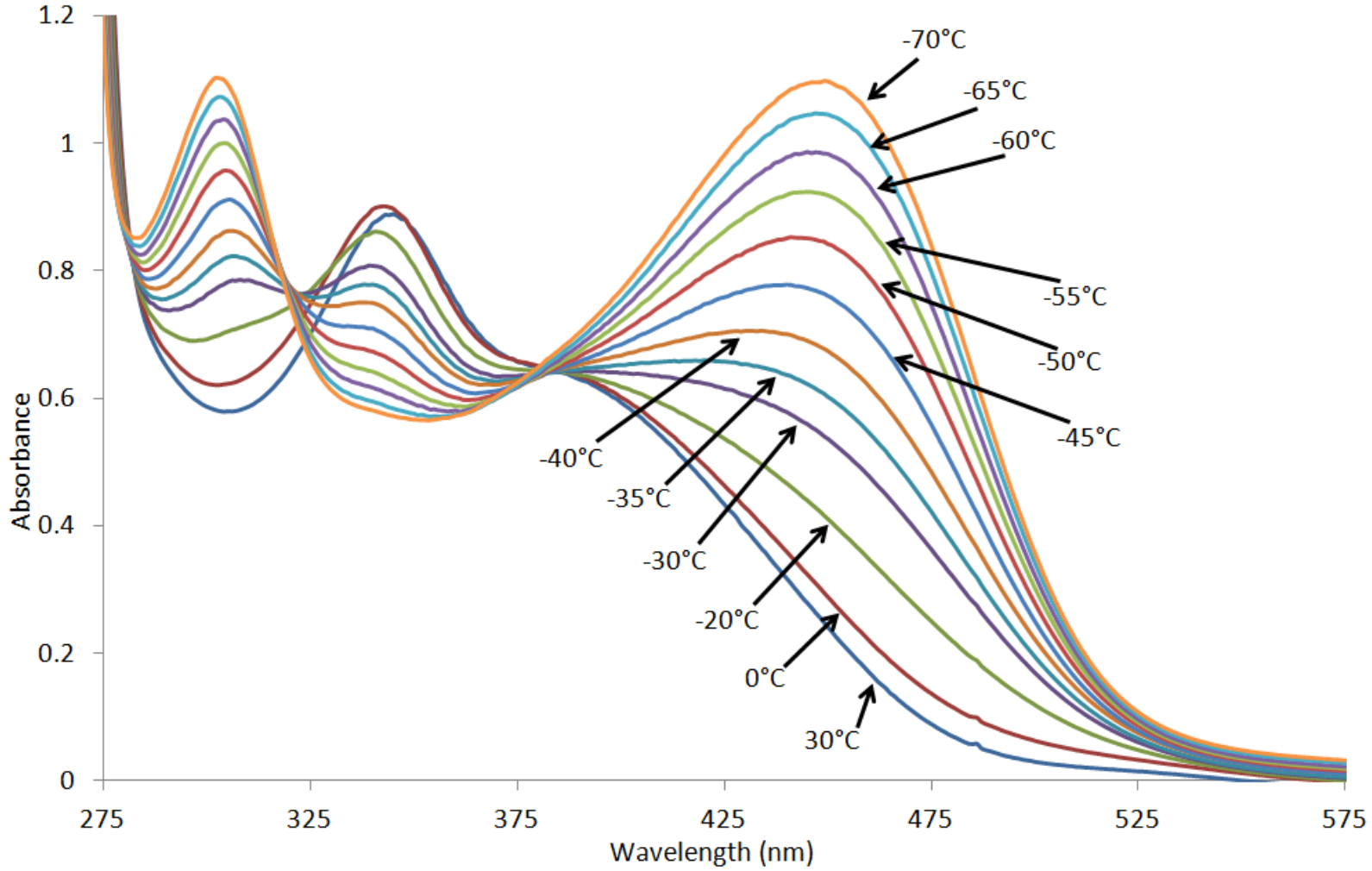


Figure 21: Temperature dependent spectra of $[Fe^{(II)}(S^{Me2}N_4(6\text{-H-DPPN}))](PF_6)$ **7** + MeOH in $CH_2Cl_2$

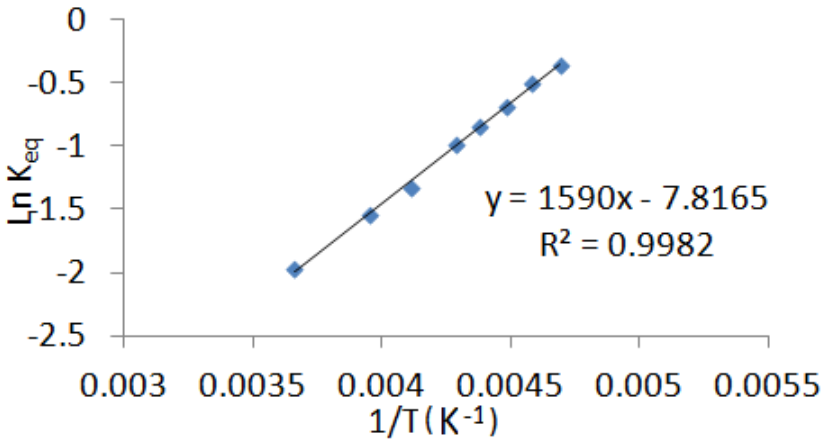


Figure 22: Van't Hoff plot of $[Fe^{(II)}(S^{Me2}N_4(6\text{-H-DPPN}))](PF_6)$ **7** + MeCN

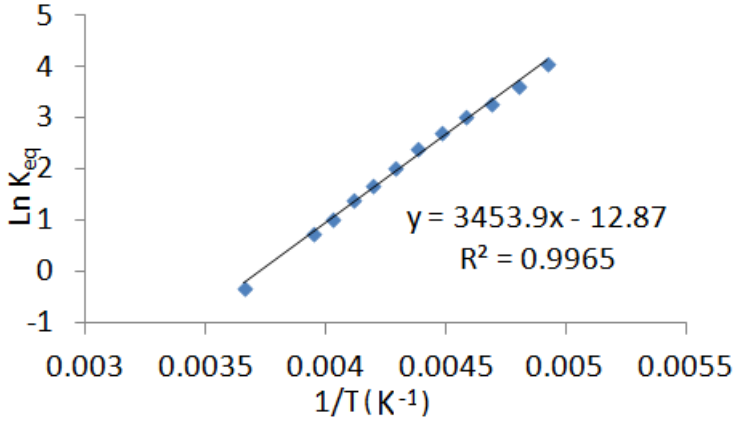


Figure 23: Van't Hoff plot of $[Fe^{(II)}(S^{Me2}N_4(6\text{-H-DPPN}))](PF_6)$ **7** + MeOH

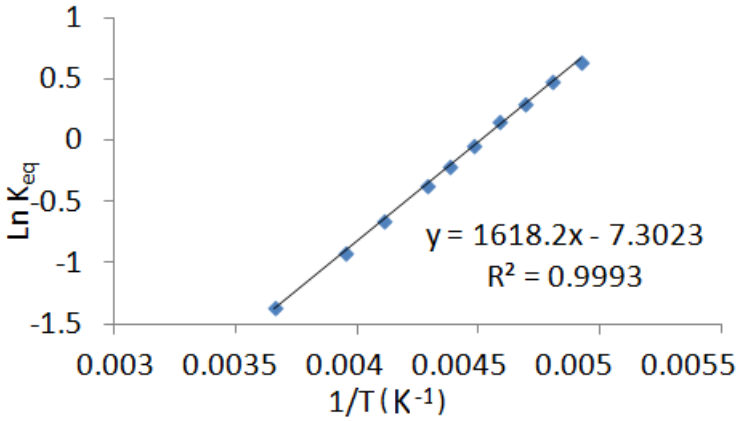


Figure 24: Van't Hoff plot of $[Fe^{(II)}(S^{Me2}N_4(6\text{-H-DPPN}))](PF_6)$ **7** + THF

*$O_2^-$ and $O_2$ Reactivity*

The reactivity of **7** with $KO_2$ was investigated by Electronic Absorption Spectroscopy (EAS) on a dipprobe instrument. Regardless of solvent, temperature or proton donor, the reactivity observed remained consistent with the growth of a band in the EAS at 512 nm. This species had been previously shown[2] to be the $\mu$-oxo dimer product $[(Fe^{(III)}(S^{Me2}N_4(6\text{-H-DPPN})))_2O](PF_6)_2$ **8**.

5-coordinate **7** was observed to be highly reactive to $O_2$. $O_2$ levels above 2ppm would result in slow conversion of the solid material to **8**. Extreme care was necessary to ensure air-free conditions of all equipment and testing apparatus. When **7** was exposed to $O_2$ in MeCN, THF, $CH_2Cl_2$ and MeOH at room temp **8** was observed in quantitative yield. Similar results were observed at low temperature in each solvent, except for MeOH. When a solution of DPPN in MeOH at -78°C was exposed to $O_2$ immediate formation of **8** was not observed.

Over the course of 25 min the growth of a band in the EAS at 532 nm was observed (Figure 25). This product (Intermediate A) did not decay into **8** and was reasonably stable to warming, decaying over several hours at room temperature. Initially Intermediate A was thought to be a product of $O_2$ inner-sphere reactivity, however, subsequent investigations showed that addition of the one electron oxidant ferricinium hexafluorophosphate ($[FeCp_2](PF_6)$) to a MeOH solution of **7** at room temperature resulted in an EAS spectrum identical to Intermediate A (Figure 26). Identical EPR spectra (X-band, 4 K) were obtained from preparation of Intermediate A from $O_2$ (Figure 27) in MeOH or from chemical oxidation with $[FeCp_2](PF_6)$ (Figure 28). The rhombic EPR spectra ($g_1 = 2.24$, $g_2 = 2.17$, $g_3 = 1.98$) are consistent with a low-spin $Fe^{(III)}$ product.

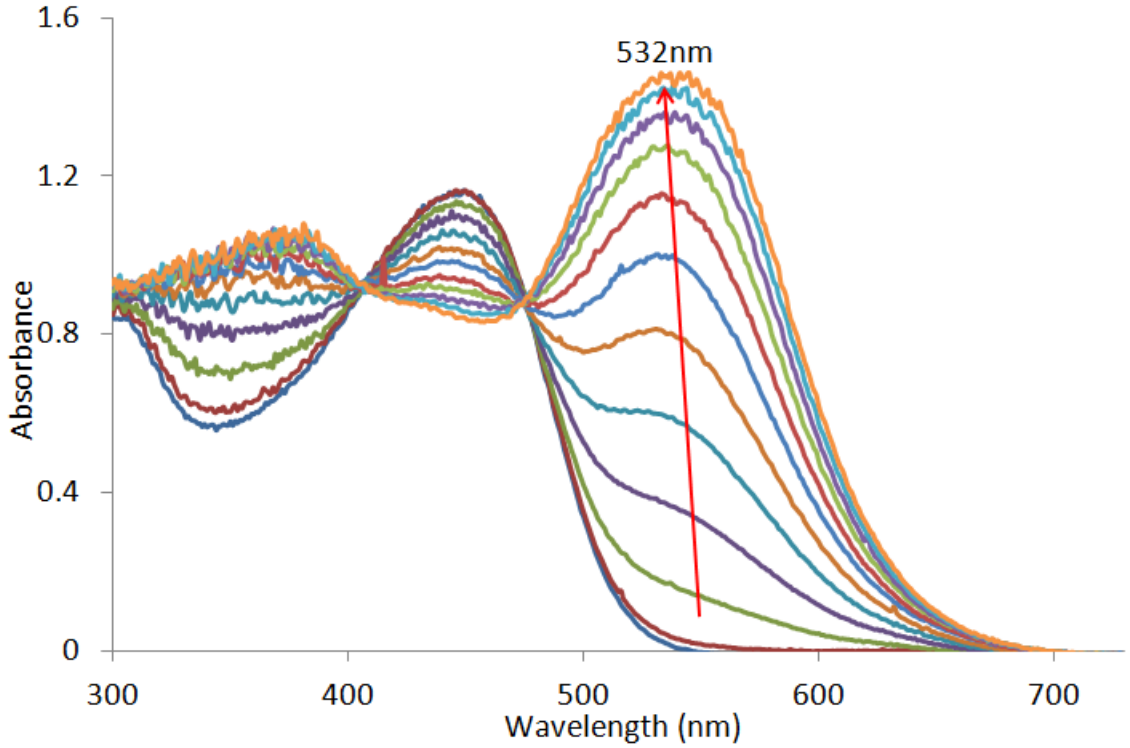


Figure 25: A solution of $[Fe^{(II)}(S^{Me2}N_4(6\text{-H-DPPN}))](PF_6)$ **7** in MeOH at -78°C exposed to $O_2$

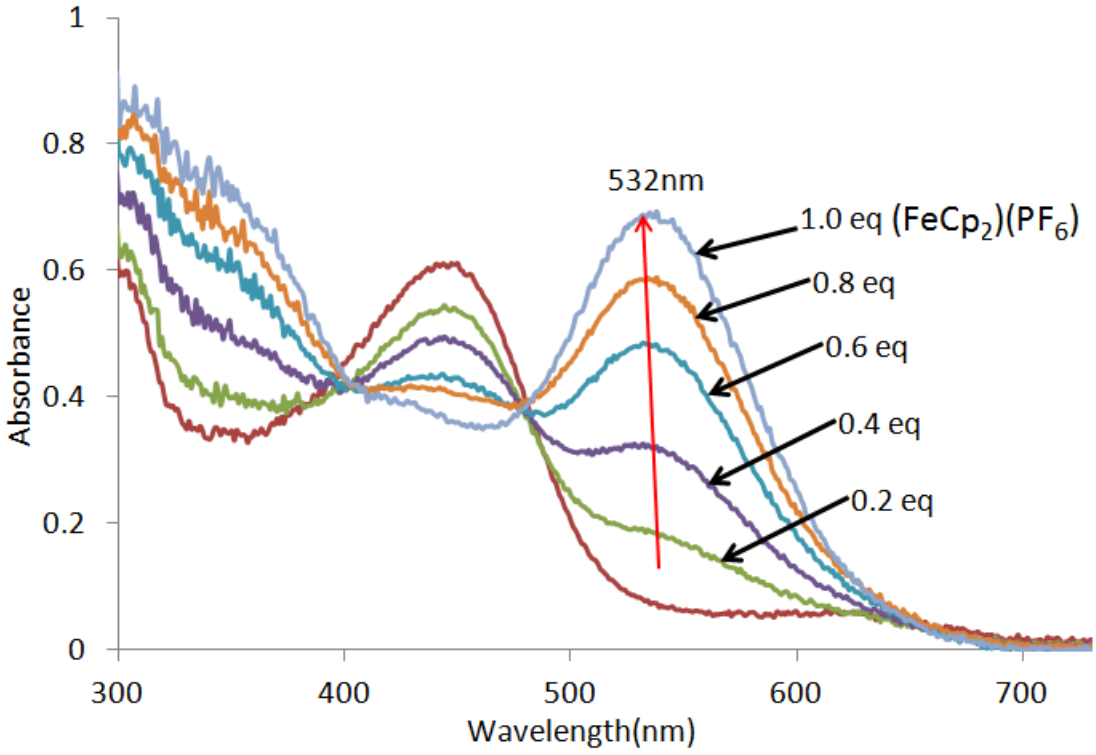


Figure 26: Titration of $(FeCp_2)(PF_6)$ to a MeOH solution of $[Fe^{(II)}(S^{Me2}N_4(6\text{-H-DPPN}))](PF_6)$ **7** at room temperature.

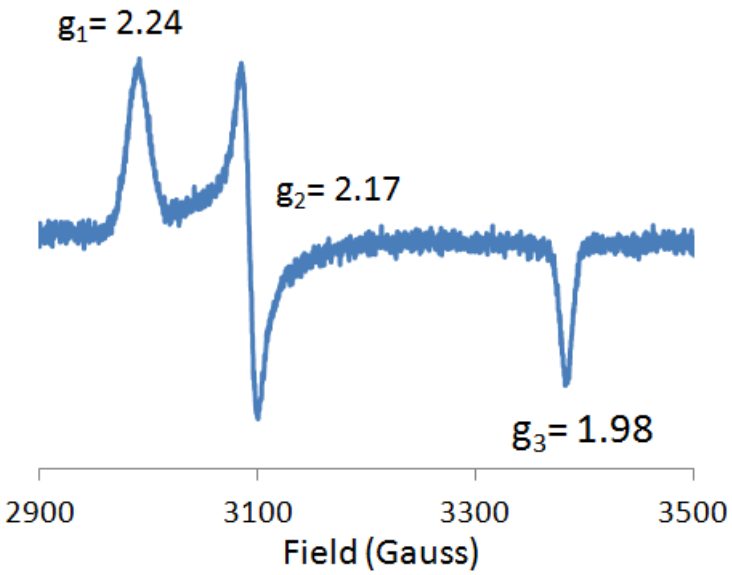


Figure 27: EPR spectrum of Intermediate A formed via $O_2$ addition

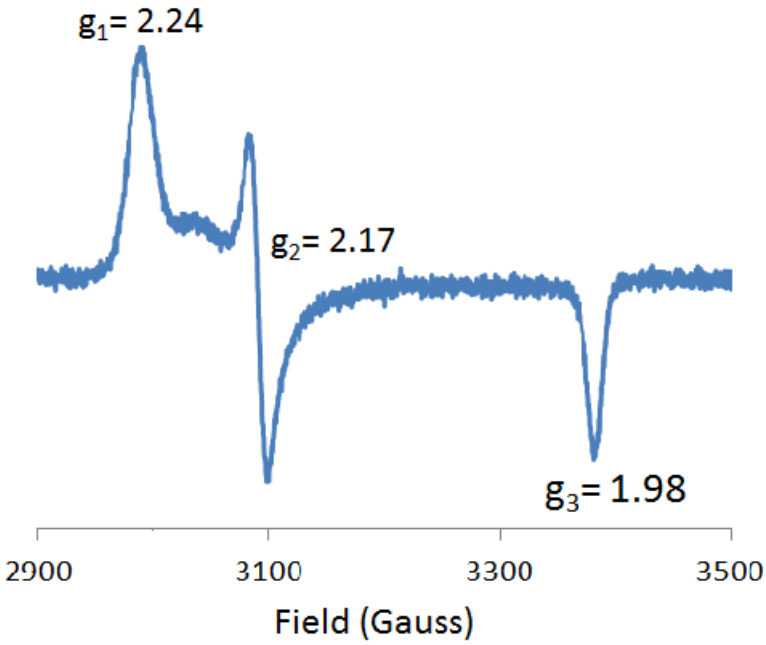


Figure 28: EPR spectrum of Intermediate A formed via $[FeCp_2](PF_6)$oxidation

## 3.4 Discussion

The original crystal structure obtained for **7** was that of the 6-coordinate [$Fe^{(II)}$($S^{Me2}N_4$(6-H-DPPN)(MeOH))]($PF_6$) compound.[2] The EAS spectra was shown to be solvent dependent suggesting **7** was dissociating the 6th ligand in solution. This hypothesis was validated when attempts to isolate the 5-coordinate complex for further study and characterization were successful (Figure 16).

The crystal structure of **7** (Figure 16) shows the complex to have a $\tau$ value of $\tau$=0.82, making it nearly trigonal bipyramidal. In contrast the majority of the ethyl linker DPEN series have values of between $\tau = 0.54$ and 0.6, placing them midway between trigonal-bipyramidal and square pyramidal. The lengthened backbone linker of **7** allows for a greater degree of flexibility of the ligand, enabling an optimized geometry around the metal center.

**7** was the first DPEN complex to exhibit reversible binding of neutral solvent ligands. This may be the result of the increased ligand flexibility, reducing the energy of rearrangement, as compared to the ethyl linker DPEN series. Obtaining parameters relevant to the binding of neutral ligands to **7** would provide a baseline for comparison to future DPEN ligands in development. To this end the thermodynamics of binding for the three solvents commonly used to study **7** were investigated as described (vida supra). $K_{eq}$, $\Delta$S and $\Delta$H values were obtained for MeCN, THF and MeOH binding. MeOH shows a greater $\Delta$H and $\Delta$S than either THF or MeCN. The greater $\Delta$S of MeOH may be explained by possible H-bonding to the thiolate resulting in a more ordered 6-coordinate complex. What is not readily apparent is why THF and MeCN have similar $\Delta$S and $\Delta$H values as MeCN would be expected to be a better ligand than THF. Comparison to future complexes may be required to more fully understand the binding properties of **7**.

The binding properties observed for **7** may explain the curious $O_2$ reactivity observed. In reactivity similar to the rest of the DPEN series, **7** forms **8** readily upon exposure to $O_2$ at room temperature in MeCN, THF, MeOH and $CH_2Cl_2$. At low temperatures, in MeCN, THF or $CH_2Cl_2$, **8** is also observed to form with no observable intermediate. However, when a solution of **7** in MeOH at -78℃ is exposed to $O_2$ **8** is not formed. Rather $[Fe^{(III)}(S^{Me2}N_4(6\text{-H-DPPN})(MeOH))]^{2+}$ is observed to form. This has been confirmed by direct oxidation of **7** in MeOH by $[FeCp_2](PF_6)$. The resulting products give the same EAS and EPR signals, strongly supporting that addition of $O_2$ is resulting in the oxidation of **7** in solution at low temperature. The tighter binding of MeOH may explain the divergent reactivity observed with $O_2$ compared to the less favorably bound ligands. At -78℃ in MeOH coordinative saturation may reduce the availability of 5-coordinate product necessary to undergo the inner-sphere reaction to produce compound **8**. Commonly $\mu$-oxo bridged dimers require that 5-coordinate material must first react with $O_2$ to form an $Fe^{III}$-superoxo, then react with another 5-coordinate complex to form $Fe^{III}$-O-O-$Fe^{III}$, followed by homolytic O-O bond cleavage to form $Fe^{IV}$=O which can react with another 5-coordinate complex to form **8**. If 5-coordinate complex concentration is significantly reduced due to forming the 6-coordinate complex then the monomeric $Fe^{III}$-superoxo may persist long enough to undergo alternate reactivity, such as accepting a proton and acting as an oxidant to 6-coordinate material to yield $Fe^{III}$-OOH and $Fe^{III}$-MeOH. Protonation of the proximal oxygen would then release $H_2O_2$ followed by coordination of MeOH to the 5-coordinate $Fe^{III}$ to form the observed MeOH bound product. In the aprotic solvents no sidereactions of this type could occur and the $Fe^{III}$-superoxo could persist long enough react with another 5-coordinate complex.

## 3.5 Conclusion

We have isolated and structurally characterized the first DPEN complex that has shown reversible coordination of solvent. Thermodynamic data of ligand coordination was obtained for MeCN, THF and MeOH as a reference to compare future DPEN complexes that exhibit similar coordination behavior, which show that MeOH binds tighter than MeCN or THF. Additionally we have shown that the reaction product of **7** formed upon addition of $O_2$ in MeOH at -78℃ is identical to the chemically oxidized product. We have yet to identify the product formed by $O_2$ through this oxidation reaction.

# Bibliography


[1] Dirk Schweitzer, Jason Shearer, Durrell K. Rittenberg, Steven C. Shoner, Jeffrey J. Ellison, Reza Loloee, Scott Lovell, David Barnhart, and Julie A. Kovacs. *Inorg. Chem.*, 41:3128–3136, 2002.

[2] S.A. Toledo. Synthesis and Reactivity of an Expanded Family of Superoxide Reductase (SOR) Model Complexes Using N-Heterocyclic, Thiolate-Containing Ligands: Towards a Better Understanding of Structural-Functional Relationships., Ph.D. Thesis, University of Washington, Seattle, Wa, 2009.

[3] Michael D. Clay, Francis E. Jenney Jr., Peter L. Hagedoorn, Graham N. George, Michael W. W. Adams, and Michael K. Johnson. *J. Am. Chem. Soc.*, 124:788–805, 2002.

[4] Julie A. Kovacs. *Science*, 299:1024–1025, 2003.

[5] Michael R. Bukowski, Kevin D. Koehntop, Audria Stubna, Emile L. Bominaar, Jason A. Halfen, Eckard Munck, Wonwoo Nam, and Lawrence Que Jr. *SCIENCE*, 310:1000–1002, 2005.

[6] Wonwoo Nam. *Acc. Chem. Res.*, 40:522–531, 2007.

[7] Carsten Krebs, Danica Galonic Fujimori, Christopher T. Walsh, and J. Martin Bollinger Jr. *Acc. Chem. Res.*, 40:484–492, 2007.

[8] Jason Shearer, Robert C. Scarrow, and Julie A. Kovacs. *J. Am. Chem. Soc.*, 124:11709–11717, 2002.

[9] Terutaka Kitagawa, Abhishek Dey, Priscilla Lugo-Mas, Jason B. Benedict, Werner Kaminsky, Edward Solomon, and Julie A. Kovacs. *J. Am. Chem. Soc.*, 128:14448–14449, 2006.

[10] A. Jalila Simaan, Susanne Dopner, Frederic Banse, Sophie Bourcier, Guy Bouchoux, Alain Boussac, Peter Hildebrandt, and Jean-Jacques Girerd. *Eur. J. Inorg. Chem.*, pages 1627–1633, 2000.

[11] Piotr J. Mak, Ilia G. Denisov, Doreen Victoria, Thomas M. Makris, Tianjing Deng, Stephen G. Sligar, and James R. Kincaid. *J. Am. Chem. Soc.*, 129:6382–6383, 2007.

[12] Xiaopeng Shan and Lawrence Que Jr. *PNAS*, 102:5340–5345, 2005.

# 4 $[Fe^{(II)}(S^{Me2}N_4(2\text{-}QuinoEN))](PF_6)$

Investigations into an intermediate of $KO_2$ reactivity

## 4.1 Introduction

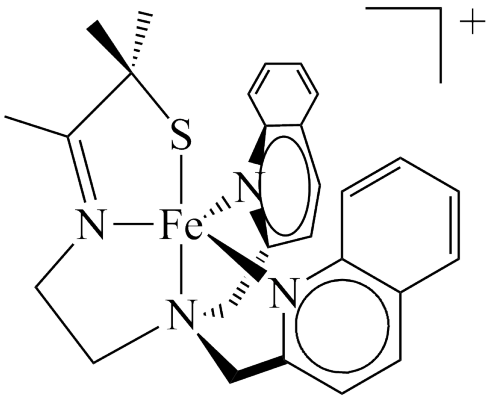


Figure 29: $[Fe^{(II)}(S^{Me2}N_4(2\text{-}QuinoEN))]^+$

$[Fe^{(II)}(S^{Me2}N_4(2\text{-}QuinoEN))]^+$ (**9**) (Figure 29) was synthesized previously in the Kovacs lab[1] as part of the first series of DPEN ligands, and had displayed reactivity with $O_2^-$ in MeOH at -78℃. Further investigations (vida infra) showed that the observed product was in fact the $Fe^{(III)}$ oxo-bridged dimer species $[(Fe^{(III)}(S^{Me2}N_4(2\text{-}QuinoEN)))_2\text{-}\mu\text{-}O]^{2+}$ (**10**), which formed with no observable intermediate. However, during recent investigations it was discovered that at -40℃ in MeCN, with t-BuOH (300 eq) present as a proton donor, an intermediate species, (**11**), of reaction with $O_2^-$ was observed to form and subsequently convert to **10**. It was proposed that the observed intermediate was a transient peroxo/hydroperoxo species.

The recent discovery of the crystal structure for the $\eta$:1:$\eta$:1 peroxo-bridged dimer $[(Mn^{(III)}(S^{Me2}N_4(6\text{-}Me\text{-}DPEN))_2\text{-}\mu\text{-}O_2)]^{2+}$ and the low resolution structure of the analogous $[(Mn^{(III)}(S^{Me2}N_4(2\text{-}QuinoEN))_2\text{-}\mu\text{-}O_2)]^{2+}$ complex (unpublished results) show that the DPEN ligand system is indeed capable of supporting metal-peroxo species. While

the manganese DPEN compounds were observed to form stable peroxo complexes at low temperatures **11** was only transiently stable and decayed even at low temperature to **10**. Investigations into the nature and properties of **11** were undertaken and are outlined below.

## 4.2 Reactivity

*General Methods*

All reactions were performed using standard Schlenk techniques under an atmosphere of dinitrogen in a glove box. Reagents were obtained from commercial sources at the highest purity available and were used without further purifications. Acetonitrile (MeCN) and diethyl ether ($Et_2O$) were dispensed under argon from a solvent delivery system. Methanol (MeOH) was refluxed over magnesium and iodine. Propionitrile (EtCN) and dichloromethane ($CH_2Cl_2$) were dried over $CaH_2$. 3-Methyl-3-mercapto-2-butanone was prepared according to a published procedure. Electron paramagnetic resonance (EPR) spectra were obtained using a Bruker E580 CW/FT X-Band EPR Spectrometer at 4 K. Electronic absorption spectra (EAS) were recorded using either a Hewlett-Packard 8453 diode array, a Cary 50 spectrometer. Standard reactions for formation of **11** were maintained for comparison between all reagents. Solutions of **9** (0.4 mM) (5 mL) were injected into a custom glass adapter dip probe cell attached to a Cary 50 spectrometer and cooled to -40℃ in a dry ice/MeCN bath. *tert*-BuOH (60 $\mu$L) (300 eq) was added to the solution of **9**. 100 $\mu$L of $KO_2$ (0.02 M) (1 eq) (solubilized by 18-crown-6 in THF) solution was added to the solution of **9** and the electronic absorption spectrum acquired once per minute at a scan rate of 600 nm/min.

*$O_2$ Reactivity Review: Formation of **10**.*

**9** was characterized by UV/Vis absorbance features at $\lambda_{max}(\epsilon)$= 479 nm (620) and 377 nm (740) in MeCN. Upon exposure of an MeCN solution of **9** to $O_2$ a rapid conversion of the EAS spectrum characterized by the growth of an absorption band at 566 nm (2700) is observed. This transformation proceeds regardless of the solvent or the temperature of the reaction. This species has been characterized as **10** by x-ray crystallography, as previously reported.[1] To date no intermediates have been detected

along the reaction path from starting material to **10** in the reaction with $O_2$.

*$O_2^-$ reactivity. Formation of Intermediate **11***

At low temperatures upon addition of $O_2^-$ (from $KO_2$ solubilized with 18-crown-6 in THF) to a solution of **9** in MeOH or MeCN the formation of **10** is observed by EAS with no indication of an intermediate. The amount of **10** formed by this reaction is only half that obtained when formed by $O_2$, as evidenced by the intensity of 566 nm absorbance in the EAS spectrum. In the case of EtCN, $CH_2Cl_2$ or THF being used as the reaction solvent the formation of **10** is very slow or is not observed over the course of several hours.

If a solution of **9** in MeCN at -40℃ was spiked with the proton donor t−BuOH (300eq) and then reacted with $O_2^-$ what was observed was the initial formation of a band at 544 nm which cleanly converts to a new species with a 566nm band over the course of 50 min. The isosbestic conversion strongly indicated the formation of an intermediate prior to formation of **10**. The amount of **10** formed by this reaction is only half that obtained when formed by $O_2$, as evidenced by the intensity of the 566 nm absorbance in the EAS spectrum.

*544 nm Intermediate **11**: EPR, rR and FT-IR characterization*

Species **11** was formed in MeCN at -40℃ in an $N_2$ atmosphere glove box. The solution was diluted 1:1 with pre-cooled toluene and frozen in an EPR tube in liquid $N_2$. Attempts to observe species **11** by EPR obtained a weak, broad signal with a value of $g_{eff} = 2.16$. To obtain resonance Raman samples **11** was formed in MeCN at -40℃ in an $N_2$ atmosphere glove box and EPR tubes of the solution were frozen in liquid $N_2$. Both $^{16}O$ and $^{18}O$ samples were prepared from appropriately labelled $KO_2$ samples. Samples of **10** from both $^{16}O_2$ and $^{18}O_2$ were also prepared. All samples were observed

by rR with an excitation wavelength of 514 nm. Comparison of the isotopically labeled samples did not reveal any observable isotopically sensitive signals.

To obtain IR spectra, **11** was formed in MeCN at -40℃ in an $N_2$ atmosphere glove box. Cold $Et_2O$ was added to precipitate solids out of solution rapidly. The solution was filtered to collect the solids. Cold nujol mulls of the isolated intermediate were prepared and placed between KBr salt plates. IR spectra of **11** derived from $K^{16}O_2$ and $K^{18}O_2$, as well as spectra of **9** and **10**, were obtained and compared. No isotope sensitive stretches were observed.

*Reactivity of **11** with select reagents*

Attempts were made to react **11** with a variety of substrates to better characterize the compound.

To a solution of **11**, in MeCN at -40℃, was added tetracyanoethylene (TCNE) (2 eq) dissolved in MeCN. Upon addition of TCNE to the solution **11** was observed to convert to **10** over the course of 3 minutes. Peaks corresponding to reduced product $TCNE^-$ were also observed in the EAS.[2] ESI-MS and GC-MS analysis of the reaction solution did not reveal any epoxide or glycol type products of reaction.

To a solution of **11**, in MeCN at -40℃, was added $PPh_3$ (20 eq) dissolved in MeCN. No effect upon the conversion to **10** was observed as compared to the control reaction. ESI-MS did not show an observable triphenylphosphineoxide peak.

To a solution of **11**, in MeCN at -40℃, was added 2,4,6-tritertbutylphenol (10 eq) dissolved in MeCN. No effect upon the conversion to **10** was observed as compared to the control reaction. EPR analysis of the reaction solution did not reveal any signal supporting an organic radical species expected from hydrogen atom abstraction.

To a solution of **11**, in MeCN at -40℃, was added 2,4-ditertbutylphenol (10 eq) dissolved in MeCN. No effect upon the conversion to **10** was observed as compared to

the control reaction. ESI-MS did not show indications of the organic dimer product expected to form upon hydrogen atom abstraction.

To a solution of **11**, in MeCN at -40℃, was added 9,10-dihydroanthracene (10 eq) dissolved in MeCN. No effect upon the conversion to **10** was observed as compared to the control reaction.

Intermediate **11** was formed as normal in a -40℃ solution of MeCN, which had previously been rigorously dried over $CaH_2$, and *t*-BuOH dried over 4Å molecular sieves. This solvent was then spiked with $H_2{}^{18}O$ (1.2 mM) prior to reaction. Isosbestic conversion from **11** to **10** was observed to occur in the same fashion as the control reaction. ESI-MS analysis of the reaction solution did not indicated that any $^{18}O$ incorporation into **10** had occurred.

To a solution of **11**, in MeCN at -40℃, was added $[Fe^{(II)}(S^{Me2}N_4)(tren)]^+$ (**1**) dissolved in MeCN. Both **10** and $[Fe^{(III)}(S^{Me2}N_4)(tren)(OOH)]^+$ were observed by EAS to form as the reaction progressed. Upon ESI-MS analysis the only **9** derived species detected was **10**. No heterobimetalic oxo-bridged dimer complex was observed.

To a solution of **11**, in MeCN at -40℃, was added $[Mn^{(II)}(S^{Me2}N_4)(6\text{-Me-DPEN})]^+$ (**12**) dissolved in MeCN. No effect upon the conversion to **10** was observed as compared to the control reaction. Upon ESI-MS analysis the only **9** derived species detected was **10**. No heterobimetalic mixed oxo-bridged dimer complex was observed.

To a solution of **9** in EtCN, with *t*-BuOH (300 eq) present in situ, at -78℃ was added $O_2^-$. Over the course of several hours no discernible reaction was observed.

To a solution of **9** in EtCN at -40℃ was added $O_2^-$. Over the course of an hour no discernible reaction was observed. If a proton donor, MeOH or *t*-BuOH, is added to solution then the gradual formation of **10** is observed. In the case of MeOH full formation of **10**, equivalent to that observed by $O_2$, results in 5 min. In the case of *t*-BuOH full formation of **10**, equivalent to that observed by $O_2$, results in 2 hours. No

intermediate species was observed during these conversions.

The amount of **10** formed was observed to differ depending on the nature of the dioxygen species added. $O_2$, $KO_2$ and $H_2O_2$ each have a different ratio of reagent to formation of **10**. When a solution of **9** was reacted with excess $O_2$ in MeCN, at room temperature or -40℃, full formation of **10** was observed, as evidenced by the known molar absorptivity of **10**.[1]

When a solution of **9** was reacted at -40℃ with $O_2^-$ (1 eq) in MeCN with *t*-BuOH (300 eq) present *in situ* it was observed to react in a 1:1 fashion but only produce 50% of the possible **10**. Excess $O_2^-$ or exposure to $O_2$ did not increase the yield of **10**. If only half an equivalent of $O_2^-$ was added to solution 25% of the possible **10** was observed to form. Upon exposure to $O_2$ the amount of **10** increased to 75% of the possible yield, indicating only half of **9** had reacted with half an equivalent of $O_2^-$.

When a solution of **9** was reacted in MeCN at -40℃ with urea hydrogen peroxide it was observed that 2 eq were required to fully react with starting material and only produced 50% of the possible **10**. Exposure of this product to $O_2$ did not result in an increase of **10**.

Attempts at characterization of **11** by spectroscopic and reactivity properties have to-date not yielded suitable evidence to confirm the proposition that **11** is a peroxo/hydroperoxo intermediate. Discussion of work-to-date is provided below.

## 4.3 Discussion

The thiolate containing, non-heme iron complex $[Fe^{(II)}(S^{Me2}N_4(2\text{-QuinoEN}))]^+$ **9** has been found to react with $O_2^-$ to form $\mu$-oxo dimer **10** at ambient temperatures. When this reaction is performed at -40°C in MeCN, with t-BuOH (300 eq) present as a proton donor, an intermediate, **11**, is observed, characterized by an absorption band with a $\lambda_{max}$ of 544 nm. This species converts to **10** over the course of 50 min (Figure 30) with an isosbestic point maintained during the conversion. When this reaction is attempted with alternate proton donors, such as MeOH, the 544 nm species is not clearly formed and there is no isosbestic conversion to **10**. In each of these cases the yield of **10** is only 50% of what would be expected for full conversion of starting material.

The possibility that **11** was a peroxo/hydroperoxo species was investigated. Attempts to characterize **11** via spectroscopic methods have been undertaken. The EPR spectra of **11** showed a weak, broad signal centred at $g_{eff} = 2.16$ (Figure 31), however, this signal was too weak to be clearly identified as the species **11**. Attempts to form $[Fe^{(III)}(S^{Me2}N_4(2\text{-QuinoEN}))]^{2+}$ for comparison by one electron chemical oxidation were unsuccessful due to the instability of the $Fe^{(III)}$ species in solution.[1]

Lacking a strong and clear EPR signal, spectroscopic observation of **11** was undertaken by resonance Raman spectroscopy, in collaboration with the Spiro group, with the assistance of Dr. Mohammed Ibrahim. For an S = 1/2 system the $\nu$(Fe-O) stretch for a peroxo/hydroperoxo would be expected to fall in the range of 600-700 $cm^{-1}$ and the $\nu$(O-O) would be in the 700-800 cm-1 range.[3,4] In the S = 5/2 state these values shift and expand to $\nu$(Fe-O) between 400-650 cm-1 and $\nu$(O-O) between 800-900 cm-1. Intermediate **11**, formed from both $^{16}O$ and $^{18}O$ isotopically labeled reagents, was investigated (Figure 32). The closest available excitation at 514 nm was used and the rR spectra analyzed, however, no isotopically-sensitive peaks were observed. It is possible that the 514 nm excitation wavelength used may be too far from the interme-

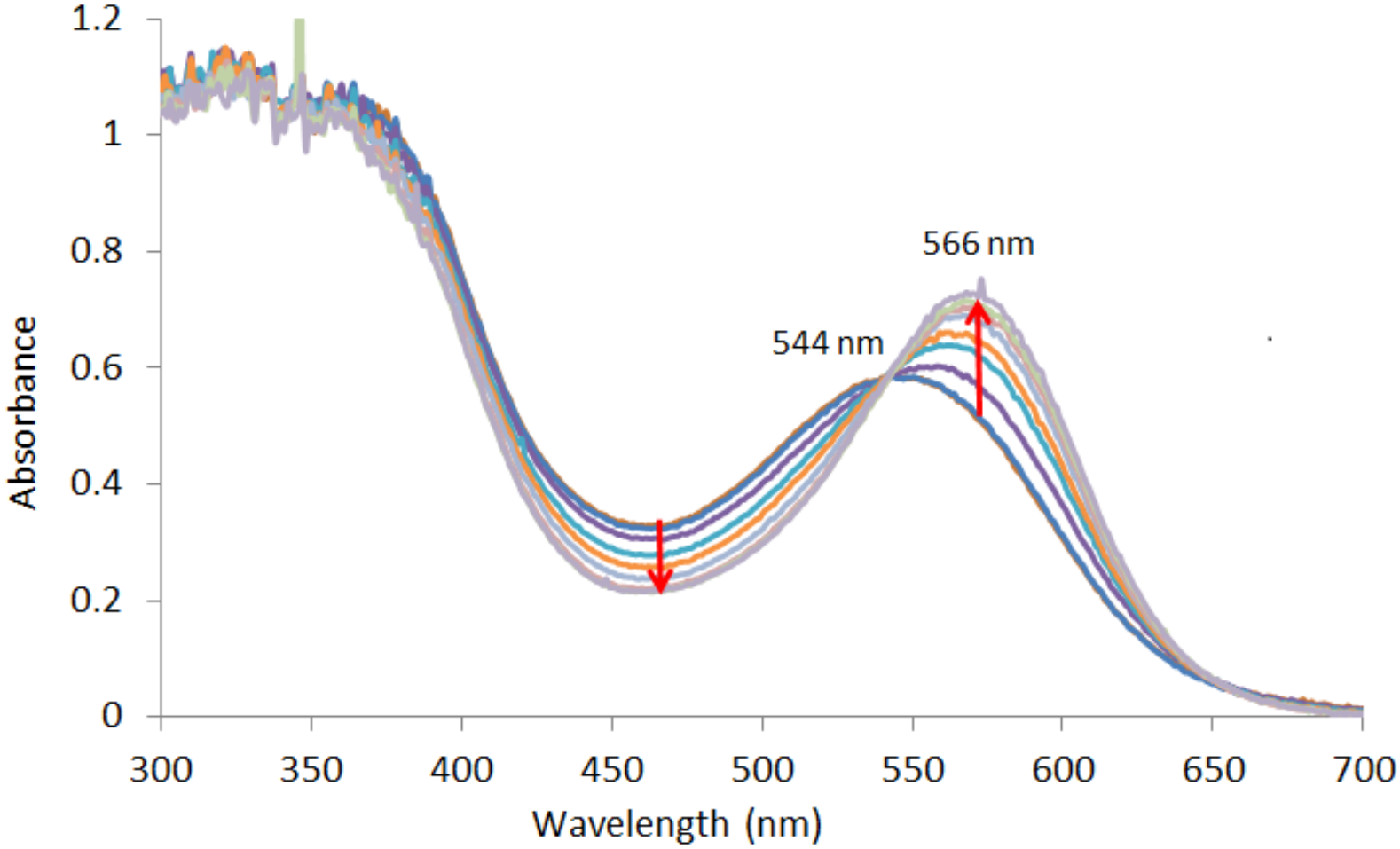


Figure 30: Electronic absorption spectra demonstrating the conversion of **11** to **10** in MeCN at -40℃ in ten minutes intervals.

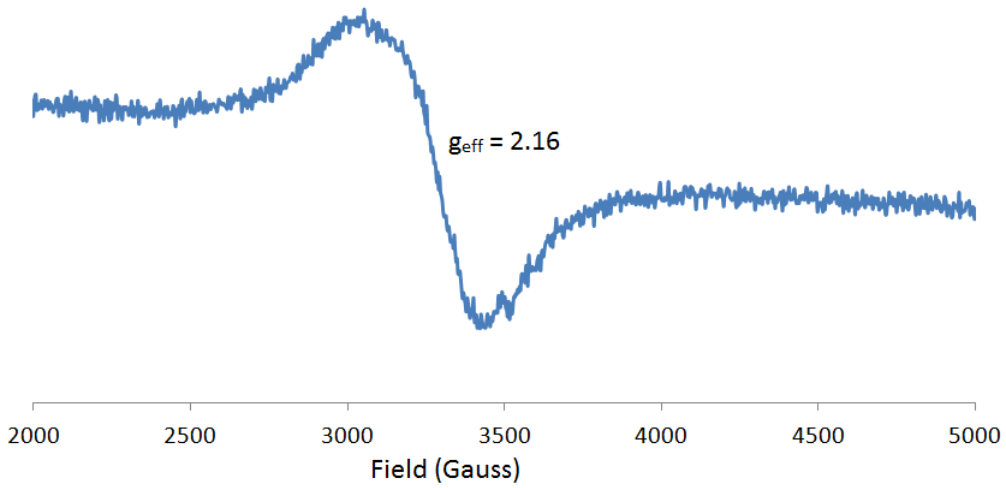


Figure 31: EPR spectrum of **11** in MeCN/Toluene glass

diate absorption maximum but a more closely targeted laser was unavailable during our enquiry.

Since rR spectroscopy was unsuccessful in observing isotopically-sensitive features, measurements of the $\nu$(Fe-O) and $\nu$(O-O) were attempted by IR spectroscopy. Towards this goal **11** was precipitated from solution with cold $Et_2O$ and the solids were collected. Kept cool with dry ice, the solids were prepared in a nujol mull and placed between KBr salt plates. Comparison of **9**, **10** and **11** indicate that **11** is a separate species with unique stretches at 882, 822 and 749 $cm^{-1}$ and is clearly not a mixture of **9** and **10** (Figure 33).

Comparison of the IR spectra of **11** derived from $^{16}O_2^-$ and $^{18}O_2^-$ did not provide spectroscopic evidence of an iron peroxo/hydroperoxo species. While stretches in the IR spectra fall within the expected range of an $\nu$O-O they did not shift with isotopically labelled $KO_2$. The broad signals in the region of interest, as well as the difficulty of removing the noise from the nujol mull, may have resulted in any spectral changes being unobserved by IR spectroscopy.

Attempts at characterizing **11** by EPR, rR and IR spectroscopy were unsuccessful

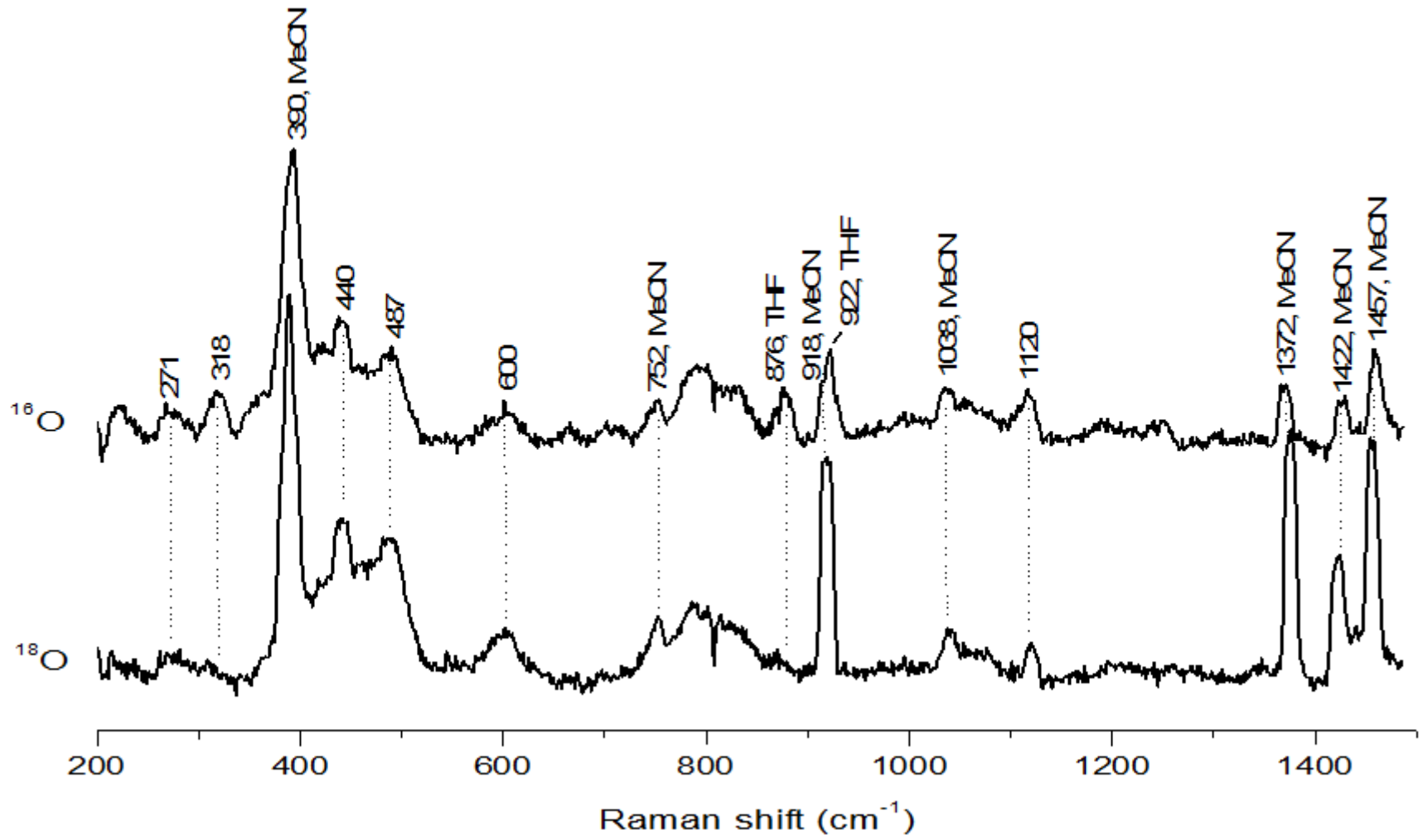


Figure 32: Resonance Raman comparison of isotopically labeled **11**. $\lambda_{ex} = 514$ nm

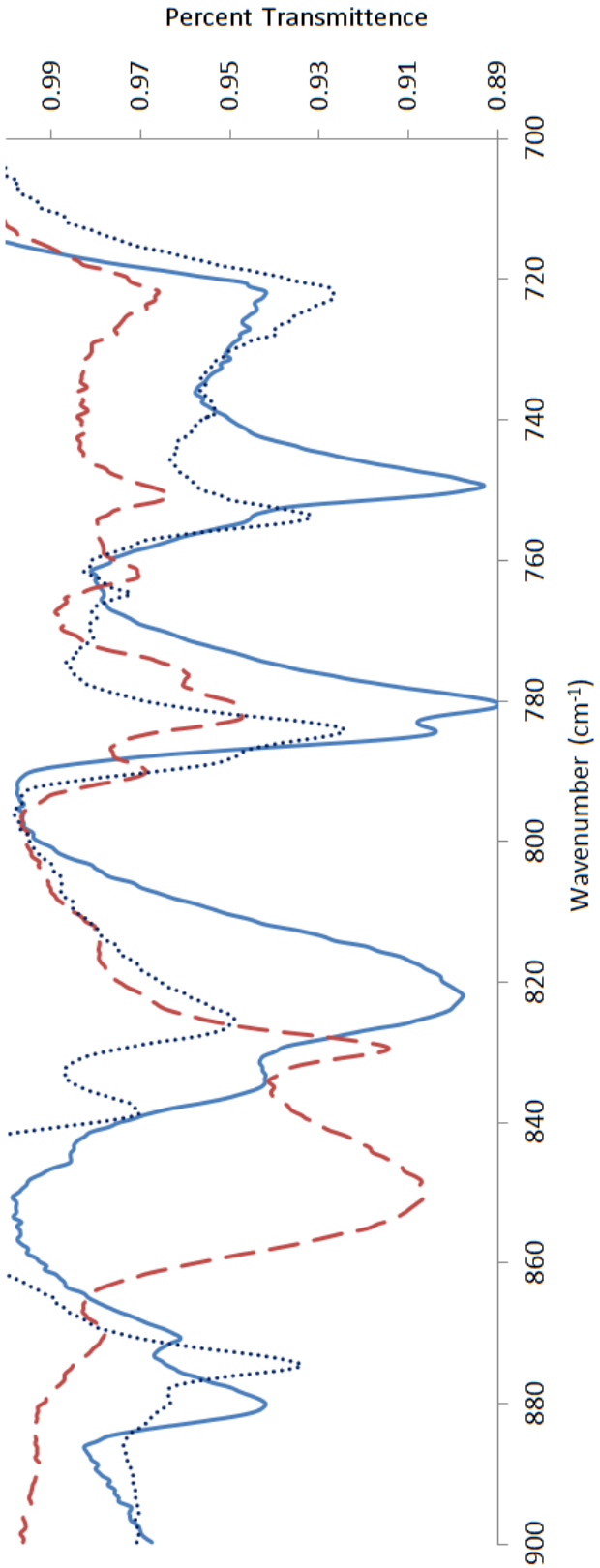


Figure 33: Infrared spectra comparison of **9** ($\cdots$), **10** (- - -) and **11**(—)

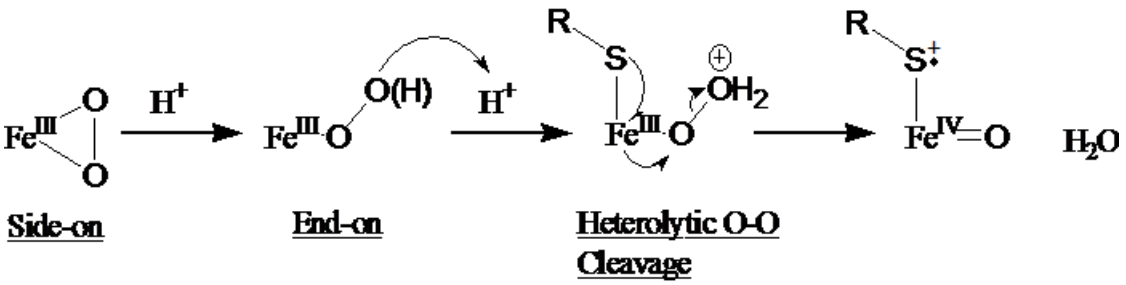


Figure 34: Proposed heterolytic O-O bond cleavage pathway for monomeric FeOOH decay

is determining the identity of the intermediate and alternative methods of investigation were undertaken. Attempts to characterize **11** via the reactivity of various reagents *in situ* were undertaken. Several possible pathways for formation of **10** via a peroxo/hydroperoxo intermediate were considered. Both side-on and end-on peroxo species were a possibility, most likely being electrophilic or nucleophilic respectively. The possibility that a mixed valent $Fe^{(II)}-O-O-Fe^{(III)}$ was being formed in solution was also considered.

In the monomeric cases a side-on peroxo species would be converted to an end-on hydroperoxo by protonation. From this point, whether the intermediate species started side-on or end-on, reactivity would follow the same path. Further protonation of the distal oxygen followed by heterolytic cleavage of the O-O bond would result in the formation of water and an $Fe^{(IV)}$=O species with a thiyl radical (Figure 34). In the case of the mixed valent $Fe^{(II)}$-O-O-$Fe^{(III)}$ dimer homolytic and heterolytic cleavage of the O-O bond would result in the same products, an $Fe^{(III)}$-$O^{-}$ and an $Fe^{(IV)}$=O species.

The reactivity of $Fe^{(IV)}$=O species has been well documented for both heme and non-heme compounds.[5–7] Both heme and non-heme Fe=O species can perform similar oxidation reactions upon a wide variety of substrates[5,6] (Figure 35). These include, but are not limited to, phosphines, olefins, aromatic compounds and alkanes. In catalytic reactions the non-heme species tend to follow an $Fe^{(II)}/Fe^{(IV)}$=O reaction that results

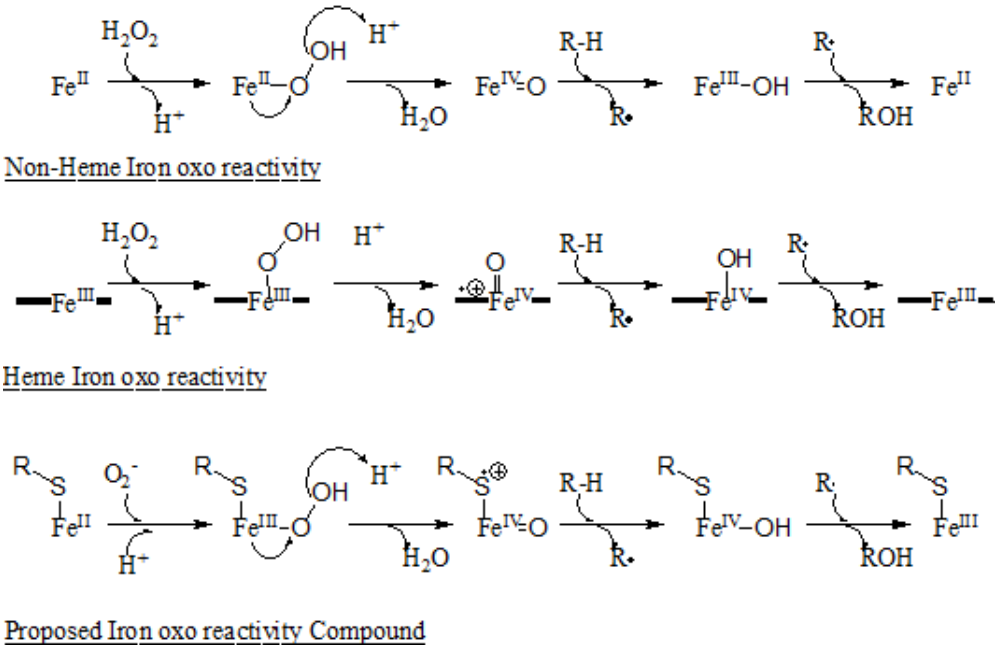


Figure 35: Comparison of reactions of heme and non-heme iron-oxo systems and possible reactivity for **9**.

in the reformation of the starting $Fe^{(II)}$ material after oxidizing substrate. In the case of heme compounds an $Fe^{(III)}/[Fe^{(IV)}{=}O\ L^{+}]$ reaction is invoked where the heme-porphyrin ligand is oxidized by one electron. After oxidation of substrate the $Fe^{(III)}$ is reformed to complete the cycle. In the case of **9** the $O_2^-$ would oxidize the $Fe^{(II)}$ to $Fe^{(III)}$ before the heterolytic O-O bond cleavage step, resulting in a formally $Fe^{(III)}/Fe^{(V)}$ couple. While this would not be expected for most other non-heme compounds it is a reasonable possibility in the case of **9** as the thiyl could fill the role as the oxidized radical ligand.[8]

If **11** were to follow similar heme type reactivity the next step after $Fe^{(IV)}{=}O$ thiyl radical cation formation would be hydrogen atom abstraction to most likely form $Fe^{(IV)}$-OH. This then could follow several paths, such as oxygen rebound or electrophilic aromatic substitution to hydroxylate another species in solution. The result would be reduction and conversion to an $Fe^{(III)}$ thiolate species. The $Fe^{(III)}$ could then condense with water in solution to form the observed **10** species.

For this type of reactivity to be occurring a source of hydrogen atoms is required

to be present in solution. Often solvent molecules may play this role but experiments involving the intermediate species took place in acetonitrile, which have C-H bonds that are likely stronger than those of the ligand of complex **9**.[9] It is perhaps more likely that the required hydrogen abstractions come from the ligand of a species derived from complex **9**. Both alkane and aromatic bonds are present in the **9** derived complexes, providing suitable targets for the proposed hydrogen atom abstraction pathways. The result of this would be that for each abstraction there would be a sacrificial equivalent of complex, resulting in less than 100% conversion of the initial complex **9** to **10**.
The expected formation of **10** can be found for each of the proposed pathways. For end-on peroxos the hydrogen atom abstraction pathway would result in only a 50% maximum formation of **10**, provided each sacrificial equivalent was abstracted from only once. In the case of a mixed valent pathway a 75% maximum yield of **10** could be expected. In comparison, the formation of **10** by $O_2$ would be expected to result in 100% conversion of complex **9**.

Metal-peroxo species are known to act as oxidants[10,11] and a selection of substrates have been added to solutions of **11** to test for this type of reactivity. An electrophilic peroxo would be expected to react with triphenylphosphine ($PPh_3$) to form triphenylphosphineoxide $OPPh_3$. Upon addition of $PPh_3$, (20 eq) in MeCN, to a solution of the intermediate **11**, in MeCN at -40°C, no reaction was observed to take place. The intermediate decayed to **10** in the same fashion and in the same time frame as when no substrate was present. ESI-MS analysis of the reaction mixture observed a peak corresponding to $PPh_3$ but not to $OPPh_3$.

A nucleophilic peroxo species would be expected to react with malononitrile and tetracyanoethylene to form epoxide or glycol type products, or with 2-phenylpropanal via deformylation. Addition of an excess of 2-phenylpropanal or malononitrile, in MeCN, to a solution of **11**, in MeCN at -40°C, resulted in no observable reaction. Upon addition

of the very electron deficient olefin tetracyanoethylene (TCNE), (2 eq) in MeCN, to a solution of **11**, it was observed that the conversion to **10** proceeded to completion in less than three minutes, compared to 50 minutes when no substrate was present. Signals corresponding to the reduced product $TCNE^-$ were also observed in the EAS spectrum,[2] however, these signals represent sub-stochiometric amounts of $TCNE^-$. Exploration of reaction mixture by GC-MS did not reveal the expected epoxide or glycol-type products. The products of TCNE reaction has not yet been definitively characterized. It has been shown that TCNE reacts with **9** and $KO_2$, forming $TCNE^-$. The presence of $TCNE^-$ as a product of reaction suggests that residual starting materials may remain when the EAS signal for **11** maximizes.

Attempts to characterize **11** by its reactivity were not successful in illuminating if the proposed peroxo species was present.

Investigations into the possible hydrogen atom abstraction step were undertaken using 2,4,6-tri-*tert*-butylphenol, 2,4-di-*tert*-butylphenol and dihydroanthracene (DHA).[5,12] Separately each substrate was placed into a solution of **11** and the amount of **10** formed was compared to reactions lacking the donor substrate. Additional spectroscopy to observe the abstracted substrate product was also performed in a manner unique to each substrate (vida infra).

Upon addition of 2,4,6-tri-*tert*-butylphenol, 2,4-di-*tert*-butylphenol or DHA, (10 eq) in MeCN, to a solution of **11** no effect upon the yield of **10** was observed. In the case of 2,4,6-tri-*tert*-butylphenol an EPR sample of the reaction solution was prepared and a spectrum taken (4K, MeCN/Toluene). No EPR signal was detected corresponding to the organic radical expected for hydrogen atom abstraction from 2,4,6-tri-tert-butylphenol. The ESI-MS spectrum for reaction performed in the presence of 2,4-di-*tert*-butylphenol did not reveal a signal for the dimer expected to form from hydrogen atom abstraction.

ESI-MS and EAS spectra of reactions performed in the presence of DHA did not reveal any anthracene product expected if hydrogen atom abstraction from DHA had occurred.

The tested hydrogen atom donors were unsuccessful in preventing the loss of complex which results in the diminished formation of **10** observed by EAS. Since the loss of an equivalent of **9** couldn't be prevented during formation of **10** attempts at trapping or identifying a possible $Fe^{(IV)}$=O species via reactivity were undertaken.

It has been shown that $Fe^{(IV)}$=O species can exchange with $H_2O$ in solution.[13,14] Allowing **11** to form and decay to **10** in MeCN spiked with $^{18}O$ labelled water would result in a detectable increase in the mass of **10** if exchange were occurring. **11** was formed in a solution spiked with $^{18}O$ water (1.2 mM) and allowed to decay to **10**. ESI-MS analysis of the reaction solution showed no detectable labelled **10**.

An $Fe^{(IV)}$=O can react with $M^{(II)}$ species to undergo incomplete atom transfer and form heterobimetalic $Fe^{(III)}-O-M^{(III)}$ products.[15] To investigate this possibility $[Fe^{(II)}(S^{Me2}N_4)(tren)]^+$ **1** and $[Mn^{(II)}(S^{Me2}N_4)(6\text{-Me-DPEN})]^+$ **12**, in MeCN, were added to solutions of **11** at -40°C. In both cases the absorbance of **11**, at 544 nm, was unaffected upon addition and continued to convert to **10**.

The reaction solutions were investigated by ESI-MS, however, the only **9** containing species observed was the known **10**. No oxo-bridged heterobimetalic species were observed. The $[(Fe^{(III)}(S^{Me2}N_4)(2\text{-QuinoEN}))\text{-O-}(Mn^{(III)}(S^{Me2}N_4)(6\text{-Me-DPEN}))]^{2+}$ product is known to form and has been observed from the addition of **9** to the intermediate of **12** + $O_2$ reactivity. The absence of this product from addition of **12** to a solution of **11** suggests that no $Fe^{(IV)}$=O species is present in solution.

An alternate method of forming the proposed $Fe^{(III)}$-OOH intermediate using $H_2O_2$ was attempted. Upon addition of urea:$H_2O_2$ to a solution of **9**, in MeCN at -40℃, **10** was observed to form immediately. However, it took 2 eq of $H_2O_2$ to fully react with starting material and formed only half the maximum **10**, the same final **10** observed for reactivity with $O_2^-$.

Comparison of the yields of **10** from the various dioxygen reagents $O_2$, $O_2^-$ and $H_2O_2$ revealed a curious trend. When **10** was formed by $O_2$, **9** was converted to **10** completely.

When the one electron reduced species $O_2^-$ is used **11** forms and then decays to form only 50% of the possible **10**. Further addition of $O_2^-$ does not result in any further formation of **10**, nor does exposing the reaction to $O_2$ after completion. In the case of addition of only 0.5 eq $O_2^-$, 25% of the **10** is observed to form. When this solution is then exposed to $O_2$ an increase in the 566 nm signal of **10** to 75% is observed. This strongly indicated that $O_2^-$ is reacting in a 1:1 ratio with **9** to yield only one half an equivalent of **10**.

When $H_2O_2$ is used the formation of **10** occurs with no observable intermediate species. The intensity of the 566 nm absorbance for **10** continues to grow in until 2 eq of reagent are added. The amount of **10** formed at that point is only 50% of the **10** possible. When this solution is exposed to $O_2$ no increase in the 566 nm absorbance is observed, indicating all **9** had been consumed. Attempts to identify products, other than **10**, by ESI-MS formed have been unsuccessful thus far for both $O_2^-$ and $H_2O_2$ reactions.

An experiment to form **11** at 10X normal concentration and let it decay was undertaken to observe if the yield of **10** was dependent on concentration. Compound **9** and $O_2^-$ were added to 1/10 the volume of MeCN and *t*-BuOH at -40℃. This reaction

was allowed to progress for an hour before being diluted with additional solvent to a concentration of 0.4 mM. The intensity of the 544 nm peak of **10** was then observed to be the same as when the reaction was run at normal concentrations, indicating that the yield of **10** was not dependent on the concentration of the reaction.

Attempts at elucidating the nature of **11** by exploring its reactivity towards various reagents were unsuccessful. No hydrogen atom abstractions were observed upon the reagents 2,4,6-tri-*tert*-butylpheonl, 2,4-di-*tert*-butylpheonl or DHA. No evidence for an $Fe^{(IV)}$=O species was found through attempted exchange with $^{18}O$ water in solution, nor from formation of heterobimetalic oxo-bridged dimers with **1** or **12**. The lack of reactivity with reagents known to react with electrophilic and neucleophilic peroxos; $PPh_3$, TCNE, maleonitrile and 2-phenylpropanal, suggest that no iron peroxo species is being formed. While the possible $Fe^{(II)}$-O-O-$Fe^{(III)}$ mixed valent species could be expected to display a lack of reactivity, due to the peroxo being buried inside the dimer, the 1:1 ratio of **9** to $O_2^-$ is not consistent with such a product. it appears from the preceding data that **11** is not an iron-peroxo/hydroperoxo species.

## 4.4 Conclusion

We have shown the clear isosbestic conversion of the intermediate **11**, resulting from addition of $O_2^-$ to **9**, to form **10**. Spectroscopic investigations by EPR, rR and IR were undertaken on **11** and while IR has show that **11** is a distinct species EPR and rR have not been able to further elucidate the nature of **11**. Specific signals characteristic of iron peroxos have not yet been observed. **11** has shown a significant lack of reactivity towards reagents expected to react with iron-peroxo compounds. Further reactivity experiments targeted at interrupting the conversion of **11** to **10**, or to increase the yield of **10** were found to not impact the decay of **11**. This preponderance of data would suggest that the observed intermediate is likely not a peroxo compound, however the

spectroscopic and reactivity data observed do not illuminate what alternative species may have formed upon the addition of $O_2^-$ to **9**.

While the nature of species **11** remains unknown the evidence of a clear and repeatable isosbestic convertion between **11** and **10**, as well as a curious stochiometry in reactions with $O_2$, $O_2^-$ and $H_2O_2$ suggests that **11** holds the promise of intriguing discovery.

# Bibliography


[1] S.A. Toledo. Synthesis and Reactivity of an Expanded Family of Superoxide Reductase (SOR) Model Complexes Using N-Heterocyclic, Thiolate-Containing Ligands: Towards a Better Understanding of Structural-Functional Relationships., Ph.D. Thesis, University of Washington, Seattle, Wa, 2009.

[2] Vellaichamy Ganesan, Sergiy V. Rosokha, and Jay K. Kochi. *J. Am. Chem. Soc.*, 125:2559–2571, 2003.

[3] Gerard Roelfes, Vladislav Vrajmasu, Kui Chen, Raymond Y. N. Ho, Jan-Uwe Rohde, Charon Zondervan, Rene M. la Crois, Ebe P. Schudde, Martin Lutz, Anthony L. Spek, Ronald Hage, Ben L. Feringa, Eckard Munck, , and Lawrence Que Jr. *Inorg. Chem.*, 42:2639–2653, 2003.

[4] Terutaka Kitagawa, Abhishek Dey, Priscilla Lugo-Mas, Jason B. Benedict, Werner Kaminsky, Edward Solomon, and Julie A. Kovacs. *J. Am. Chem. Soc.*, 128:14448–14449, 2006.

[5] Wonwoo Nam. *Acc. Chem. Res.*, 40:522–531, 2007.

[6] Carsten Krebs, Danica Galonic Fujimori, Christopher T. Walsh, and J. Martin Bollinger Jr. *Acc. Chem. Res.*, 40:484–492, 2007.

[7] Jan-Uwe Rohde, Jun-Hee In, Mi Hee Lim, William W. Brennessel, Michael R. Bukowski, Audria Stubna, Eckard Munck, Wonwoo Nam, and Lawrence Que Jr. *Science*, 299:1037–1039, 2003.

[8] Shuji Kimura, Eckhard Bill, Eberhard Bothe, Thomas Weyhermu1ller, and Karl Wieghardt. *J. Am. Chem. Soc.*, 123:6025–6039, 2001.

[9] Jeffrey J. Warren, Tristan A. Tronic, and James M. Mayer. *Chem. Rev.*, 110:6961–7001, 2010.

[10] Marlene F. Sisemore, Matthias Selke, Judith N. Burstyn, and Joan Selverstone Valentine. *Inorg. Chem.*, 36:979–984, 1997.

[11] R.A. Sheldon and J.A. Van Doorn. *J. Organomet. Chem.*, 94:115–129, 1975.

[12] Jasmine R. Bryant, Janelle E. Taves, and James M. Mayer. *Inorg. Chem.*, 41:2769–2776, 2002.

[13] Mi Sook Seo, Jun-Hee In, Sun Ok Kim, Na Young Oh, Jongki Hong, Jinheung Kim, Lawrence Que Jr, and Wonwoo Nam. *Angew. Chem.*, 116:2471–2474, 2004.

[14] Marlene Martinho, Frederic Banse, Jean-FrancÃ¼ois Bartoli, Tony A. Mattioli, Pierrette Battioni, Olivier Horner, Sophie Bourcier, and Jean-Jacques Girerd. *Inorg. Chem.*, 44:9592–9596, 2005.

[15] L. Keith Woo. *Chem. Rev.*, 93:1125–1136, 1993.

# 5 New DPEN Ligand Design and Synthesis

## 5.1 Introduction

Previous work in the Kovacs lab by Jason Shearer with the $[Fe^{(II)}(S^{Me2}N_4)(tren)]^+$ complex, **1**, resulted in the first spectroscopically characterized $Fe^{(III)}OOH$ complex with a coordinated thiolate ligand.[1] Functionally modelling SOR **1** was observed to form a stable iron-peroxo compound at low temperature upon reaction with $O_2^-$ in MeOH. The ligand incorporated a thiolate *cis*- to the binding site rather than *trans*- as found in the SOR active site, however release of $H_2O_2$ was still observed. A second thiolate containing iron-hydroperoxo complex was developed in the Kovacs group, $[Fe^{(II)}(cyclam\text{-}PrS)]^+$ **2**, which contained a tethered thiolate in the *trans*- position to the binding site.[2] **2** was found to be both a structural and a functional model for SOR, releasing $H_2O_2$ upon addition of AcOH to the $Fe^{(III)}OOH$. The rR spectra of **2** suggests that the *trans*-thiolate significantly weakens the Fe−O bond. These two compounds shows that the *trans*-thiolate promotes the weakening of the Fe-O bond but $H_2O_2$ release is not dependent on the trans positioned sulphur. To better understand what properties govern the release of $H_2O_2$ and the reactivity of the SOR models, variations of the ligands needed to be explored.

Replacement of the primary amines of **1** with pyridines provided an opportunity for extensive modification of the ligand framework. Modifications to the *ortho*-, *meta*- and *para*- substituents with donating, withdrawing and/or sterically congestive groups would provide a wide range of modified ligand properties to investigate.

The first of the DPEN series of ligands synthesized by Toledo were the 6-H, 6-Me pyridine derivatives and the change of the pyridine ring for a quinoline ring.[3] In the case of the ethyl backbone based ligands the $[Fe^{(II)}(S^{Me2}N_4)(6\text{-Me-DPEN})]^+$ **13**

and $[Fe^{(II)}(S^{Me2}N_4)(2\text{-QuinoEN})]^+$ **9** were isolated and characterized. In the case of the propyl backbone based $[Fe^{(II)}(S^{Me2}N_4)(6\text{-Me-DPPN})]^+$ **14** and $[Fe^{(II)}(S^{Me2}N_4)(6\text{-H-DPPN})]^+$ **15** were isolated and characterized. However, these compounds were unsuccessful in the goal of forming stable and characterizable intermediates of $O_2$ and $O_2^-$ reactivity. The formation of an $Fe^{(III)}$ oxo-bridged dimer was the most common result of these reactions. Comparison of the primary amines of **1** to the pyridine rings of the DPEN series reveals that the pyridine rings are more electron withdrawing ligands. This is clearly seen in the change in the potentials of the $Fe^{(II)}/Fe^{(III)}$ redox couple from -150 mV vs SCE for **1** to +407 mV for **13**, +401 mV for **9** and +433 mV for **14**. Decreasing the electron density around the metal could result in strengthening the Fe−O bond and subsequently favoring O−O bond cleavage over Fe−O cleavage observed for the more donating primary amines. The next series of proposed DPEN ligands have been designed with the intention of disfavoring the $Fe^{(III)}$ oxo-bridged dimer formation, either by adjusting the substituents on the pyridine rings to be more donating or to create enough steric bulk as to prevent dimer formation and potentially trap reactive intermediates. Sterically bulky ligands were devised for the *meta* substituted -phenyl DPEN ligands. Planned electron-donating substituents include the *para* substituted -methoxy, -amino, -dimethylamino and the 3,5-dimethyl-4-methoxy groups to compensate for the withdrawing capacity of the pyridine ring. The electron withdrawing substitutions *para* -nitro and -chloro could also be readily synthesized and would serve as an excellent comparison against the electron-donating ligands.

These substitutions of the pyridine ring have been synthesized previously[4–7] and in some cases it has been shown that the more donating pyridine systems tend to counter productively result in slightly weaker O-O bonds in low-spin $Fe^{(III)}$. However **1** contained donating primary amines but still formed a low temperature stable peroxo complex. Likewise the *trans*-arylthiolate containing compounds synthesized by Goldberg et.

al.[8] saw a weakening of the Fe-O bond of iron alkylperoxo species with more donating substituents on the aryl ring. It is clear from the range of observations that greater understanding of the effects of the ligand in such systems is required.

## 5.2 Experimental

*General Methods*

All reactions were performed using standard Schlenk techniques under an atmosphere of dinitrogen. Reagents were obtained from commercial sources at the highest purity available and were used without further purifications. Acetonitrile (MeCN), Tetrahydrofuran (THF) and Diethyl ether ($Et_2O$) were dispensed under argon from a solvent delivery system. Methanol (MeOH) was refluxed over magnesium and iodine, dimethylformamide (DMF) was dried over 4Å molecular sieves and dichloromethane ($CH_2Cl_2$) was dried over $CaH_2$. Solvent removal was performed on a Buchi rotary evaporator. 3-Methyl-3-mercapto-2-butanone was prepared according to a published procedure. NMR spectra were recorded on a Bruker AV 301, Bruker AV 300, Bruker AVX 500 or Bruker DVR 499 FTNMR spectrometer and referenced to the residual protio solvent.

*Synthesis of 2-[Bis-(4-methoxy-3,5-dimethyl-pyridin-2-ylmethyl)-amino]-ethyl-carbamic acid* tert-*butyl ester* **16**: (Figure 36)

2-chloromethyl-3,5-dimethyl-4-methoxypyridine hydrochloride (1.66 g, 7.47 mmol) and (3-amino-propyl)-carbamic acid tert-butyl ester (0.8 g, 4.99 mmol) were dissolved in 5 M NaOH (2.5 mL). Solution turned pink after stirring for 1 minute. After 48 hours the brown/orange solution was diluted with $H_2O$ (20 mL) and extracted with $CH_2Cl_2$ (3 x 20 mL). Organic layers were combined and dried over $Na_2SO_4$. Solvent was removed by vacuum to obtain **16** (1.42 g, 82% yield) as an orange/brown oil. $^1$H NMR (301 MHz, $CDCl_3$) $\delta$ 8.15 (s, 2 H), 6.31 (s, 1 H), 3.77 (s, 4 H), 3.69 (s, 6 H), 3.12 (m, 2 H), 2.69 (m, 2 H), 2.20 (s, 6 H), 2.11 (s, 6 H), 1.42 (s, 9 H)

*Synthesis of N,N-Bis-(4-methoxy-3,5-dimethyl-pyridine-2-ylmethyl)-1,2-diaminoethane*

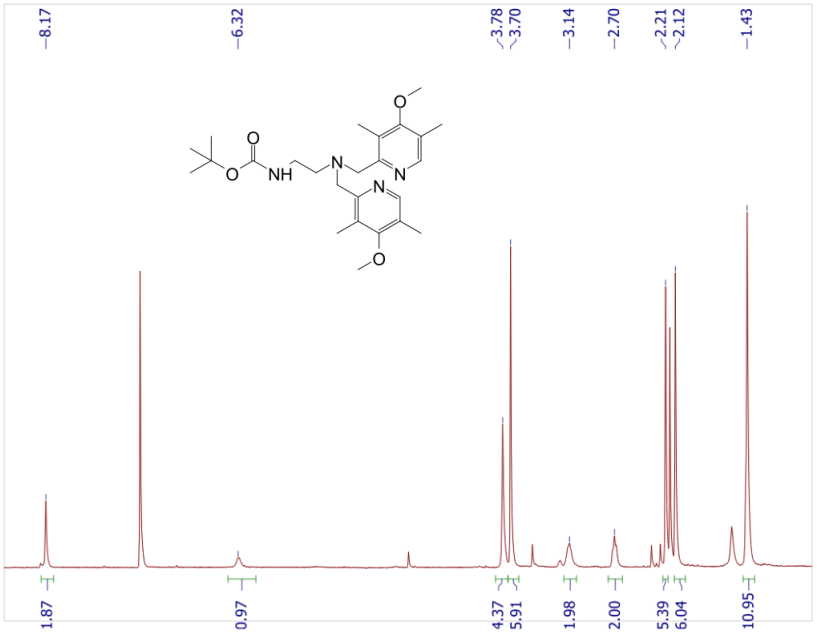


Figure 36: NMR spectra of 2-[Bis-(4-methoxy-3,5-dimethyl-pyridin-2-ylmethyl)-amino]-ethyl-carbamic acid *tert*-butyl ester **16**

**17**: (Figure 37)

2-[Bis-(4-methoxy-3,5-dimethyl-pyridin-2-ylmethyl)-amino]-ethyl-carbamic acid *tert*-butyl ester **16** (1.42 g, 3.10 mmol) was dissolved in $CH_2Cl_2$ (10 mL) and TFA (2 mL) was added dropwise over 5 min. The mixture was allowed to stir at room temperature for 2 hours. Volatiles were removed by rotary evaporation. Residue was dissolved in 2 M NaOH (30 mL) and extracted with $CH_2Cl_2$ (2 x 20 mL). Combined organic layers were dried over $Na_2SO_4$ and solvent removed by vacuum to obtain **17** (0.8 g, 72% yield) as an orange/brown oil. $^1$H NMR (301 MHz, $CDCl_3$) $\delta$ 8.18 (s, 2 H), 3.74 (s, 4 H), 3.71 (s, 6 H), 2.20 (m, 2 H), 2.65 (m, 2 H), 2.22 (s, 6 H), 2.11 (s, 6 H)

*Synthesis of 5-Bromo-2-formylpyridine* **18**: (Figure 38)

2,5-Dibromopyridine (10 g, 42.2 mmol) was dissolved in $Et_2O$ (150 ml) and cooled to -78℃. Care was taken to prevent any material plating out on the flask wall when cooled. A solution of 2.5 M n-BuLi in hexanes (16.88 mL, 42.2 mmol) was added via syringe

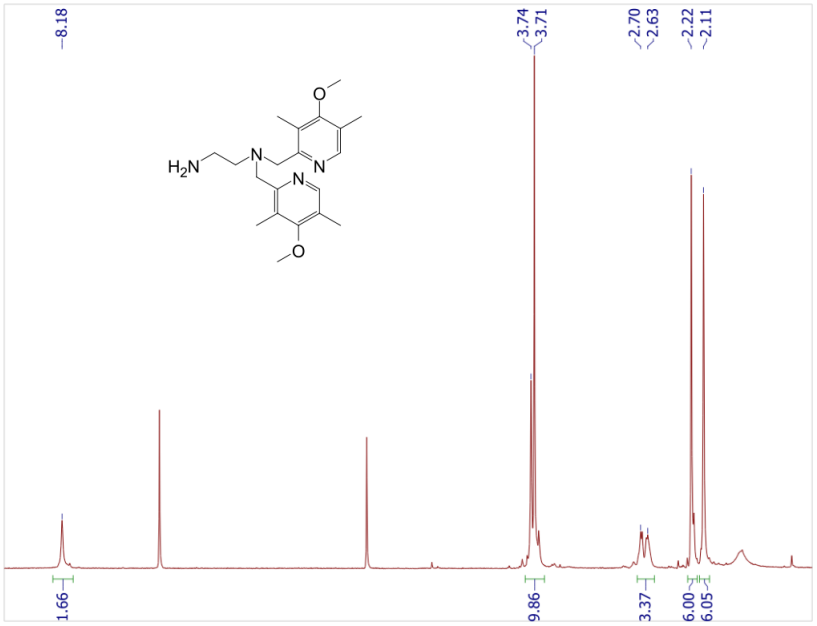


Figure 37: NMR spectra of N,N-Bis-(4-methoxy-3,5-dimethyl-pyridine-2-ylmethyl)-1,2-diaminoethane **17**

over 15 min to the $Et_2O$ solution. The solution was warmed to -40℃ and stirred for 20 min then cooled to -78℃ and 4.84 M DMF in $Et_2O$ (9.6 mL, 46.5 mmol) was added via syringe over 10 min. After 2 h solution was warmed to room temperature and 6 M HCl (30 mL) was added to solution. The $Et_2O$ layer was collected and the aqueous layer was extracted with further $Et_2O$ (3 x 50 mL). Organic layers were combined to obtain a light yellow solution. Activated charcoal was added to the $Et_2O$ solution and filtered to obtain a colorless solution. Organics were dried over anhydrous $Na_2SO_4$. $Et_2O$ was removed by vacuum to obtain **18** as a white crystaline solid (5.42 g, 70% yield) as a white solid. $R_f$ = 0.2 (6:1 Hexane/Acetone). $^1$H NMR (301 MHz, $CDCl_3$) $\delta$ 10.09 (s, 1 H), 8.83 (d, J = 2.2 Hz, 1 H), 8.02 (dd, J = 2.37 Hz, 8.21 Hz, 1 H), 7.68 (d, J = 8.21 Hz, 1 H)

*Synthesis of 5-phenyl-2-formylpyridine* **19**: (Figure 39)

5-Bromo-2-formylpyridine **18** (5.4 g, 29.0 mmol) and $Pd(PPh_3)_4$ (1 g, 0.86 mmol) were

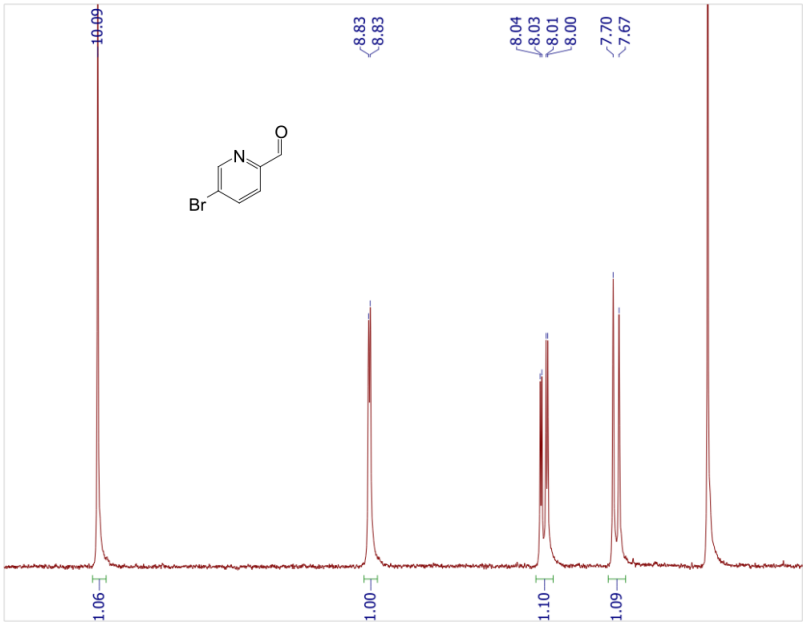


Figure 38: NMR spectra of 5-Bromo-2-formylpyridine **18**

added to degassed toluene (60 mL) under nitrogen. $PhB(OH)_2$ (4.4 g, 36.1 mmol) was dissolved in degassed MeOH (20 mL) and added to toluene solution. Degassed 2 M $Na_2CO_{3(aq)}$ (30 mL) was added to toluene solution and a reflux condenser was attached. Reaction was refluxed under $N_2$ for 8 hours then removed from heat. $CH_2Cl_2$ (100 mL) was added to solution and organics were washed with 2 M $Na_2CO_3$ (50 mL). Organics were dried over $Na_2SO_4$. Solvent was removed by vacuum to obtain orange oil. The residue was purified by a short plug silica gel chromatography using $CH_2Cl_2$ to obtain **19** (4.0 g, 75% yield) as a yellow solid. $R_f = 0.2$ (100% $CH_2Cl_2$). $^1$H NMR (301 MHz, $CDCl_3$) $\delta$ 10.14 (s, 1 H), 9.13 (d, 1 H), 8.23 (dd, 1 H), 8.09 (m, 2 H), 7.91 (d, 1 H), 7.52 (m, 3 H)

*Synthesis of 5-phenyl-2-pyridinemethanol* **20**: (Figure 40)

5-Phenyl-2-formylpyridine **19** (4.0 g, 21.8 mmol) was dissolved into MeOH (40 mL). Separately $NaBH_4$ (1.12 g, 29.6 mmol) was dissolved in $H_2O$ (20 mL). Aqueous solution

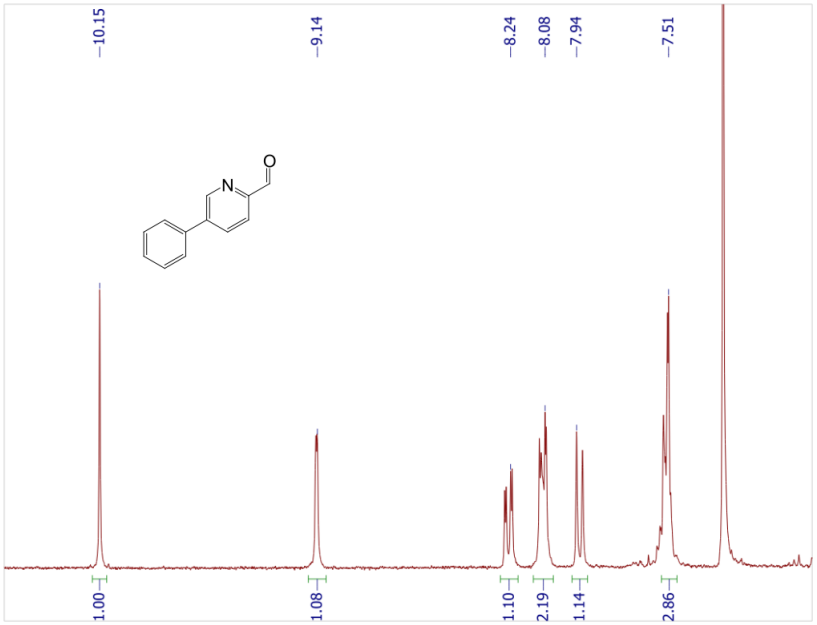


Figure 39: NMR spectra of 2-formyl-5-phenylpyridine **19**

was added dropwise to MeOH solution over 10 min. After addition the mixture was refluxed for 1.5 h. Solution was removed from heat and 6 M HCl was added until pH = 1. The solution was stirred for 10 min then 4 M NaOH was added until pH = 12. Solution was extracted with $CH_2Cl_2$ (50 mL) and the organic layer was filtered to remove insolubles. Organics were dried over $Na_2SO_4$ and solvent was removed by vacuum to obtain **20** (4.0 g, 99% yield) as a brown oil. $^1$H NMR (301 MHz, $CDCl_3$) $\delta$ 8.67 (d, 1 H), 7.99 (d, 2 H), 7.80 (dd, 1 H), 7.74 (dd, 1 H), 7.46 (m, 3 H), 4.78 (d, 2 H), 1.83 (t, 1 H)

*Synthesis of 2-Chloromethyl-5-phenylpyridine Hydrochloride* **21**: (Figure 41)

5-Phenyl-2-pyridinemethanol **20** (4.0 g, 21.6 mmol) was dissolved in $CH_2Cl_2$ (40 mL) and thionylchloride (2 mL) was added dropwise over 5 min. Solution was refluxed for 1 h then all volatiles were removed by vacuum to obtain **21** (4.1 g, 80% yield) as a brown/grey powder. $^1$H NMR (301 MHz, $CDCl_3$) $\delta$ 9.03 (s, 1 H), 8.44 (d, 1 H), 8.22

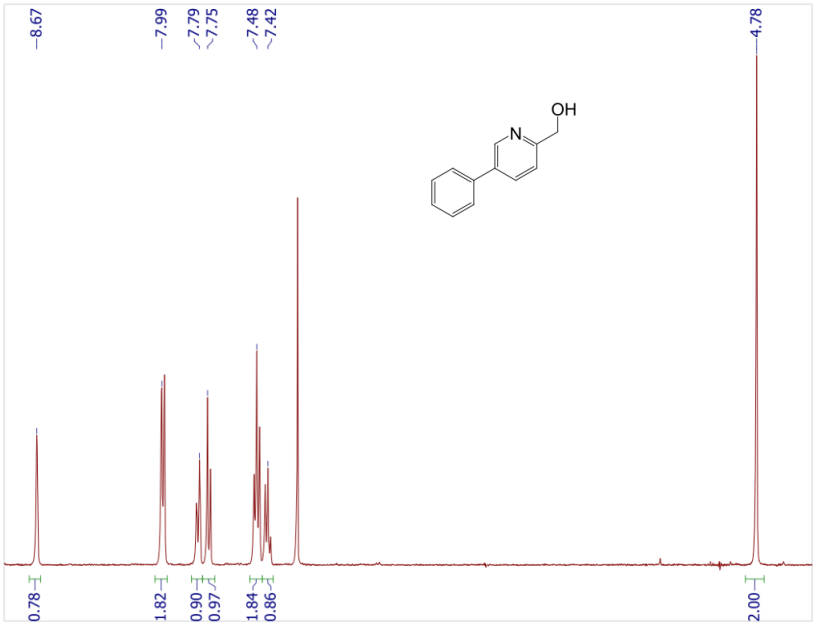


Figure 40: NMR spectra of 5-phenyl-2-pyridinemethanol **20**

(m, 2 H), 8.12 (d, 1 H), 7.66 (m, 3 H), 4.74 (s, 2 H)

*Synthesis of {3-[Bis-(5-phenyl-pyridin-2-ylmethyl)-amino]-propyl}-carbamic acid tert-butyl ester* **22**: (Figure 42)

(3-Amino-propyl)-carbamic acid tert-butyl ester (0.508 g, 2.92 mmol) was dissolved in 2 M NaOH (20 mL). 2-Chloromethyl-5-phenylpyridine hydrochloride **21** (1.128 g, 4.70 mmol) was added to aqueous solution and $CH_2Cl_2$ (5 mL) was added to dissolve solid material that remained. Biphasic mixture was allowed to stir 3 weeks. $H_2O$ (20 mL) was added to solution and mixture was extracted with $CH_2Cl_2$ (3 x 50 mL). Organic layers were combined and washed with brine. Dried organics over $Na_2SO_4$ and removed solvent by vacuum to obtain **22** (0.9 g, 75% yield) as an orange/brown oil. $^1$H NMR(499 MHz, $CDCl_3$) $\delta$ 8.63 (s, 2 H), 7.98 (d, 4 H), 7.77 (dd, 2 H), 7.71 (d, 2 H), 7.47 (t, 4 H), 7.41 (t, 2 H), 3.63 (s, 4 H), 3.15 (m, 2 H), 2.56 (t, 2 H), 1.75 (t, 2 H), 1.41 (s, 9 H)

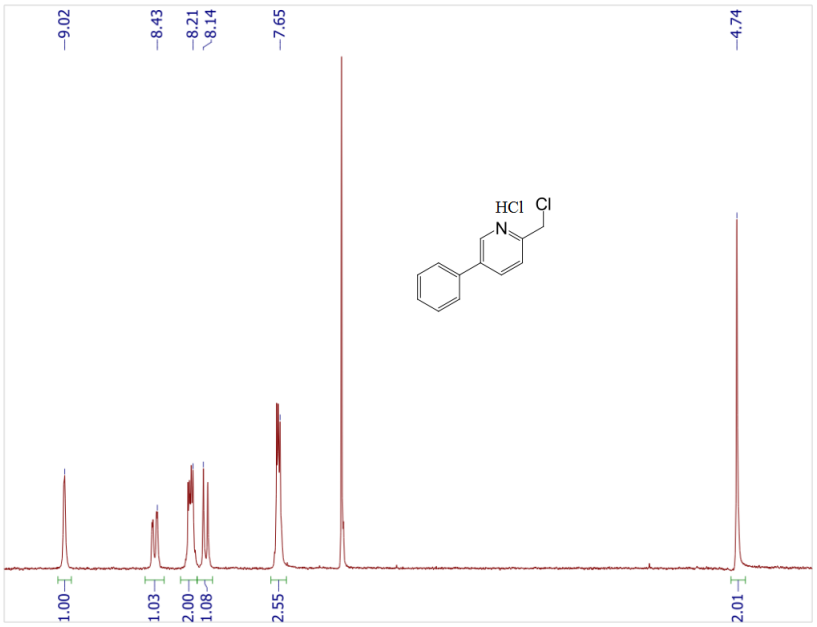


Figure 41: NMR spectra of 2-Chloromethyl-5-phenylpyridine Hydrochloride **21**

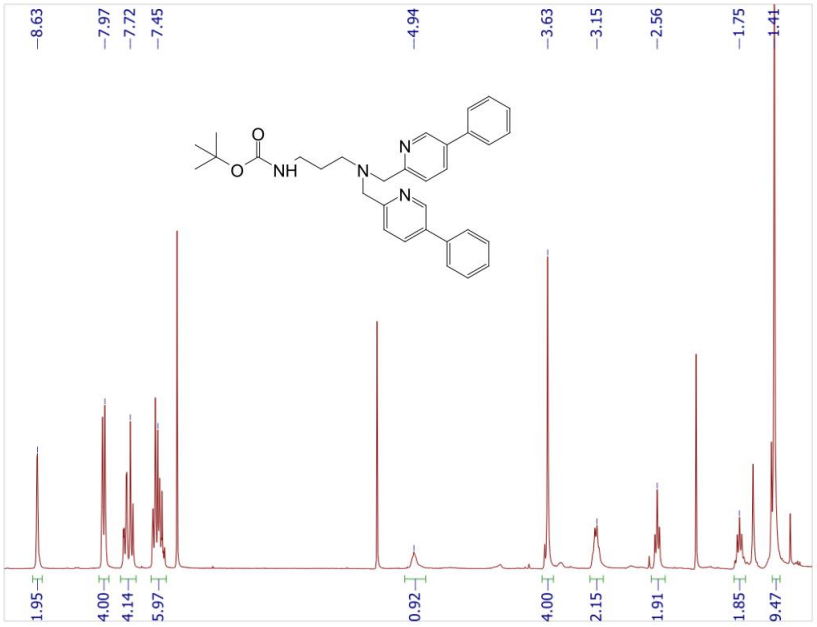


Figure 42: NMR spectra of {3-[Bis-(5-phenyl-pyridin-2-ylmethyl)-amino]-propyl}-carbamic acid tert-butyl ester **22**

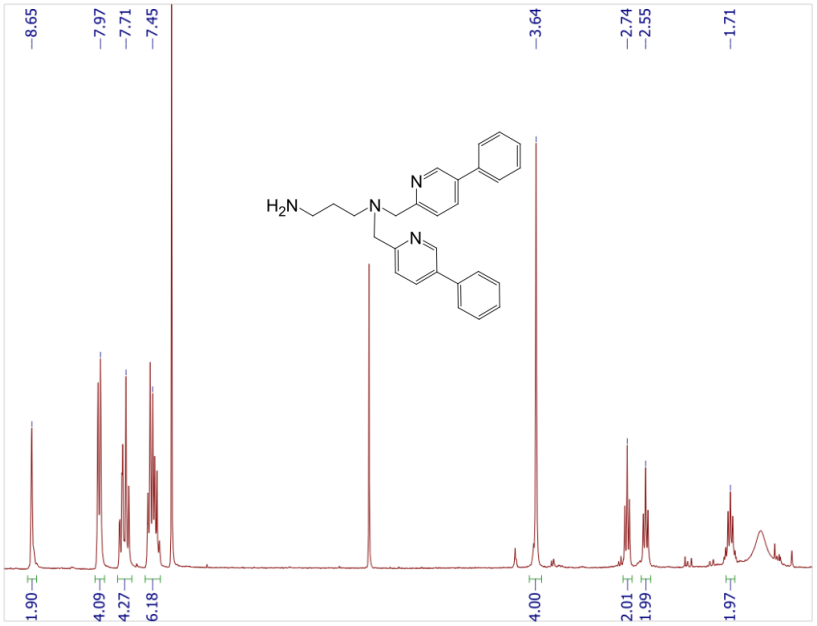


Figure 43: NMR spectra of N,N-Bis-(5-phenyl-pyridin-2-ylmethyl)-1,3-diaminopropane **23**

*Synthesis of N,N-Bis-(5-phenyl-pyridin-2-ylmethyl)-1,3-diaminopropane* **23**: (Figure 43)

{3-[Bis-(5-phenyl-pyridin-2-ylmethyl)-amino]-propyl}-carbamic acid tert-butyl ester **22** (0.9 g, 1.77 mmol) was dissolved in $CH_2Cl_2$ (10 mL) and TFA (3 mL) was added dropwise to solution over 5 min. After 1.5 h all volatiles were removed by vacuum. $CH_2Cl_2$ (20 mL) and 2 M NaOH (20 mL) were added to residue. Organic layer was collected and washed with brine. Organic layer was dried over $Na_2SO_4$ and organics were removed by vacuum to obtain **23** (0.662 g, 85% yield) as an orange/brown oil. $^1$H NMR (301 MHz, $CDCl_3$) $\delta$ 8.65 (s, 2 H), 7.98 (d, 4 H), 7.72 (m, 4 H), 7.46 (m, 6 H), 3.64 (s, 4 H), 2.74 (t, 2 H), 2.56 (t, 2 H), 1.71 (m, 2 H), 1.25 (bs, 2 H)

*Synthesis of N-{3-[Bis-(5-phenyl-pyridin-2-ylmethyl)-amino]-propyl}-2-bromo-2-methyl-propionamide* **24**: (Figure 44)

N,N-Bis-(5-phenyl-pyridin-2-ylmethyl)-1,3-diaminopropane **23** (0.3 g, 0.734 mmol) was

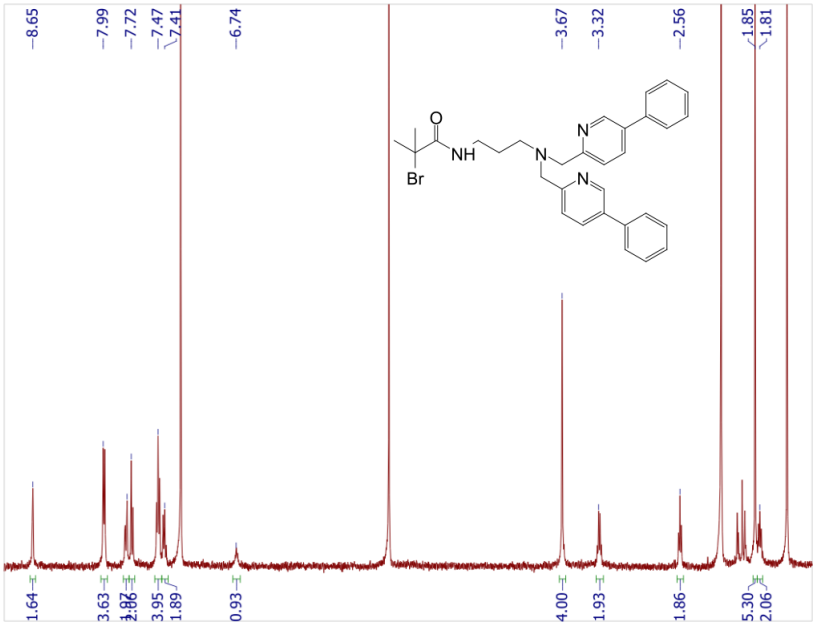


Figure 44: NMR spectra of N-{3-[Bis-(5-phenyl-pyridin-2-ylmethyl)-amino]-propyl}-2-bromo-2-methyl-propionamide **24**

dissolved in $CH_2Cl_2$ (5 mL) and DIPEA (0.177 g, 1.01 mmol) was added to solution followed by 2-Bromo-2-methylpropionyl bromide (0.26 g, 1.13 mmol). Reaction was allowed to stir overnight. Added $CH_2Cl_2$ (10 mL) and washed with conc. $NH_4Cl_{(aq)}$ (2 x 10 mL) and 2 M NaOH (2x10 mL). Dried organics over $Na_2SO_4$ and removed solvent by vacuum to obtain **24** (0.302 g, 74%) as an orange/brown oil. $^1$H NMR (499 MHz, $CDCl_3$) $\delta$ 8.65 (s, 2 H), 7.99 (d, 4 H), 7.78 (dd, 2 H), 7.72 (d, 2 H), 7.47 (t, 4 H), 7.41 (m, 2 H), 6.73 (bs, 1 H), 3.67 (s, 4 H), 3.31 (m, 2 H), 2.56 (t, 2 H), 1.85 (s, 6 H), 1.81 (m, 2 H); ESI-MS: 557 m/z, 559 m/z.

*Synthesis of N-{3-[Bis-(5-phenyl-pyridin-2-ylmethyl)-amino]-propyl}-2-thioacetyl-2-methyl-propionamide* **25**: (Figure 45)

N-{3-[Bis-(5-phenyl-pyridin-2-ylmethyl)-amino]-propyl}-2-bromo-2-methyl-propionamide **24** (0.208 g, 0.373 mmol) was dissolved in DMF (2.5 mL) and solution was degassed and exchanged with $N_{2(g)}$. Under a stream of $N_{2(g)}$ excess potassium thioacetate (0.162 g,

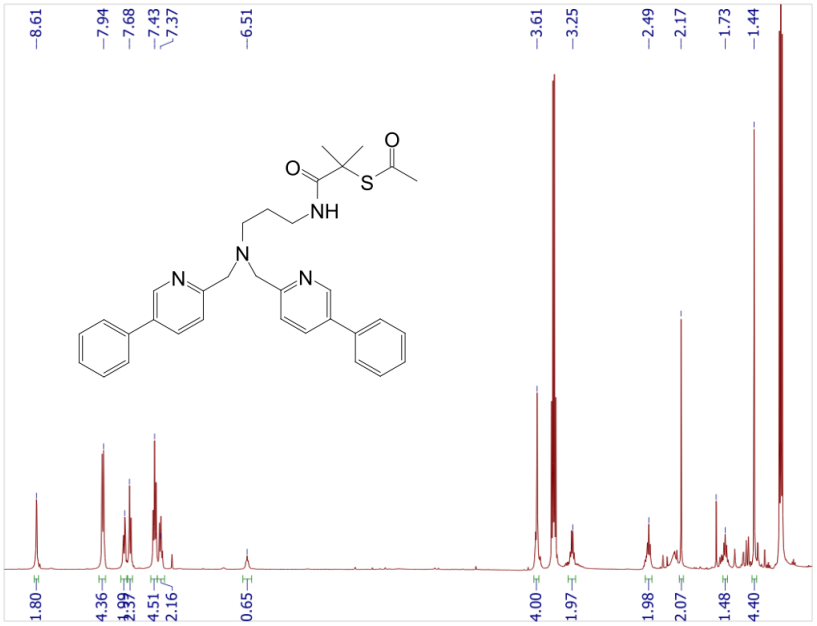


Figure 45: NMR spectra of N-{3-[Bis-(5-phenyl-pyridin-2-ylmethyl)-amino]-propyl}-2-thioacetyl-2-methyl-propionamide **25**

1.42 mmol) was added to solution followed by a catalytic amount of potassium iododide (0.038 g, 0.23 mmol). Reaction was allowed to stir overnight. After 36 hours ESI-MS showed no starting material and a prominent peak at 591 m/z corresponding to the product plus potassium. $Et_2O$ (10 mL) was added to solution and organic layer was washed with $H_2O$ (4 x 10 mL) then brine (1x10 mL) to remove DMF and salts. Dried $Et_2O$ over $Na_2SO_4$ and removed solvent by vacuum to obtain **25** as a light brown oil. $^1$H NMR (500 MHz, $CDCl_3$) $\delta$ 8.61 (s, 2 H), 7.94 (d, 4 H), 7.73 (dd, 2 H), 7.68 (d, 2 H), 7.43 (t, 4 H), 7.37 (m, 2 H), 6.51 (bs, 1 H), 3.61 (s, 4 H), 3.25 (q, 2 H), 2.49 (t, 2 H), 2.17 (s, 3 H), 1.73 (t, 2 H), 1.44 (s, 6 H); ESI-MS: 553 m/z

## 5.3 Discussion

Investigations into the products of reaction of $O_2$ or $O_2^-$ with the first series of DPEN ligands yielded several compounds of interest, but few intermediates that were well behaved and fully characterized. Low stablility, spectroscopic ambiguity and a propensity to form the $Fe^{(III)}$ oxo-bridged dimer products were characteristic of the original DPEN ligands. Changes to the ligand framework needed to be employed to adjust the strength of the Fe-O and O-O bonds of potential iron-peroxo species. The importance of the strength of the Fe-O and O-O bonds towards reactivity is nicely illustrated by comparing the resonance Raman (RR) data for the hydroperoxo species of the high-spin E114A SOR mutant[9] and the low-spin P450 (CYP101) enzyme.[10] Both systems contain the $N_4S_1$ coordination sphere and are presumed to form $Fe^{(III)}$-O-OH species but P450 cleaves the O-O bond while SOR forms $H_2O_2$. In P450 (CYP101) the $\nu$(Fe−O) and $\nu$(O−O) are 559 and 799 $cm^{-1}$ respectively while in the E114A SOR mutant 567 and 838 $cm^{-1}$ are observed. SOR actually possesses a slightly stronger $\nu$(Fe-O) by 8 $cm^{-1}$ but the $\nu$(O-O) is 39 $cm^{-1}$ stronger. DFT calculations by Hall (ref HallIC10a) have suggested that SOR release of $H_2O_2$ is strongly promoted by weakening the Fe-O bond but is realized not just through the coordination sphere but by the surrounding environment as well. Changing solvents can effect environmental influences but stabilizing the O-O bond while weakening the Fe-O bond must be carefully pursued through ligand design to overcome the $Fe^{(III)}$ oxo-bridged dimer formation common to first generation DPEN ligands.

Two methods were devised to overcome the observed instability of intermediates prior to $\mu$-oxo dimer formation. The first would be introduction of donating groups to the pyridine ring which could counter the electron withdrawing effect, directing greater electron density towards the metal center. This would potentially result in weakening

the M-O bond sufficiently to favor peroxide release over O-O bond cleavage, as seen in **1** by creating a less Lewis acidic metal center. The second method was to prevent the formation of $Fe^{(III)}$ oxo-bridged dimers by incorporation of steric bulk to create a protective pocket around the 6th coordination site.

Only one ligand with donating groups has been completely synthesized as of this writing. The 2-hydroxymethyl-3,5-dimethyl-4-methoxypyridine starting material was available commercially and so compound **17** was readily formed by methods used for previous DPEN ligands. The ligand underwent the metal-templated Schiff-base condensation with 3-mercapto-3-methylbutanone and $Fe(OAc)_2$ and was observed to form complex by ESI-MS. The complex, however, was not amenable to crystallization and appeared to dissociate from the metal during crystalization attempts as the oily product obtained showed only free condensed ligand when investigated by ESI-MS. Attempts to isolate the complex by rapidly crashing out of solution can obtain crude complex but recrystalization is required to obtain usable purity.

Modified pyridine rings containing para-substituted donating groups are favored for future synthesis. The increasingly donating series of *para*-methoxy, -amino and -dimethylamino modified pyridines are known[5,11,12] and are ideal targets for incorporation into future complex syntheses. By placing the donating group in the para position intramolecular steric interactions can be minimized in regard to the geminal methyls adjacent to the sulphur atom. The necessity of reduced intramolecular sterics has been shown in the crystal structures of previous DPEN complexes where the 6-Me substituent resulted in exceptionally long bond $N_{(py)}$-Fe bonds in the 6-coordinate $Fe^{(III)}$ oxo-bridged dimers.[3]

An alternate means of preventing $Fe^{(III)}$ oxo-bridged dimers was investigated

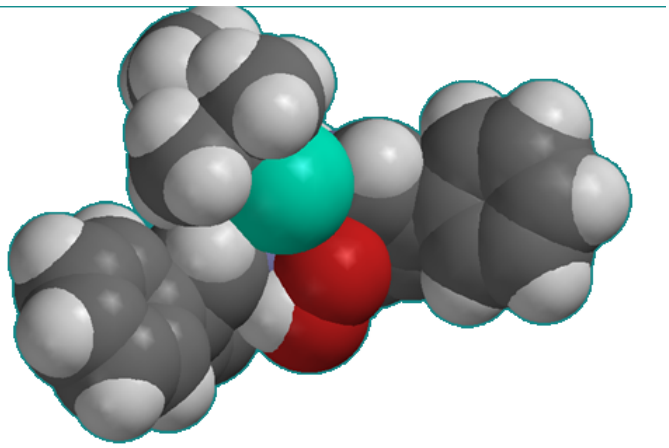

Figure 46: Molecular mechanics model of $[Fe^{(II)}(S^{Me2}N_4)(5\text{-Ph-DPPN})]^+$ **23** with proposed hydroperoxo:

through the use of stericly bulky substituents. A single phenyl ring in the 5-position was shown by molecular mechanics modelling (Figure 46) to provide a sufficiently deep protective pocket around the sixth coordination site to likely prevent the oxo-bridged dimer formation. A modified synthetic scheme developed from literature preps for the 6-phenyl pyridine derivative[13–15] was undertaken to synthesize the 5-phenyl pyridine component (Figure 47).

Standard complexation methods for the DPEN series involving the metal templated Schiff-base condensation of 3-methyl-3-mercaptobutanone to the primary amine of compound **23** in the presence of $Fe(OAc)_2$ were unsuccessful. Neither condensed ligand nor complex was observed by the ESI-MS. Despite various conditions success was not achieved towards the desired product. The lack of free condensed ligand raised the possibility that the ligand, prior too condensation, was too bulky to allow the metal templated Schiff-base condensation. In an attempt to alleviate the problem of condensing the thiol onto the ligand an alternate synthesis was devised which incorporated the thiol into a complete 5-coordinate ligand prior to addition of a metal. The primary amine of

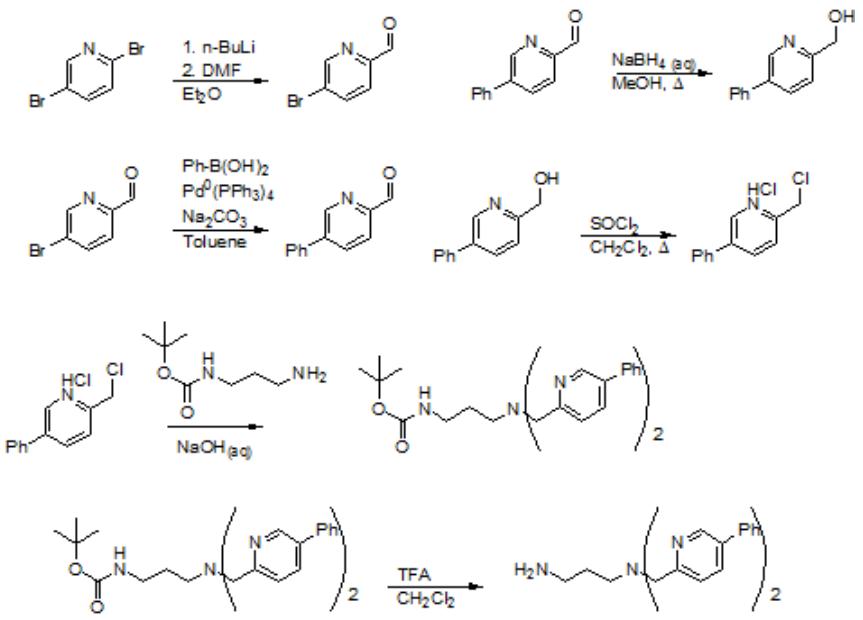


Figure 47: Synthetic scheme of 5-Ph-DPEN ligand **23**

**23** was alkylated with 2-Bromo-2-methylpropionyl bromide to form an amide. Reaction with potassium thioacetate in dry DMF displaced the bromide to yield the final -acetyl protected thiol ligand **25**. When reacted with $Fe(OAc)_2$ and base the ligand failed to form the desired complex as monitored and determined by ESI-MS. Deprotected ligand was observed by ESI-MS at (511 m/z) but no peak corresponding to metal and ligand was observed. To ensure that the lack of complex formation was not due to incomplete amide deprotonation dry DMA was used as the solvent in place of methanol. By removing alternate proton sources the amide could be reliably deprotonated prior to coordination to the metal. To prevent the possibility that the base was reacting with the metal preferentially the non-coordinating base potassium bis(trimethylsilyl)amine was used. Despite these efforts no evidence of a metal-ligand complex was observed.

The target ligands **25** and **43** may simply be too large and bulky to complex first row transition metals. In this case a smaller functional group may achieve the desired balance between protection of the reactive product and the ability to form the desired metal complex. The use of isopropyl substituents in place of a phenyl may achieve these

goals. Future work with the next series of DPEN ligand should focus on the synthesis of the para substituted donating groups; -OMe, -$NH_2$, -$NMe_2$ and on less bulky meta substituents.

## 5.4 Conclusion

In conclusion, we have reported the syntheses and characterization of three new DPEN series ligands. Addition of significant steric bulk as well as significantly donating substituents, on the pyridine ring have been shown to inhibit complex formation. Less bulky and only single donating substituents on the pyridine rings should be focused on for future ligand synthesis. The para-position series of modifications offers excellent capacity to fine-tune the electronic donating capacity while avoiding the problems with intramolecular steric interactions and should be aggressively pursued in the near future. The 5-$^i$Pr ligand offers a synthetic route to continue attempting to utilize ligand bulk as a protective element while reducing the quantity of bulk to a lesser degree than the phenyl rings provided. Investigations of bulky ligands would be well served to target this modification next.

# Bibliography

[1] Jason Shearer, Robert C. Scarrow, and Julie A. Kovacs. *J. Am. Chem. Soc.*, 124:11709–11717, 2002.

[2] Terutaka Kitagawa, Abhishek Dey, Priscilla Lugo-Mas, Jason B. Benedict, Werner Kaminsky, Edward Solomon, and Julie A. Kovacs. *J. Am. Chem. Soc.*, 128:14448–14449, 2006.

[3] S.A. Toledo. Synthesis and Reactivity of an Expanded Family of Superoxide Reductase (SOR) Model Complexes Using N-Heterocyclic, Thiolate-Containing Ligands: Towards a Better Understanding of Structural-Functional Relationships., Ph.D. Thesis, University of Washington, Seattle, Wa, 2009.

[4] Yan Zang and Lawrence Que Jr. *Inorg. Chem.*, 34:1030–1035, 1995.

[5] Bernhard Kohl, Ernst Sturm, Jorg Senn-Bilfinger, W. Alexander Simon, Uwe Kruger, Hartmann Schaefer, Georg Rainer, Volker Figala, and Kurt Klemm. *J. Med. Chem.*, 35:1049–1057, 1992.

[6] J. H. Hutchinson, D. Riendeau, C. Brideau, C. Chan, D. Delorme, D. Denis, J.P. Falgueyret, R. Fortin, J. Guay, P. Hamel, T. R. Jones, D. Macdonald, C. S. McFarlane, H. Piechuta, J. Scheigetz, P. Tagari, M. Thgrien, and Y. Girard. *J. Med. Chem.*, 36:2771–2787, 1993.

[7] Gerard Roelfes, Vladislav Vrajmasu, Kui Chen, Raymond Y. N. Ho, Jan-Uwe Rohde, Charon Zondervan, Rene M. la Crois, Ebe P. Schudde, Martin Lutz, Anthony L. Spek, Ronald Hage, Ben L. Feringa, Eckard Munck, , and Lawrence Que Jr. *Inorg. Chem.*, 42:2639–2653, 2003.

[8] Frances Namuswe, Gary D. Kasper, Amy A. Narducci Sarjeant, Takahiro Hayashi, Courtney M. Krest, Michael T. Green, Pierre Moenne-Loccoz, and David P. Goldberg. *J. Am. Chem. Soc.*, 130:14189–14200, 2008.

[9] Gergely Katona, Philippe Carpentier, Vincent Niviere, Patricia Amara, Virgile Adam, Jeremy Ohana, Nikolay Tsanov, and Dominique Bourgeois. *Science*, 316:449–453, 2007.

[10] Piotr J. Mak, Ilia G. Denisov, Doreen Victoria, Thomas M. Makris, Tianjing Deng, Stephen G. Sligar, and James R. Kincaid. *J. Am. Chem. Soc.*, 129:6382–6383, 2007.

[11] Masakazu Tamura, Yasuteru Urano, Kazuya Kikuchi, Tsunehiko Higuchi, Masaaki Hirobe, and Tetsuo Nagano. *Chem. Pharm. Bull.*, 48:1514–1518, 2000.

[12] Christiana Xin Zhang, Susan Kaderli, Miguel Costas, Eun il Kim, Yorck-Michael Neuhold, Kenneth D. Karlin, and Andreas D. Zuberbuhler. *Inorg. Chem.*, 42:1807–1824, 2003.

[13] J. E. parks, B. E. Wagner, and R. H. Holm. *Inorg. Chem.*, 10:2472–2478, 1971.

[14] Chang lin Chuang, Kitae Lim, Qiu Chen, Jon Zubieta, and James W. Canary. *Inorg. Chem.*, 34:2562–2568, 1995.

[15] Magdalena M. Makowska-Grzyska, Ewa Szajna, Crystal Shipley, Atta M. Arif, Michael H. Mitchell, Jason A. Halfen, and Lisa M. Berreau. *Inorg. Chem.*, 42:7472–7488, 2003.